STUDIES ON
MIXED LAYER DEPTH IN THE ARABIAN SEA

Thesis submitted to the

Cochin University of Science and Technology

For the Degree

of

DOCTOR OF PHILOSOPHY

IN

## PHYSICAL OCEANOGRAPHY

UNDER FACULTY OF MARINE SCIENCES

By

M. G. JOSEPH, M. Sc.

NAVAL PHYSICAL AND OCEANOGRAPHIC LABORATORY

COCHIN - 682 004

DECEMBER 1986

C E R T I F I C A T E

    This is to certify that this Thesis is an authentic record of research work carried out by Sri M.G. Joseph, M.Sc, under my supervision and guidance in Naval Physical and Oceanographic Laboratory for the Ph.D. Degree of the University of Cochin and no part of it has previously formed the basis for the award of any other degree in any University.

<div style="text-align: right;">
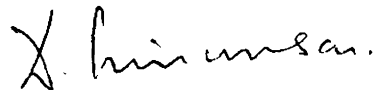
Dr. D. SRINIVASAN
(Research Guide)
Visiting Professor
Ocean Engineering Centre
Indian Institute of Technology

</div>

Madras - 600 036
December, 1986

ACKNOWLEDGEMENTS

C O N T E N T S

PREFACE

The surface layers of the oceans are fairly
stratified with a top mixed layer of nearly uniform
temperature (also density) over a layer of negative
thermal gradient called thermocline. The mixed layer
depth in the ocean has important significance in
performance for sonar/under water communication,
fisheries and biological productivity. Prediction of
mixed layer can be based on an understanding of mixed
layer dynamics, controlled by wind forcing, heat exchanges
at the surface mixing by turbulence and convection,
advection, convergence/divergence and internal waves.

The mixed layer depth distribution in the Arabian
Sea is mainly influenced by southwest and northeast
monsoons and the respective reversals of currents and
gyre systems. The mixed layer depth characteristics
in the Arabian Sea with special reference to its annual
and short term predictability is the aspect of study
in this thesis. Climatological data from the atlases
of Wooster et al. (1967), Hastenrath and Lamb (1979)
and Robinson et al. (1979) and BT/hydrometeorological
data collected during OCEANAVEX (1973-74),MONSOON (1977)
and the local cruise of MV PRASIKSHANI have been
analysed to present the variability of the mixed layer
depth in relation to the causative factors.

The break up of the thesis into the different
chapters is as follows:

Chapter I presents a general introduction on the mixed layer depth, its characteristics and causative factors with a review of earlier works on the topic followed by the details of the study area, data sources and quality and methodology of the analysis.

Chapter II has two sections. Section I deals with the variability of surface wind field, net heat gain and sea surface temperature in the Arabian Sea. In Section II a discussion on the variability of wind (mechanical) and convective mixing in relation to observed mean monthly mixed layer depth for the Arabian Sea subareas is presented.

Chapter III presents a discussion on advection, convergence/divergence and internal oscillations, influencing the mixed layer variability.

Chapter IV deals with the spatial and seasonal variability of the mixed layer depth in the Arabian Sea.

In Chapter V, short term predictive characteristics of mixed layer depth for deep oceanic and shallow coastal stations in the Arabian Sea are discussed by presenting an evaluation of a simple one dimensional prediction scheme.

A summary of the above studies is presented with conclusions on variability of mixed layer depth in relation to the causative factors and its predictability in the Arabian Sea in Chapter VI.

ABBREVIATIONS

^{o}C	:	degree centigrade
cal	:	calorie
$cal\ cm^{-2}\ min^{-1}$	:	calorie per square centimetre per minute
$cal\ cm^{-2}\ hr^{-1}$	:	calorie per square centimetre per hour
$cal\ g^{-1}\ ^{o}C^{-1}$	:	calorie per gram per degree centigrade
cm	:	centimetre
$cm\ sec^{-1}$	:	centimetre per second
Fig.	:	Figure
$g\ cm^{-3}$	:	gram per cubic centimetre
kts	:	knots
M, m	:	metre
MLD	:	mixed layer depth
ppt	:	part per thousand
SST	:	sea surface temperature
$W\ m^{-2}$	:	Watt per square metre

CHAPTER I

CHAPTER I

INTRODUCTION

1.1 Mixed layer depth and its importance

The top layer of the ocean forms the link between the atmosphere and the deeper waters. As a result of turbulent mixing at the surface under the predominant effects of wind stress and heat exchange the vertical distribution of water characteristics is purely uniform. The bottom of this layer marks the limit of atmospheric influence and generally coincides with the Ekman depth of frictional influence. This surface layer absorbs the solar energy incident at the surface and contains the momentum imparted by the wind stress at the surface, thus acting as a buffer modifying the exchanges between the atmosphere and the deeper waters. The atmosphere in turn derives an immense energy back in the form of cyclonic heat potential stored, from the surface layers, thereby influencing the weather and climate. Convergence, divergence, eddies and internal waves affecting the surface layer depth leads to the modification and change in circulation in the deeper waters. The mixed layer depth sets a vertical limit for fisheries exploitation, as it is related to the productivity of waters with nutrients stirred up from the bottom. Variation in the mixed layer depth affects the sonar propagation limiting the horizontal range characteristics. The mixed layer depth

information to be used in general circulation models
and atmospheric boundary layer models cannot be overlooked
(Meehl, 1984).

1.2   Definition of Mixed Layer Depth (MLD)

The surface mixed layer can be easily identified
from the vertical thermal structure of the ocean. Usually
the vertical temperature profile in the ocean will have
an isothermal part in the top layer followed by steeper
thermal gradients (thermocline) overlying deeper layers
with mild gradients. The thickness of the turbulent,
homogeneous surface layer experiencing greater seasonal
changes in temperature is referred to as the mixed layer
depth (MLD). A number of definitions are in use
depending on the purpose for which the information on
MLD is required.

Schott (1902) defined mixed layer depth as the
depth upto the top of the thermocline having a minimum
gradient of 2^OC in 25 m. According to Defant (1961) the
top of the thermocline in the tropical Indian Ocean is
to be fixed at a depth where the average gradient in
temperature is equal to or more than 0.5^OC in 10 m.
For climatological purposes the MLD is defined as the
depth at which the temperature drops by 1 or 1.1^OC from
the surface value (Laevastu and Hela, 1970; Robinson et al.,
1979; Wyrtki, 1971). Wyrtki (1971) proposed two criteria
for MLD and used the average of the two values for
presenting MLD distribution in the Indian Ocean. In the

first method the shallowest 5 m depth interval of the bathythermograph data with a temperature difference of $0.5^{\circ}C$ is located. The depth of intersection of a tangent joining the depths defining the above interval and the vertical from the sea surface temperature (SST) is taken as the MLD. According to the second criterion the mixed layer depth is the depth where $1^{\circ}C$ fall from the surface temperature is observed. Colborn (1975) followed the same criterion for his extensive work on thermal structure of the Indian Ocean.

1.3   Variability of Mixed Layer Depth (MLD)

1.3.1   Diurnal variability

The day time heating of the surface layers increases the negative temperature gradients in the upper layer and results in the decrease of surface layer depth. According to La Fond (1954) the MLD gets capped by transient thermoclines in the afternoon due to heating from 0900 hrs to about 1500 hrs when maximum surface temperature is observed. Following this, the surface layers get cooled owing to a reduction in solar radiation. The convection resulting from cooler and denser surface waters extends to greater depths, destroying the gradients created in the afternoon. The cooling continues in the night making the surface layer isothermal at 0000 hrs. Slight positive gradients are noticed at 0600 hrs in the morning due to a delay in the subsurface cooling. The response of the upper ocean layer to diurnal cycle has also been discussed by

Defant (1961). The shallowing of the layer during day
heating and deepening due to night cooling have been
recently asserted by Woods et al. (1986) Gargett et al.
(1979) and Gregg et al. (1985). Variation of MLD from
this observed diurnal cycle depends on the location,
season and the meteorological conditions. For instance
a change in the diurnal cycle may be induced by stormy
weather and overcast sky.

1.3.2 Seasonal variability

Seasonal variability of MLD shows a similarity
in heating and cooling to that of the diurnal cycle, but
on an extended time scale in the annual cycle. The
surface layer is isothermal and deeper in autumn and
winter when the sea loses heat to the atmosphere, except
in areas near current boundaries. The net heat gain
during spring and summer causes shallow seasonal
thermoclines and lower values of MLD. However, this
pattern of MLD variation in the annual cycle can be
disturbed by several factors. For instance in the North
Indian Ocean, reversing monsoonal winds and currents
and the resulting convergence/divergence patterns change
the annual. variability of MLD. Regional differences in
the coastal upwelling/sinking and net heat transfer also
cause perturbations in the cycle.

Both unimodal and bimodal oscillation of MLD
have been observed in the Arabian Sea. In the bimodal
pattern the mixed layer deepens during winter and shoals

during spring and summer. Late summer cooling deepens
the surface layers again. The secondary warming during
August/September makes the MLD shallower with a subsequent
cooling and deepening towards winter. In the unimodal
oscillations the mid summer deepening is supressed due
to localised coastal phenomena such as surface convergence/
divergence causing upwelling and sinking. In the central
and western Arabian Sea areas bimodal oscillations are
commonly observed in the annual cycle while in the
northeastern and eastern coastal areas a unimodal pattern
is apparent (Sharma, 1968; Colborn, 1975; Narayana Pillai
et al., 1980).

1.4   Factors affecting MLD variability

The factors controlling the MLD can be grouped
under 4 major heads, viz., heat exchange at the surface,
mixing by wind stress and convection, vertical and
horizontal advection resulting in convergence/divergence
and internal oscillations (Laevastu and Hela, 1970). The
variation in intensity of the above processes in time and
space decides the vertical extent of the mixed layer
depth in the oceans. For short periods from a few hours
to a month the vertical one dimensional processes of heat
and momentum transfers at the surface controls the vertical
structure of the temperature and the mixed layer depth
(Niiler and Kraus, 1977). For longer periods of more than
a month to a year or more, horizontal processes due to

advection are equally dominant as the net poleward
transport of heat by currents is to be taken into account
(Pond and Pickard, 1983).

1.4.1 Surface wind stress and waves

The classical work of Ekman (1905) analysed the
influence of wind stress on the surface boundary layer.
Theoretical studies of Rossby and Montgomery (1935)
established the depth of wind mixed layer as a function of
wind speed and latitude. Using this steady state theory,
Lumby (1955) calculated layer depth as a function of
mean wind for 10° squares. Laevastu (1960) obtained an
empirical relationship for turbulent mixing based on
trochoidal characteristics of wave spectrum corresponding
different wind speeds. There are a number of empirical
approaches relating forced mixing to wind and waves
(Neumann, 1955; Mazeika, 1960). Miropolsky (1970) pointed
out the important role of surface wind in supplying the
mechanical energy required for mixing. Pollard and
Millard (1970) and Gonella (1971)demonstrated the effect
of variability of local wind on the dynamics of the marine
upper layer. Increase in layer depth and decrease in
surface temperature was related to high wind speeds and
upward heat flux and conversely decrease in the layer
depth to low wind speed and downward heat flux (Elsberry
and Camp, 1978; Elsberry and Raney, 1978). Prangsma and
Cruseman (1984) observed that the MLD generally responded
to changes in wind speed within a few hours. Longuet-

Higgins and Turner (1974) and Toba et al. (1975) have extended wave theories to the mechanical turbulence at the surface. Turner (1981) relates mixing to the Langmuir Cells produced by wind driven current.

1.4.2 Heat exchange, absorption and convective mixing

Heat exchange between the ocean and the atmosphere changes the surface density and affects the buoyancy fluxes. Kitaigorodskii (1960) proposed a balance between the kinetic energy due to wind stress and the stabilising buoyancy flux at an equilibrium depth. This argument requires MLD to be shallow during heating and deep during cooling. When there is net heat input to the sea surface, an increasing stabilising density gradient inhibits mixing. When there is net cooling at night or in the winter, convection extends to the mixed layer entraining colder waters from below (Foster, 1965; Mc Alister and Mc Leish, 1969; Katsaros et al., 1977). Laevastu (1960) Defant (1961) and James (1966) have formulated methods to calculate the depth of convective mixing from heat loss and density structure. Woods (1980) examined the variation of convection in the mixed layer for diurnal as well as annual cycles.

The surface fluxes of radiation heat and momentum affecting the buoyancy and turbulent mixing have been examined by many workers (Berliand, 1960; Lumb, 1964; Laevastu and Hubert, 1965; James, 1966; Matsuike et al., 1970; Pond, 1971; Budyko, 1974; Smith and Banke, 1975;

The investigation of penetration of solar energy
and the net heat available at the surface must clearly
take into account the properties of absorption and
scattering of sea water. Studies on this aspect both
theoretical and experimental, have been reported by
several authors (Jerlov, 1968; Tyler, 1968; Tyler and
Smith, 1970). The fraction of solar energy absorbed by
the top 5 m   is about 69% for clear water and about
89% for the turbulent water. The vertical thermal
gradient created by the difference in absorption at
different levels and in water types determines the vertical
extent of mechanical and convective mixing due to wind stress
and buoyancy fluxes.

5 Advection and convergence/divergence

The effects of advection and convergence/divergence
have an important influence on MLD (La Fond, 1954;
Laevastu and Hela, 1970). Advection transports heat,
thereby causing changes in the surface layer temperature.
However, density currents in the northern hemisphere
results in deeper surface layers on the right hand side
and shallower on the left hand side (Sverdrup et al., 1947).
The upwelling motion near the coasts induced by convergence/
divergence have been examined by O'Brien and Hurlbert (1972)
and Gill and Clarke (1974) who found correlation between
the movements of thermocline (and the mixed layer) and long
shore wind stress variations. The horizontal convergence/
divergence associated with storm induced inertial rotation

of the currents can lead to significant vertical displacements of the thermocline along the path of storms (Leipper, 1967; O'Brien et al., 1977). Wind stress curl-driven vertical velocity determines the horizontal distribution of MLD, according to De Szoeke (1980). He observed enhancement of deepening in downwelling regions of convergence (negative wind stress curl) and attenuation of deepening or even shallowing in upwelling regions of divergence (positive curl).

1.4.4   Internal oscillations

Internal waves affect the time variation of the mixed layer depth by virtue of the oscillations about the mean position, with periods ranging from Brunt Vaisala to inertial ranges. Internal waves contribute to mixing in the thermal/density fine structure (Munk, 1981). Linden (1975) and Kantha (1977) observed that mixed layer deepening by entrainment of colder water from below was reduced by internal waves radiating energy away from the area.

1.5   Theoretical models of MLD

A number of models have been proposed simulating time variability of MLD. In general these can be classified into the integral or slab models and the differential or multilevel models. Examples of the first class of models are those of Laevastu and Hubert (1965), James (1966), Kraus and Turner (1967), Kitaigorodosky and Miropolsky (1970), Pollard et al. (1973), Denman (1973),

Denman and Miyake (1973), Niiler (1975), Gill and
Turner (1976) and De Szoeke and Rhines (1976). The second
class of models includes those proposed by Mellor and
Durbin (1975), Marchuk et al. (1977), Madsen (1977)
and Kondo et al. (1979).

The integral models are based on the principles
that mechanical turbulence generated by the surface wind
stress changes the potential energy of the temperature
profile by mixing buoyant water down-ward from the surface.
The equations are derived from energy balance considerations
assuming the pre-existence of a homogeneous mixed layer
and ignoring eddy diffusivities. The governing expressions
for slab models are obtained by integrating the equation
for surface exchange of heat and momentum. The second class
of models is based on one dimensional diffusive processes
assuming the upper layer not to be well mixed. A closure
system of turbulence and thermodynamic equations determines
the vertical temperature structure in details.

Both types of models are one dimensional and
neglect advective and horizontal processes. The integral
models are conceptually simple. But the closure schemes
of the differential methods lead to a rigorous
mathematical formulation of the turbulent exchanges. The
second method closely reflects rapid changes in MLD while
the first (integral) method simulates closely persistent
and gradual changes in MLD (Miyakoda and Rosati, 1984).

1.6 Earlier studies on the MLD in the Arabian Sea

In the Arabian Sea earlier works on MLD are mainly on the distributional aspects. Sewell (1929) analysed the properties of temperature and salinity of surface waters in the Arabian Sea and Bay of Bengal. He reported bimodal oscillations with peaks in July and January in the Laccadive area. The variation of MLD and hydrographic parameters in the pre and post-monsoon seasons was studied by various authors (Ramasastry and Myrland, 1959; Patil et al., 1964). Ramamirtham and Jayaraman (1960) reported MLD variations off Cochin while studying the hydrographic features of the area. Hydrographic features in relation to the mixed layer depth characteristics around the Laccadive islands was also reported by Jayaraman et al. (1960) and Patil and Ramamirtham (1962)with a range in variability of 65-80 m in winter. Murty (1964) observed that MLD is low (10-40 m) during southwest monsoon, moderate (20-50 m) during summer and deep (100 m) near the southwest coast of India. He also observed a shoreward sloping of the surface of MLD during summer in this area. Wyrtki (1971) reported shallower MLD (about 20 m) during upwelling season from May to September off Arabia and during July to August off the southwest coast of India. Rao et al. (1963) studied the wind regime of hydrographic characteristics of Gujarat and observed MLD upto 40 m with a weak slope of isotherms northeastward.

MLD values of 65-80 m around Laccadives during
winter were reported by Patil and Ramamirtham (1962).
Shallow MLD (20-30 m) was observed off Gujarat by
Patil et al. (1964). Panikkar and Jayaraman (1966)
analysing the contrast between Arabian Sea and Bay of
Bengal attributed a higher range of MLD in the Arabian
Sea to upwelling. Sharma (1966, 1968) reported upwelling
in spring and summer and sinking in winter in the coastal
waters between Cape Comorin and Mangalore as indicated by
annual oscillations in the thermal structure and
thermocline depth. He attributed the oscillations to the
upwelling and sinking induced mainly by the oceanic currents.
Variability of MLD in the eastern and central Arabian Sea
during southwest monsoon has been related to the
circulatory pattern by Sastry and D'Souza (1970). Colborn
(1975) in his extensive treatment on vertical thermal
structure of north Indian Ocean observed bimodal
oscillations in MLD and temperature with a range of 20-100 m
in the Arabian Sea. Ramesh Babu (1976) ascribed the
deepening of MLD (15 - 40 m) during May-July north of
Bombay due to strong monsoonal wind stress. The MLD
deepening of about 40 m and associated cooling of the
surface temperature during this period (by 2°C) was
reported by Ramam et al. (1979). Rao et al. (1981) and
Ramesh Babu and Sastry (1984) attributed the deepening of
MLD during June-July in the central and eastern Arabian
Sea to heat losses at surface and current shear at the
base of MLD.

In the northeastern Arabian Sea a progressive
reduction in MLD during March was observed by Ramesh
Babu et al. (1980). Varma et al. (1980) and Kesavadas et al.
(1980)associated the deep MLD upto 200 m off Pakistan in
November/December with winter cooling and anticyclonic
eddy structures. Narayana Pillai et al. (1980) observed
the top of thermocline deepest during December-February
and shallowest (surface) during June-September south of
Cochin and October-November north of Cochin. Thicker
mixed layers in the deep waters in comparison to shallow
waters in the Arabian Sea north of Goa was reported by
Qasim (1982).

Considerable study has been made on the influence
of upwelling and sinking on MLD along the Indian coasts
(Banse, 1959, 1968; Sharma, 1966, 1968; Darbyshire, 1967;
Narayana Pillai et al., 1980; Basil Mathew, 1982).

The role of meteorological factors in deciding
the wind stress, energy exchange and heat transfer
processes in the Araiban Sea has been studied in great
detail especially after the Monex programmes.
Wooster et al. (1967) discussed the winds, currents
and temperature in the Arabian Sea based on average
conditions in 2° quadrangles. Ramage et al. (1972) gave
a detailed presentation of the surface climate based on
IIOE data from the Indian Ocean. A detailed survey of
the surface climate, atmospheric circulation and heat

budget in the Arabian Sea and the Indian Ocean have been made by Hastenrath and Lamb (1979). Duing and Leetma (1980)computed the heat budget of the upper layers of the Arabian Sea and attributed the cooling in the western Arabian Sea to the dominant upwelling. The recent works by Ray (1984) and Reddy et al. (1984) on the net heat transfer at the surface and Joseph and Pillai (1986) on air-sea interaction in the Arabian Sea and north Indian Ocean are of interest in this context.

The characteristics of general circulation in the Arabian Sea was discussed in relation to convergence/ divergence by Varadachari and Sharma (1964, 1967). Duing (1970) examined monsoonal influence on the seasonal variation of the currents and MLD in the Arabian Sea and north Indian Ocean. The effect of wind stress curl and the related convergence/divergence zones on MLD in the Arabian Sea was examined by Ramesh Babu and Sastry (1984). Convergence/divergence in relation to upwelling/sinking along the southwest coast of India has been discussed by Basil Mathew (1982).

As regards the effect of internal waves on MLD in the Arabian Sea, there is very little published information (Ramam et al., 1979).

The seasonal and spatial variation of thermal and salinity structure and MLD in relation to oceanographic and marine meteorological parameters in the Arabian Sea is presented in the atlases of U.S. Navy Hydrographic Office

(1960),Deutsches Hydrographisches Institut (1960) and

Koninklijk Nederlands Meteorologisch Institut (1952).

Similar atlases have also been prepared by Wooster et al.

(1967), Wyrtki (1971), Hastenrath and Lamb (1979) and

Robinson et al. (1979). But they are mainly based on

average data from $1^O - 5^O$ quadrangles and finer details

are lost as a result of averaging and sparseness of data

in some areas.

1.7   Description of the study area

Arabian Sea is the oceanic area in the north Indian

Ocean bounded by the Asiatic subcontinent and peninsular

India to the north and east and African continent to the

west, with a southern limit as the latitude of Cape Comorin

$(8^O 15'N)$,though by some definitions the seas around the

Laccadives have been excluded. On the northern and

western sides, the Arabian Sea is connected to Persian

Gulf and Red Sea which exchanges high saline waters with

it. While Indus River discharges dilute the waters in the

northeastern corner, high evaporation rate during much of

the year makes it more saline. On the eastern side the

Indian continental shelf is broader at the southern tip,

narrowing down to about $11^O N$ and again broadens off Gulf

of Cambay and northwards. On the western side the Arabian

shelf is narrower.

The Arabian Sea is greatly influenced by the

reversals in the two major monsoonal wind systems. The low

pressure developing over the Indian subcontinent causes

intense southwesterly winds which flow for longer periods
from May to September in the Arabian Sea. During winter
a high pressure system over the Tibetan region initiates
the northeasterly winds which are weaker over the Arabian
Sea lasting for a shorter duration from December to
January. Regional variations in intensity, direction and
duration of the winds are, however, noticed. Precipitation
is more during southwest monsoon than the northeast monsoon.

The circulation in the Arabian Sea is dominantly
controlled by the wind reversals. As a result during
summer a major anticyclonic system of currents is present.
The system persists for a longer duration (March-September)
intensifying during June-August. Along the western coastal
areas of the Arabian Sea, a western boundary flow is
present between 6° N and 10° N. The northerly coastal
flow in this area during May-October is strong (greater
than 350 cm sec^{-1}) (Duing et al., 1980). Along the
Arabian Coast the easterly/northeasterly currents are
present during this time with average speeds upto
50 cm sec^{-1}. Along the eastern coastal areas southerly
currents with maximum speeds upto 50 cm sec^{-1} are observed
during July-August. In winter a weak cyclonic circulation
system is present from November to January (Deutsches
Hydrographisches Institut , 1960). Along the western
coastal areas off the Arabian coast weak southerly or
variable currents are observed during this period. Reversal
of flow towards north takes place after October and weak
northerly coastal currents are apparent along the west coast

of India from November to January. The winds and currents
during the transitional months of March/April and October/
November are variable and complex.

In rhythm with the semi-annual changes in winds and
currents, Arabian Sea exhibits cyclic characteristics of
upwelling during southwest monsoon and sinking during
northeast monsoon along much of the coastal zone. Regions
of extensive upwelling along the Somali and Arabian coasts
are caused by strong offshore windstress components while
the upwelling observed along the southwest coast of India
is mainly related to the geostrophic flow. The reversals
in the monsoon and current system also influence the surface
heat transfer processes, thermal structure and mixed layer
depth variations, resulting in bimodal annual response.

Warm and cold core eddies are observed along
Somali/Arabian coasts, off Pakistan and Iran coasts and
also in the Indus Cone area (Banse, 1980; Bruce, 1968;
Quraishee, 1984).

For the present study in the Arabian Sea an area
limited between 60° E and 75° E longitudes and 10° N and
25° N latitudes is selected (Fig. 1.1). This area has
been divided into 8 subareas of 5° quadrangles numbered
from 1 to 8 for the purpose of presenting the average
conditions in the annual cycle. Subarea 1 comprises of
the northeastern Arabian Sea areas at the mouth of Gulf of
Oman, off Arabian, Iran and Pakistan coasts bounded between
20° - 25° N and 60°-65° E. Subarea 2 includes the

northeastern Arabian Sea areas in the Indus Cone,

off Kutch and Porbandhar of the Gujarat coast limited

between $20^{\circ} - 25^{\circ}$ N and $65^{\circ} - 70^{\circ}$ E. Subarea 3 is on

the western side of the central Arabian Sea between

$15^{\circ} - 20^{\circ}$ N and $60^{\circ} - 65^{\circ}$ E. Subarea 4 belongs to the

eastern side of the central Arabian Sea within $15^{\circ}-20^{\circ}$

and $65^{\circ}-70^{\circ}$E. The offshore and coastal areas of Bombay,

Ratnagiri and Goa come under subarea 5. Subarea 6 is

at the southwestern edge of the study area between $10^{\circ}-15^{\circ}$ N

and $60^{\circ}-65^{\circ}$ E. Southeastern part of the central Arabian

sea bounded between $10^{\circ}-15^{\circ}$ N and $65^{\circ}-70^{\circ}$ E is included in

subarea 7. Areas around Laccadive islands and offshore/

coastal zone off the southwest coast of India from

Mangalore to Cochin limited between $10^{\circ}-15^{\circ}$ N and $70^{\circ}-75^{\circ}$ E

are included in subarea 8.

This area has been slightly exceeded to the west

for including the entire data set of Oceanographic Naval

Expedition - OCEANAVEX (1973-74) in presenting seasonal

variations of MLD and the related parameters during

winter and premonsoon (Fig. 1.2).

1.8   Scope of the present study

Studies on MLD in the Arabian Sea have been mostly

confined to the distributional aspects with little work

done to correlate with the controlling parameters. These

studies have been, in most cases, the offshoots of

hydrographic studies in the area. The present work aims

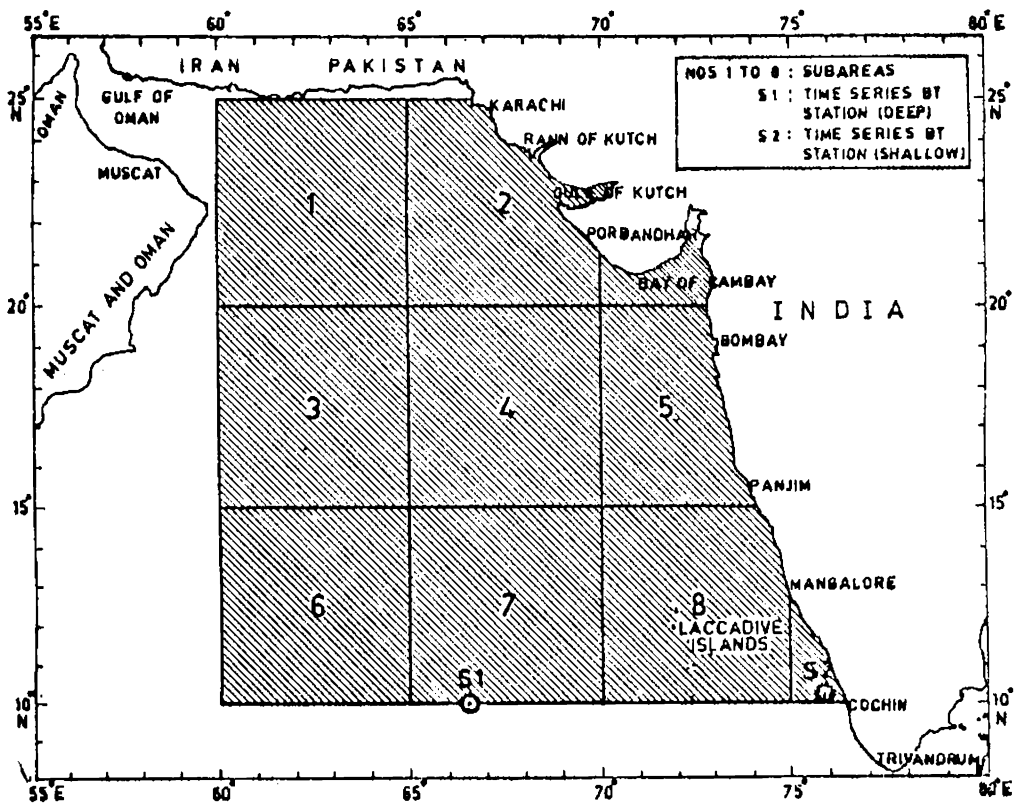to analyse in depth the time variation of MLD in
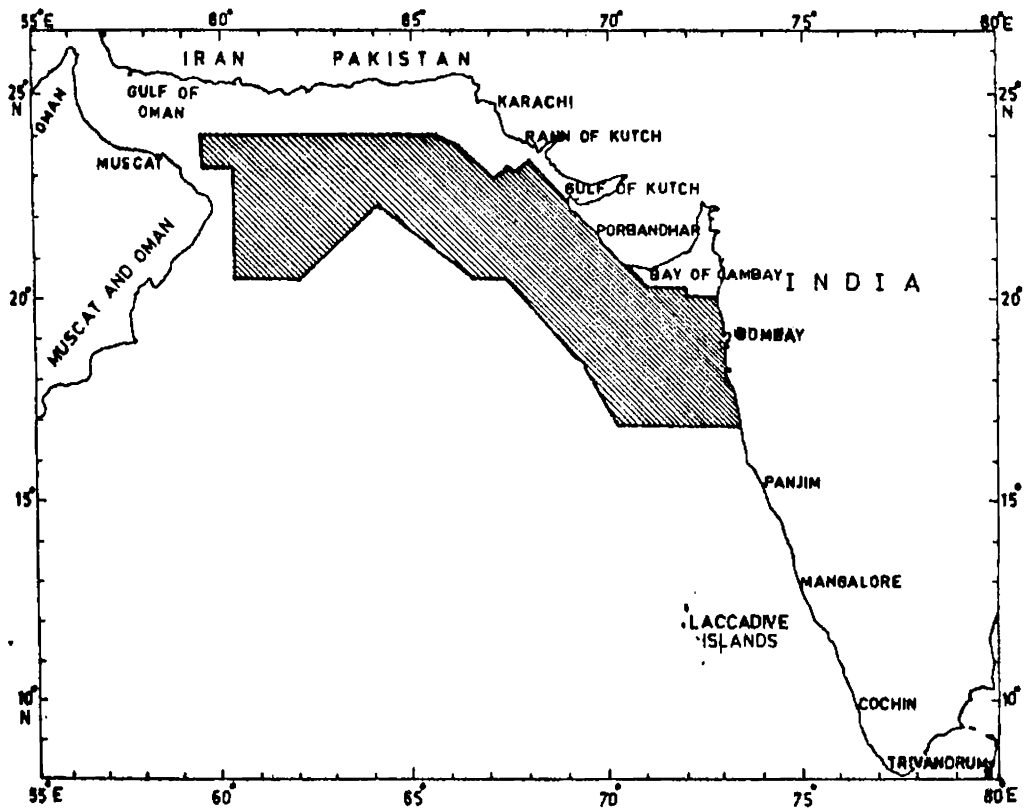
FIG.1.1 AREA OF STUDY

FIG.1.2 AREA OF OBSERVATIONS IN THE NORTHERN ARABIAN SEA
DURING - OCEANAVEX (1973-74)

representative oceanic domains in the Arabian Sea, in relation to the variations in the primary controlling factors, viz., the surface wind field, net heat transfer, sea surface temperature (SST) and the resulting mechanical and convective mixing. The corresponding changes in the annual cycle of surface currents (advection) and surface divergence are examined with reference to upwelling and sinking motions of MLD in the annual cycle. The importance of internal waves on the variation of MLD is examined in a limited manner using a sample data set from deep oceanic station only.

To analyse the meridional distribution of MLD , variation along 60° E, 65° E, 70° E and 75° E lontigudes is examined. A comparison of the two seasonal regimes corresponding to winter and premonsoon conditions in the northern Arabian Sea is presented with corresponding changes in surface wind speed and sea surface temperature for the area.

A simple one dimensional model for prediction of MLD is applied for short durations ranging from 3 - 6 hrs and the results are compared with the observed MLD characteristics at two stations, one representing oceanic deep water conditions and other representing coastal shallow water conditions in the Arabian Sea.

1.9   Data inputs

The data sets used for the study have come from various sources. Table 1.1 gives the details of the data,

TABLE - 1.1

DETAILS OF DATA UTILISED FOR THE STUDY

S.No.	Parameter/ observation	Area/ position(s)	Source of data	No. of stations/ data	Period of data/obser vation
1	2	3	4	5	6
1.	Surface wind speed/ direction	$60^{\circ}E-75^{\circ}E$, $10^{\circ}N-25^{\circ}N$	Hastenrath and Lamb (1979)	3072 values of 1° quadr- angles for 12 months	1911-70
2.	Net heat transfer	-do-	-do-	-do-	-do-
3.	Sea surface temperature	-do-	-do-	-do-	-do-
4.	Surface current	-do-	Wooster et al. (1967)	768 values of 2° quadr- angles for 12 months	-do-
5.	Mixed layer depth	-do-	Robinson et al. (1979)	3072 values of 1° quadr- angles for 12 months	1853-1967
6.	Average temperature difference from surface 120 m (T_0-T_{120})	-do-	-do-	-do-	-do-

TABLE - 1.1. (Contd)

1	2	3	4	5	6
7.	BT data (space)	Northern Arabian Sea	INS DARSHAK-OCEANAVEX (1973-74) NPOL Data Base	665	23 December 1973 to 12 May 1974
8.	Surface wind speed	-do-	-do-	-do-	-do-
9.	Sea surface temperature	-do-	-do-	-do-	-do-
10.	Time series BT and salinity data (200 m)	S1 ($10^o30'N$, 66^oE and 4360 m depth)	R.V.PRILIV (Monsoon-1977) NPOL Data Base	92 obser-vations each (3 hourly)	7-19 June 1977
11.	Time series BT and salinity data	S2 ($10^o15'N$, $75^o48'E$ and 200 m depth)	M.V.PRASIKSHANI NPOL Data Base	21 obser-vations each (hourly)	19 January 1983.

their source and the purposes for which they are used.
Data on surface wind field, net heat transfer and sea
surface temperature are derived from the atlas of
Hastenrath and Lamb (1979). 1^O quadrangle mean values of
the parameters for every month have been digitised from
the monthly distribution charts and averaged to obtain
monthly means for the 8 subareas. The MLD criterion
selected for this analysis is that of 1.1^O C difference
from the surface and it tallies well with the data of
Robinson et al. (1979). MLD and the difference in
temperature from surface to a depth of 120 m $(T_O - T_{120})$
have been derived from this atlas.

The surface currents (advection) for the subareas
have been derived from the mean surface current values
available for 2^O quadrangles in the Arabian Sea area
presented in the Atlas of Wooster et al. (1967).

The bathythermograph (BT) data set collected from
665 stations in the northern Arabian Sea during OCEANAVEX
(1973-74) along with supplementary surface meteorological
data (India Meteorological Department, 1975) including wind
and SST was used for the presentation of surface wind speed,
sea surface temperature and MLD distributions during winter
and premonsoon regimes.

The time series data set of thermal and salinity
structures upto 200 m used for presenting predictive
characteristics of MLD at the deep station, S1 ($10^O30'N$,
66° E and 2000 m depth) relates to 'Monsoon - 77' BT
and hydrographic observations during 7 - 19 June, 1977

(92 observations) on board R.V. PRILIV. At the shallow
station S2 (10°15' N, 75°48' E and 200 m depth) time series
BT and salinity data collected on board MV PRASIKSHANI
on 19 January 1983 (21 observations each)were used. In
both cases the supplementary data on wind, cloudiness, air
and SST were also utilised. The long time series BT data
at S1 has also formed the basis for spectrum analysis (FFT)
of MLD oscillations (64 observations) due to internal waves.

1.10   Data quality and density

Data base for the atlas of Hastenrath and Lamb (1979)
is the National Climatic Centre's Tape Data Facility
(TDF-11) consisting of 4.5 million data for the entire
Indian Ocean received during 1911-70. TDF-11 deck was
compiled from ship logs, weather reports and data from
buoys and several meteorological agencies in the Indian
Ocean. The National Climatic Centre (1968) indicates that
the data are quality controlled. The data density indicated
for the Arabian Sea on the Atlas is 100-5000 observations
per 1° quadrangle. For the derived data on net heat
transfer available from this atlas, relative and absolute
errors of less than 10 and more than 20% are reported.

The surface current data derived from the atlas of
Wooster et al. (1967) is based on the KNMI Atlas
(Koninklijk Nederlands Meterologisch Institut, 1952) which
has presented average currents in 2° quadrangles. The
direction is reported to be nearest 45° and speeds in 0-5,
6-20, 21-35, 36-50, 51-65, 66-80 and greater than 80 cm sec^{-1}

ranges. The data density in many quadrangles especially
in the coastal zones in the Arabian Sea is indicated to
be between 0-5 or less per month. This may affect
seriously the mean values of currents and surface
divergence.

Data on MLD and T_0-T_{120} (Table 1.2)from the atlas
of Robinson et al. (1979) is based on BT and hydrographic
observations available with U.S. National Weather Records
Centre Marine Deck (1853-1966) and with Wyrtki's Indian
Ocean Data Tape (1930-1967). Majority of this data are
quality controlled and processed by Woods Hole Oceanographic
Institution and Scripp's Institute of Oceanography, U.S.A.

In all the above cases an over all personal error
of digitisation to a maximum of 2% is to be added on the
final data taken for this analysis. The time series/space
BT data have been digitised at 5 m intervals after applying
corrections with respect to the SST values. Salinity data
from time series hydrographic observations were linearly
interpolated to read the corresponding 5 m values for
computing densities.

1.11   Methodology of computations, data analysis and
        presentation

1.11.1 Wind (mechanical) and convective mixing depth

Computation of depths of wind mixing and convective
mixing is made using equations of Laevastu and Hubert
(1965), James (1966) and Darbyshire (1959). The mechanical
mixing due to wind/wave turbulence is obtained by

$$D_M = 12.5 \ H_S \qquad \dots \qquad (1.1)$$

where D_M = depth of mixing in metres

H_S = significant wave height in metres.

The significant wave height is calculated using the relationship of Darbyshire (1959).

$$H_S = 0.027 \ W^2 \qquad \dots \qquad (1.2)$$

where W = wind speed in knots.

The depth of convective mixing is calculated using an equation (after James, 1966),

$$D_C = \left(D_0^{\ 2} + \frac{2 \ Q_L}{C_p \rho \Delta T} \right)^{\frac{1}{2}} \qquad \dots \qquad (1.3)$$

where D_C = convective mixing in metres

D_0 = initial MLD in metres

Q_L = average net heat loss for the month

C_p = specific heat of sea water at constant pressure (taken as 1.023 cal g^{-1} $°C^{-1}$)

ρ = average density of the surface layers (taken as 1.023 g cm^{-3})

ΔT = average temperature difference in degree C at the bottom of the initial MLD for a depth interval of 30 m.

The average temperature difference for 30 m below MLD is computed for the 8 subareas as follows. With an assumption of uniform temperature in the MLD, the difference in temperature from surface to a depth of 120 m $(T_0 - T_{120})$ values digitised is equal to the difference in temperature from the bottom of MLD to 120 m. Thus the difference in temperature for 30 m depth interval below the MLD is

calculated as,

$$T = \frac{30 \ (T_0 - T_{120})}{(120 - L)} \qquad \dots \qquad (1.4)$$

where L = MLD in metres.

The average values of $T_0 - T_{120}$ for the 8 subareas derived from Robinson, et al. are presented in Table 1.2.

The initial values of average wind speed, MLD and temperature difference below MLD for 30 m depth interval are used to arrive at the final mixing values for the next month assuming a period of forcing of 30 days from the middle of the month. This assumption is adopted for the use with average monthly temperature value in the annual cycle.

1.11.2 Surface current divergence

The surface current divergence is calculated using an equation after Laevastu and Hubert (1965),

$$- \frac{\partial W}{\partial Z} = \frac{\partial U}{\partial X} + \frac{\partial V}{\partial Y} \qquad \dots \dots \qquad (1.5)$$

where U, V and W = components of surface currents

$(cm \ sec^{-1})$ in east-west, north-south

and vertical directions.

Positive values of the sum of terms on the right hand side will imply divergence at the surface or upwelling motion. The negative values of the sum will indicate convergence at the surface or sinking motion. The convergence/divergence values are expressed in units of $5 \times 10^{-8} \ sec^{-1}$.

TABLE 1.2

AVERAGE MONTHLY VALUES OF T_0-T_{120} FOR THE SUBAREAS

OF STUDY DERIVED FROM ROBINSON et al. (1979) IN
DEGREE CENTIGRADE

Sub-area	Jan	Feb	Mar	Apr	May	Jun	Jul	Aug	Sep	Oct	Nov	Dec
1	4.2	2.8	3.5	5.8	7.5	8.8	8.3	7.8	7.8	8.0	7.5	5.8
2	2.8	2.0	2.3	3.5	6.0	7.0	7.0	6.8	6.3	6.3	6.0	4.8
3	3.5	4.5	5.8	5.5	6.6	6.8	6.1	5.0	6.0	7.3	7.0	5.3
4	6.5	4.8	6.3	5.8	6.3	6.8	7.3	6.5	6.5	6.9	5.6	6.6
5	6.0	4.0	4.5	5.8	6.5	8.8	9.0	8.0	7.5	8.3	7.8	8.7
6	4.3	5.8	6.5	7.8	7.8	7.8	5.0	3.0	3.5	5.5	8.0	6.8
7	6.0	7.0	6.3	6.8	7.8	7.3	6.3	6.0	5.8	7.1	9.8	9.5
8	7.5	5.2	5.0	6.8	5.3	5.8	9.0	8.8	9.0	9.3	9.0	8.3

1.11.3 Internal waves

The analysis for obtaining amplitudes and periods
of the harmonics in the spectrum of MLD oscillations is
made using standard Fast Fourier Transform (FFT) methods
(Jenkins and Watts, 1968). MLD data from the deep station
S1 is sampled following the power law 2^n where n is an
integer. The sample strength is 64 observations at
3 hourly intervals. The data is smoothed with a "Hanning
window" and the spectral estimates are obtained. The
values are normalised with respect to the predominant
amplitude.

1.11.4 Data averages for subareas

1° quadrangle values of each parameter are averaged
over 5° quadrangles (subareas) for each month. The
annual variation is presented for surface wind speed
(knot), surface wind direction (degree), net heat
gain (Watt per sq.metre), sea surface temperature
(degree centigrade), mechanical mixing (metre), convective
mixing (metre), MLD (metre), surface current speed
(centimetre per second), surface current direction (degree),
east-west current component (centimetre per second),
north-south current component (centimetre per second) and
surface current divergence (5 x 10^{-8} sec^{-1}).

1.11.5 Presentation of time-space variability of MLD

The MLD distribution is also presented in
latitude-time diagrams along 4 longitudes namely 60^oE,
65^oE, 70^oE and 75^oE for representing simultaneous time/space

variability in the annual cycle. For doing this the values of MLD for 1° quadrangles adjacent to the longitude are averaged to represent the mean values along that longitude.

Similarly the surface wind speed, SST and MLD values analysed from the OCEANAVEX data were grouped under two seasons namely winter (December, January and February) and premonsoon (March, April and May). The MLD values are analysed, in this case, following the criterion of Wyrtki(1971). The seasonal data were grouped in half degree quadrangles and averaged to smooth out the diurnal influences on the data to the extent possible. The average values thus obtained are plotted and isopleths are drawn. For representing space sections of MLD, the diagonal sections were represented by the half degree quadrangle averages along the section. For sections parallel to the longitudes and latitudes half degree quadrangle averages lying opposite and adjacent to the latitude or longitude of the section were averaged to represent mid values to fall on the latitude or longitude of the section.

1.11.6 MLD prediction and evaluation

MLD and associated SST have been predicted using methods of Laevastu and Hubert (1965) and James (1966). The MLD values used as input, observed and predicted have been analysed using average criterion of Wyrtki (1971) discussed earlier. For the sake of preserving the continuity of the prediction scheme and routine,

details of analysis are presented in chapter V. The heat transfer units reported in chapter V is in cal cm^{-2} min^{-1} and cal cm^{-2} hr^{-1}. This is mainly because of the series of equations used in the scheme requiring this version for integration of heat energy values in terms of calories received for the duration of forecast. Hence, the difference of units presented for the annual variation and the prediction models are retained.

1.11.7 Data handling, computations and plots

Handling of data except that of OCEANAVEX, computations and original plots were done on PDP 11/60 computer system using standard Fortran programs.

CHAPTER II

CHAPTER II

SECTION I

VARIABILITY OF SURFACE WIND FIELD, NET HEAT GAIN AND SEA SURFACE TEMPERATURE

A major factor influencing the mixed layer depth (MLD) is the wind stress acting on the sea surface. The wind blowing over the sea produces waves, which in turn results in the turbulent mixing and drift currents. The mixed layer results from the combined action of wave mixing and wave current - turbulence induced by the surface wind field and its depth has been computed from wind distribution data by Lumby (1955).

Heat exchange between the atmosphere and the ocean surface is related to convective mixing in the upper layers and affects the MLD. The variation of solar radiation affects the annual/diurnal cycle of air and sea surface temperatures, cloudiness and the pressure and wind fields directly or indirectly. The effects of these parameters on the sea surface conditions and the reflectance characteristics, in turn, influence the other heat budget components such as net long wave radiation (back radiation), latent heat flux (evaporation-condensation) and sensible heat transfer.

Changes in the net heat transfer and the convective processes in the surface layer influence the MLD reflecting in changes of sea surface temperature (SST). An increase

in SST results generally in the shoaling of MLD, and a decrease in deepening it (Davis et al., 1981; Halpern,1983).

In this section annual variation of wind speed, direction, net heat gain and SST in respect of the 8 subareas of study is examined and discussed with respect to Figs. 2.1 to 2.8.

2.1.1 Subarea 1 (Fig. 2.1)

2.1.1.1 Surface wind field (Figs. 2.1 a & b)

A unimodal structure in the annual variation can be seen for the wind speed in the subarea (Fig.2.1 a) with a maximum of 8 kts in July during the southwest monsoon and low values (1.7 kts) in February during the northeast monsoon. The predominant wind direction in the subarea is southwesterly from April to August and northeasterly from December to January. Northwesterly winds are active during spring transition.

2.1.1.2 Net heat gain (Fig. 2.1 c)

The annual variation pattern of net heat gain shows double maxima in the subarea. A net heat gain from February to June is followed by cooling in July, heating in August-September and cooling again in December-January.   Heating maxima are in May (123 W m^{-2})and in September (58 W m^{-2}), whereas the minima (cooling) are in December/January (-40 W m^{-2}) and in July (-13 W m^{-2}).

The spring and summer heating can be attributed to reducedcloudiness and increased solar radiation.   The

mid-summer cooling in July can be attributed to the southwest monsoonal wind regime causing upwelling along Arabian coasts (Colborn, 1975) and cold advection enhanced by a decrease in incoming solar radiation as a result of increased cloudiness. The wind induced upwelling and the resulting cold advection reduces the sea-air temperature differences to zero and even changes sign during August thereby suppressing latent heat flux to the atmosphere (Hastenrath and Lamb, 1979). This explains a secondary maximum in the net heat gain in September.

2.1.1.3   Sea surface temperature (Fig. 2.1 d)

The annual variation in SST for the subarea is also bimodal with a maximum of $28.8^\circ C$ in May and a secondary maximum of $27.5^\circ C$ in October and a minimum of $24.5^\circ C$ in January/February and $27.5^\circ C$ in August. The SST pattern shows a close correlation to the net heat gain pattern with a lag of about 1 month. The increase in surface temperature is delayed upto October as a result of advection and upwelling (Colborn, 1975). The annual range of SST variation is about $3.4^\circ C$.

2.1.2   Subarea 2 (Fig. 2.2)

2.1.2.1   Surface wind field (Figs. 2.2 a & b)

A unimodal annual pattern of wind speed variation similar to that of subarea 1 is observed in this case with maximum speed upto 9 kts in July and minimum speed of 2.4 kts in February. Persistent increase in wind speeds

from February to July and then a decrease to October is

followed by a slight increase in December/January

(3.2-3.4 kts). The wind direction is mainly southwesterly

during May to September and the longest of the annual cycle

for the subarea. Northwesterly winds are observed in

October and spring transition while northeasterly winds are

prevalent during December/January.

2.1.2.2 Net heat gain (Fig. 2.2 c)

The net heat transfer in subarea 2 is positive from

February to June with a maximum of 120 W m^{-2} in April as a

result of spring and summer heating. Mid-summer cooling

is evident in July with values of heat loss upto about

-30 W m^{-2}. The delay in cooling in the subarea compared

to the central and southern Arabian Sea areas has been

confirmed by Privett (1959) and Wooster et al. (1967). The

net heat transfer changes sign in August mainly due to the

reduction in evaporative heat loss and reaches a secondary

maximum of 57 W m^{-2} in September. Cooling starts from

October leading to net heat loss maximum of -40 W m^{-2} in

December/January. Colborn (1975) observed that both

reduced surface heat transfer and localised upwelling are

responsible for the winter cooling of this area.

2.1.2.3 Sea surface temperature (Fig. 2.2 d)

The SST variation is bimodal with maximum (29.1^{o}C)

in June and secondary maximum (28°C) in October and minima

in January (23.4^{o}C) and September (27°C) showing a response

lag of 2 months to the annual heating cycle. The annual

range of SST variation is about 6°C for the subarea.

2.1.3   Subarea 3 (Fig. 2.3)

This area is under the major influence of the changing surface circulation and gyres in the central Arabian Sea, with strongest and most consistent currents developing towards east during southwest monsoon and weaker westerly drifts during northeast monsoon.

2.1.3.1 Surface wind field (Figs. 2.3 a & b)

The surface wind speeds in the subarea are maximum upto 13 kts in July during southwest monsoon regime. The speeds decrease to a minimum in November (1.6 kts) reaching a winter maximum of 5 kts in December. The transition periods during March/April/October are characterised by minimum wind speeds ranging from 1.7 kts in April to 1.6 kts in October (lowest). The southwest monsoon regime is indicated to be predominant by magnitude and persistent with a duration of 5 months from May to September. From November to February/March, northeasterly winds with comparatively weaker magnitudes prevail. Northwesterly winds are transitional from both southwest to northeast monsoon regimes and vice versa especially during August and October.

2.1.3.2 Net heat gain (Fig. 2.3 c)

The annual cycle of net heat gain in the subarea is bimodal with heating (positive) during February-April and during August-September. Cooling is active during June/July and October-January. Maximum heating occurs

during April (about 117 W m^{-2}) and is followed by a decrease in heating due to change in sign of heat transfer in June. Progressive cooling takes place upto July when an annual maximum of cooling rate(about -48 W m^{-2}) is observed. Reversal of sign of the net heat transfer takes place in August and September mainly due to the supression of latent heat loss as a result of strong negative sea-air temperature difference (Hastenrath and Lamb, 1979). In September, the secondary maximum heating takes place (about 47 W m^{-2}). Cooling starts from October reaching a secondary maximum (-40 W m^{-2})in December which persists upto January. Reduction in the net radiation due to the annual march of sun during winter causes cooling after October (Colborn, 1975).

2.1.3.3 Sea surface temperature (Fig. 2.3 d)

The SST variation shows bimodal oscillation with high values in March and April and low values in February and August with an average delay of 1 month in response to the annual cycle of net heat gain. Winter minimum of 24.9^{o}C in February is followed by spring heating from March through May reaching the annual maximum of 29°C at the end of this period. The mid summer cooling due to cold advection and the net heat loss during June-July results in the secondary minimum of 25.9^{o}C in August. Following heating during September results in the secondary maximum of 27.5^{o}C in October. The SST falls from November through January to the winter minimum in February. The annual range in variation of SST for the subarea is about 4°C.

2.1.4   Subarea 4 (Fig. 2.4)

As in the case of subarea 3 this subarea is also
influenced by the two monsoons causing changes in the
major oceanic circulation gyres from cyclonic to anticyclonic
and vice versa.

2.1.4.1   Surface wind field (Figs. 2.4 a & b)

The surface wind speeds are strongest during July
under the influence of the southwest monsoon and weakest
during spring and fall. The highest wind speeds are found
in July with a value of 11 kts. The summer monsoonal force
decreases to a secondary minimum of 2.6 kts in October.
The wind force increases during winter to a high value of
4.4 kts in December and the same speed persists upto
January during the northeast monsoon. This is followed by
the weakening of wind speed during February to May while
southwest monsoonal winds are predominant during May to
September. Northeast monsoon is active from November to
February. Transitional north/northwesterly winds are
present during March, April and October.

2.1.4.2   Net heat gain (Fig. 2.4 c)

The net oceanic heat transfer distribution in the
annual cycle for the subarea exhibits bimodal characteristics
with a first maximum heating occuring during April(95 W m^{-2})
and a second maximum in September (44 W m^{-2}). First
maximum of cooling is observed during July (-25 W m^{-2}) and
second maximum in December (about -8 W m^{-2}). The maxima
in heating during April and September are mainly due to

the increase in net solar radiation corresponding to the
annual march of the sun (Colon, 1964) and low evaporation
(Colborn, 1975). The heating season starts from February
to May during spring and summer seasons and is followed by
the mid-summer cooling in June and July mainly due to the
combined effect of reduction of net solar radiation with
increased cloudiness enhanced by maximum latent heat flux
during the period of southwest monsoon (Hastenrath and Lamb,
1979). The change in vapour pressure gradient from sea to
air reduces the evaporative loss during August/September.
The resulting increase in net heating is augmented also
by an increase in solar radiation by the reduction in
cloudiness. From December to January the winter cooling is
active mainly due to the maximum reduction in the net
radiation during the annual march of the sun.

2.1.4.3 Sea surface temperature (Fig. 2.4 d)

The SST variation in the subarea is very much
similar to that of subarea 3 and bimodal in pattern, with
a response delay of 1-2 months behind the annual heating
cycle. The annual maximum sea surface temperature in May/
June is $29^{\circ}C$ followed by a decrease upto $27^{\circ}C$ due to the
mid-summer cooling. The secondary increase of $28^{\circ}C$ occurs
in November. The SST progressively decreases thereafter
to the winter minimum of $26^{\circ}C$ in January. The subarea has an
annual range of about $3^{\circ}C$ in the surface temperature
variation.
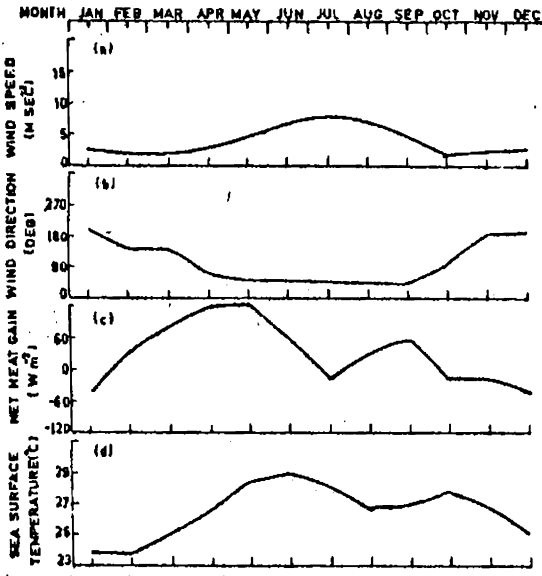
FIG. 2.1 ANNUAL CYCLE OF (a) WIND SPEED (b) WIND DIRECTION
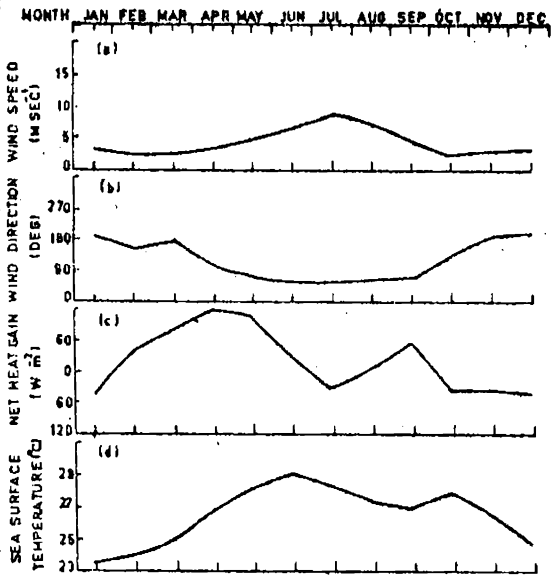(c) NET HEAT GAIN AND (d) SEA SURFACE TEMPERATURE
(SUBAREA-1)

FIG. 2.2 ANNUAL CYCLE OF (a) WIND SPEED (b) WIND DIRECTION
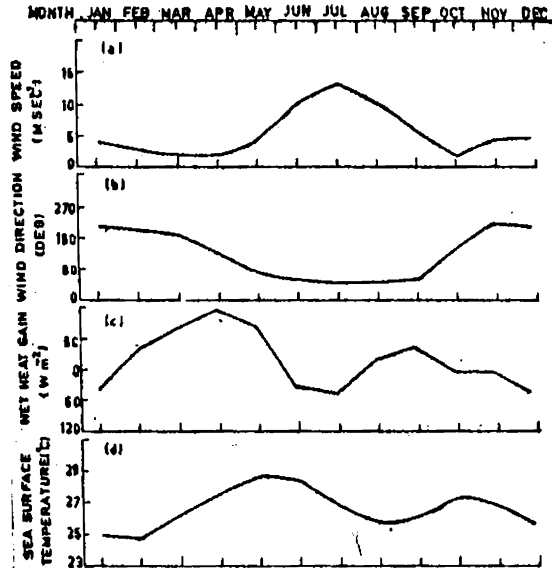(c) NET HEAT GAIN AND (d) SEA SURFACE TEMPERATURE
(SUBAREA-2)

FIG. 2.3 ANNUAL CYCLE OF (a) WIND SPEED (b) WIND DIRECTION
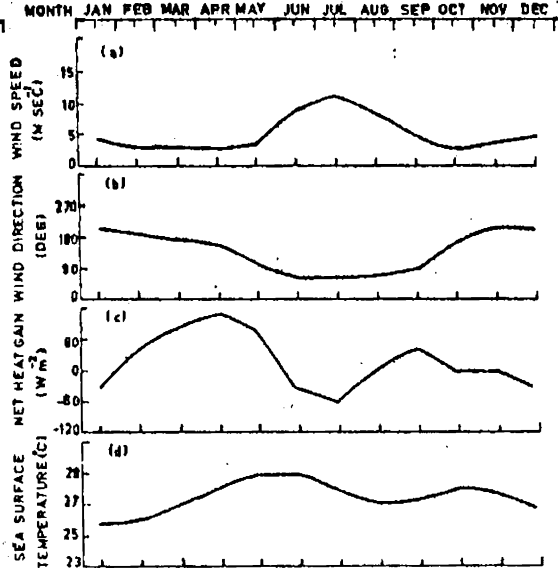(c) NET HEAT GAIN AND (d) SEA SURFACE TEMPERATURE
(SUBAREA-3)

FIG. 2.4 ANNUAL CYCLE OF (a) WIND SPEED (b) WIND DIRECTION
(c) NET HEAT GAIN AND (d) SEA SURFACE TEMPERATURE
(SUBAREA-4)

2.1.5   Subarea 5 (Fig 2.5)

2.1.5.1 Surface wind field (Figs. 2.5 a & b)

The annual variation of surface wind speed shows
peak values during southwest monsoon and weak during
October transition period from southwest to northeast
monsoon regime. The intensity of northeasterly winds are
much less compared to those during southwest monsoon,
showing the dominance of the latter over the eastern
coastal regions of the Arabian Sea. The winter speeds of
about 4 kts persist or decrease through the spring season
rising again to peak in July (about 9 kts). The wind speeds
decrease to a minimum of about 2 kts in October. From
November/December wind speeds increase gradually to a value
of about 4 kts in January. The wind direction is
predominantly southwesterly from June to September in the
subarea. Northeasterly winds are active during November
to January. The weak and variable winds from February to
May and in October are mostly northwesterly in direction.

2.1.5.2 The net heat gain (Fig. 2.5 c)

Bimodality in the annual cycle of net oceanic
heat gain is exhibited in subarea 5. The net heating is
positive from February to May corresponding to the spring
and summer heating followed by cooling mainly due to the
excess evaporation losses and reduction in radiation from
increased cloudiness. Upwelling (vertical advection)is
also accountable for cooling in the subarea by June/July
(Narayana Pillai et al., 1980). The mid-summer cooling

is followed by heating from August to November as a

result of decrease in the latent heat loss by reversal of

vapour pressure gradient during late southwest monsoon.

Annual maximum of heating is about 95 W m^{-2} in April and

the maximum of cooling is about -25 W m^{-2} in July. This

is followed by a secondary maximum heating of about

44 W m^{-2} in September with a decrease in heating towards

November. Maximum winter cooling of about -8 W m^{-2} is

observed in December and the cooling persists through

January due to the reduction in solar radiation.

2.1.5.3 Sea surface temperature (Fig. 2.5 d)

The annual cycle of SST in the subarea is bimodal

with a lag of 1-2 months with respect to the net heat gain.

Maximum value of 29° C is observed during July. The

mid-summer cooling after July decreases SST to a secondary

minimum of $27^{o}C$ in September which is partly due to the

reduction in net radiation by increased cloudiness and

latent heat flux (Hastenrath and Lamb, 1979). The cooling

is also due to the result of upwelling off the coast of

Karwar and Ratnagiri (Narayana Pillai et al., 1980). The

secondary maximum sea temperatures at the surface are

observed in October (about $28^{o}C$). SST decreases to a

minimum of 26° C in January/February. Spring heating

results in the progressive rise of SST towards a maximum

in June. The annual range of the SST in the subarea is

about 3° C.

2.1.6   Subarea 6 (Fig. 2.6)

2.1.6.1   The surface wind field (Figs. 2.6 a & b)

The variation of surface wind field in this subarea shows higher speeds during southwest monsoon from May to September with a maximum of more than 12 kts in July. Intensity of wind force decreases from August to a low value of less than 3 kts in October and gradually increases thereafter to a winter maximum speed of 5 kts in December/ January. The wind speed gradually decreases to the annual minimum in April (about 2 kts). The mean sea surface winds in this subarea is predominantly northeasterly from November to February, persisting upto April. The strongest southwesterly winds are active from May to September. Transitional months of May and December are characterised by the presence of westerly and northwesterly winds respectively.

2.1.6.2   Net heat gain (Fig. 2.6 c)

The annual variation in the net oceanic heat gain is characterised by pronounced bimodal heating and cooling as in the case with the majority of Arabian Sea areas (Colborn, 1975).Heating starts by February and increases during spring and a maximum of 106 W m^{-2} is reached in April. The following mid-summer cooling in June/July due to increase in evaporation and decrease in incident radiation has a maximum value of -60 W m^{-2} in June. Cooling is reduced in July with a change of sign in heat transfer by August. As a result of the reduction in evaporation and increase in incident radiation by reduced cloudiness

(Hastenrath and Lamb, 1979) secondary heating continues upto November with maximum of 60 W m^{-2} in September. Reduction in intensity of solar radiation from November causes cooling with a maximum of -32 W m^{-2} in December and January.

2.1.6.3 Sea surface temperature (Fig. 2.6 d)

SST in the subarea varies in a similar manner to the neighbouring areas, in the central Arabian Sea. The double oscillations in the SST variation lags generally behind the heat transfer oscillations by one month. The surface temperature decreases to the maximum (26° C) in January/February which is also supported by the earlier observations of Colborn (1975). The spring heating causes the surface water temperature to rise to a maximum of 29°C in May followed by the mid-summer cooling causing the water temperature to lower upto a secondary minimum of 26.1° C. Apart from the net cooling acting to lower the temperature of surface waters, advection of colder upwelled waters from coastal regions of Somalia and Arabia might enhance the lowering of the SST during southwest monsoon. This has been earlier indicated by Saha (1974). The secondary warming from August results in the rise of surface temperature from September reaching a secondary peak in October (27.4° C). The temperature of the surface waters decreases to the winter minimum from November.

2.1.7 Subarea 7 (Fig. 2.7)

2.1.7.1 Surface wind field (Figs. 2.7 a & b)

Strong winds are present during June to September under southwest monsoonal regime in the subarea with a

maximum of 10 kts in July. The mean winds decrease to a minimum speed of about 3 kts in October/November. The winter speeds are a little over 4 kts during December and January. Fairly low wind speeds prevail from February to May with magnitudes ranging from 2 to 3 kts. The wind directions in the subarea show a symmetry of both southwest and northeast monsoon in the annual cycle spreading over equal periods separated by transitional months of May and October with Northwesterly winds.

2.1.7.2 Net heat gain (Fig. 2.7 c)

The annual variation of net oceanic heat gain is double moded with heating periods limited between February-May and August-November. Cooling takes place during June/July and December/January. The annual heating initiated in February is mainly the result of increased net radiation under reduced cloudiness with reduction in latent heat flux (Hastenrath and Lamb, 1979). Influence of these favourable factors for heating increases from March to May with a maximum heating of more than 86 W m^{-2} occurring during April. The mid-summer cooling due to increased evaporation and cloudiness - induced reduction in radiation results in the maximum cooling of about -60 W m^{-2} in June. The net heat transfer is positive (heating) again from August to ·November. This change in sign of the heat transfer is the result of surface cooling in June/July reversing the sea-air temperature difference. The annual reduction in the solar radiation causes net transfer to become negative from December with a maximum cooling (about -15 W m^{-2}) in January.

As in the case of coastal subarea 5 the cooling in winter is very much less (4 to 5 orders less) than the mid summer cooling. This effect may be due to the coastal influence.

2.1.7.3 Sea surface temperature (Fig. 2.7 d)

SST variation in the subarea exhibits a bimodal pattern with a delay in response to the annual heating cycle of one month. SST shows an increase from $27.1^{\circ}C$ in February to March when a maximum temperature of 29° C is observed. The surface temperature lowers following the mid-summer cooling to a minimum of 27.2° C in August/ September. The secondary warming period from August results in increase of sea surface temperature upto November with a secondary maximum of $27.9^{\circ}C$. The winter cooling reduces the surface temperature to an annual minimum of 26.9° C. The months of maximum and minimum surface temperature coincide with those of maximum and minimum mixed layer depths (Fig. 2.10). A similar observation has been made by Colborn (1975) for this area. The annual range of SST in the subarea is 2.1° C.

2.1.8 Subarea 8 (Fig. 2.8)

This subarea presents peculiar characteristics of surface circulations responding to the shifting monsoon conditions (Duing, 1970). Laccadive island chains influence the variational characteristics of the parameters affecting the mixed layer depth (Colborn, 1975).

2.1.8.1 Surface wind field (Figs. 2.8 a & b)

The annual wind speed maximum is associated with the southwest monsoon in this subarea, ranging from 4 to 8 kts. Wind speed generally decreases after September to the annual minimum of about 2 kts during the northeast monsoon. Wind speed increases from October to a winter maximum of about 3 kts in January. The wind speeds are fairly persistent with more or less the same magnitude upto March. The wind direction is southwesterly during June through August which changes to northwesterly from September to October. The wind stress during this period is indicated to have southerly components as evident from the distribution of wind direction during the period. This

has been pointed out earlier by several works (Narayana Pillai et al., 1980; Shetye, 1984). The southward wind stress components have been indicated to be decisive for upwelling or enhancing the upwelling induced by the ocean circulation. From December the northeasterly winds are active and continue till January. The wind direction is mostly northerly and northeasterly. During the southwest monsoon season winds are southwesterly only in June/July.

2.1.8.2 Net heat gain (Fig. 2.8 c)

Heating starts from January in this subarea unlike the other subareas in the north and west. Maximum heating takes place during March (80 W m^{-2}). While cooling is observed during June and July with a maximum value of about -50 W m^{-2}, the rest of the annual cycle is found to have only

heating (positive heat transfer) including winter. Minimum

heating occurs in December (about 10 W m^{-2}). This

observation is peculiar to the offshore oceanic waters only

and can be explained by the fact that the winter cooling

usually observed in other areas with increase in negative

heat transfer is due to reduction in intensity of solar

radiation enhanced by moderately high evaporation. In this

subarea the evaporative loss during the winter month is less

and hence the heat transfer is still retained positive with

minimum values(about 10 W m^{-2}) in December. The bimodal

oscillatory nature of the annual cycle of net heat transfer

is observed in this subarea too.

2.1.8.3   Sea surface temperature (Fig. 2.8 d)

The surface temperature of the waters in this

subarea has an annual minimum of about 27.1^{o} C in January.

The temperature increases during spring to reach a maximum

value of 29° C in May. The surface temperature decreases

to a secondary minimum (about 27.2^{o}C) in September as a

result of negative heat transfer and upwelling. The effect

of upwelling in the near shore waters are earlier reported

by Narayana Pillai et al. (1980) and Colborn (1975). The

surface temperature increases during October/November to a

secondary maximum of 28° C as a result of increase in net

heating with reduction in evaporative loss (Hastenrath and

Lamb, 1979). The sea surface temperature decreases from

December due to the reduction in intensity of solar
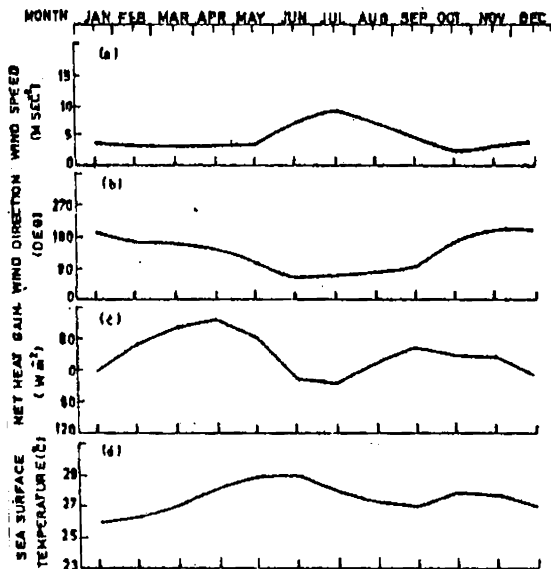
radiation.

(a)

(b)

(c)

(d)

FIG.2.5 ANNUAL CYCLE OF (a)WIND SPEED(b) WIND DIRECTION
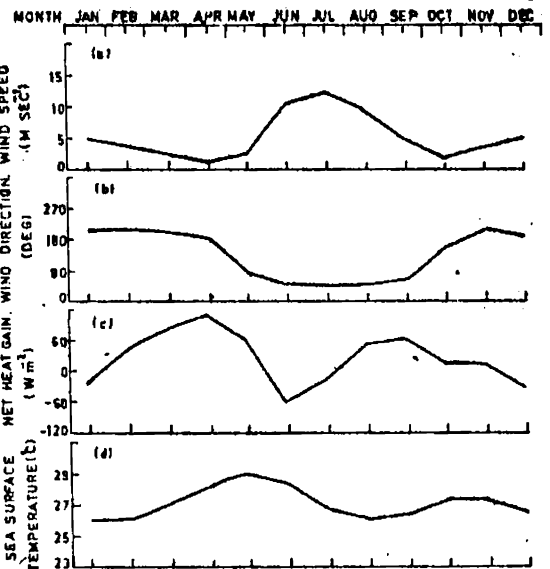(c)NET HEAT GAIN AND (d)SEA SURFACE TEMPERATURE
(SUBAREA-5)

(a)

(b)

(c)

(d)

FIG.2.6 ANNUAL CYCLE OF (a)WIND SPEED (b)WIND DIRECTION
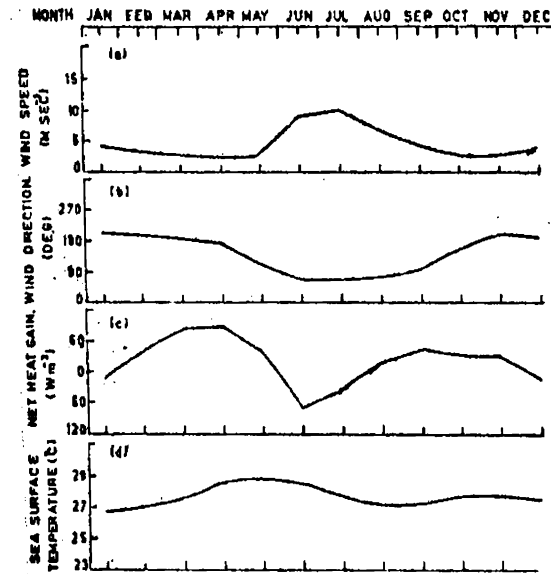(c)NET HEAT GAIN AND (d)SEA SURFACE TEMPERATURE
(SUBAREA-6)

(a)

(b)

(c)

(d)

FIG.2.7 ANNUAL CYCLE OF (a)WIND SPEED (b)WIND DIRECTION
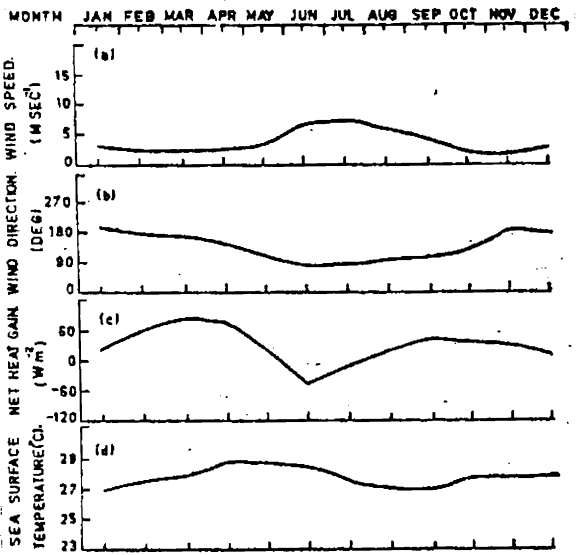(c)NET HEAT GAIN AND (d)SEA SURFACE TEMPERATURE
(SUBAREA-7)

(a)

(b)

(c)

(d)

FIG.2.8 ANNUAL CYCLE OF (a)WIND SPEED (b)WIND DIRECTION
(c)NET HEAT GAIN AND (d)SEA SURFACE TEMPERATURE
(SUBAREA-8)

SECTION - II

VARIABILITY OF MECHANICAL AND CONVECTIVE MIXING

The mixing processes controlling the mixed layer depth can be grouped under two categories namely, (1) wind or turbulent mixing (mechanical) and (2) convective mixing. Though both processes can occur together, convective mixing dominates in winter while wind mixing can be significant in summer. During summer surface cooling is limited to night time and is not pronounced. The temperature profiles will have negative gradient near the surface due to diurnal heating which will be mixed by wind. Under this condition wind mixing becomes important. Convective mixing occurs as a result of change in stability of the water column caused by diurnal and seasonal change in density produced due to cooling at surface or increase in surface salinity, both factors acting to increase the density of the surface waters. The resulting heavier water sinks to the appropriate depth of equilibrium under stability. The depth to which the wind mixing is active depends on the wind force, duration, fetch and degree of gustiness. The convective mixing depends on the rate of cooling and the vertical density distribution. When both processes occur simultaneously the resulting mixing can be accumulated beyond the limits of their independent effects. Wind mixing may act rapidly and irregularly while convective mixing acts slowly but steadily.

In this section the effects of wind mixing and convective mixing are examined separately and compared to the observed MLD variation in the annual cycle for the subareas of study in the Arabian Sea. For doing this, the average conditions of surface wind field and net heat transfer analysed and discussed in Section I are converted to the respective mixing values as per procedures described in chapter I. For the purpose of comparison and assessment of predominance of the types of mixing in the annual cycle the curves of wind mixing and convective mixing are plotted against the mean MLD (climatological) for the 8 subareas (Figs. 2.9 & 2.10).

2.2.1   Subarea 1 (Fig. 2.9)

The mechanical mixing due to the wind action is found to decrease from January (about 3 m) to a minimum in March/April (about 1 m). From May onwards wind speeds are on the increase causing a maximum mechanical mixing of about 22 m.   This is followed by a decrease in wind speed reducing the mixing in November (about 1 m). The annual cycle of wind mixing for this subarea has a range of about 2 m.

Convection is very high in magnitude compared to the mechanical mixing during January-May and October-December. The convective mixing depth closely follows the variation of the mean monthly MLD with a maximum difference only in March (about 25 m). The convective mixing is decisive in the annual distribution of MLD from January to

May as evident from Fig. 2.9. From June to September mechanical mixing is closer to the MLD indicating the predominance of mechanical mixing during this period.

The reduction in MLD during March to October is the result of spring and summer heating and the depth of mechanical mixing is nearer to the convective mixing during this period. The mean monthly MLD for the subarea shows a maximum value (64 m) in February owing to winter deepening which reduces during spring heating to an annual minimum (22 m) in June. Cooling from July deepens the MLD to 30 m in August and September. The reversal in net heat transfer results in shoaling of MLD upto October. The winter cooling due to net surface heat loss and resulting convective deepening increase the mixed layer to the winter maximum. The annual range of MLD variation is about 41 m.

2.2.2   Subarea 2 (Fig. 2.9)

Wind produced mechanical mixing is minimum in March and November (about 2 m). The mechanical mixing increases to an annual maximum of about 27 m in August corresponding to the maximum wind speeds during southwest monsoon. Forced mixing due to wind turbulence is reduced to minimum again after August. This is followed by an increase in the wind mixing to a maximum of 3 m in December. The range of mechanical mixing in the subarea is found to be about 25 m.

Annual cycle of convection shows a value of 85 m in February corresponding to the winter maximum. Mixing

by convection is greatly reduced in June to about 27 m
as a result of spring and summer heating. Further mid-
summer cooling increases the surface layer to about 50 m
in August followed by a decrease during the secondary
warming period upto September (28 m). Winter convection
is the maximum in the annual cycle.

The annual variation of the mean monthly MLD
shows a maximum of 66 m in February decreasing to 27 m in
June in the subarea. Unlike the other areas, the mixed
layer increases continuously following the mid-summer
cooling from July to a maximum during winter. The annual
range of MLD variation is about 37 m.

A comparison of the results of mechanical and
convective mixing in the subarea reveals that convective
mixing dominates in deciding the MLD during winter, spring
and summer months from January to July while wind mixing
is closer to the actual MLD values observed during August.

2.2.3   Subarea 3 (Fig. 2.9)

Mixing by wind/wave action is stronger from July
to September during the southwest monsoon when a maximum
mixing of about 59 m is observed in August. Forced mixing
is diminished during the winter months with values upto 7 m
in January. A further decrease during spring with a minimum
of about 1 m in May is observed. The wind mixing is minimum
with the same magnitude during November. The annual range
of mechanical mixing for the subarea is about 35 m.

The extent of convection in the subarea closely
follows the annual cycle of mean monthly MLD distribution
with the maximum difference of about 26 m in March and 22 m
in October. A maximum of 88 m in February due to convective
mixing is observed. This is followed by a decrease to 33 m
in June which is the minimum value of the convective mixing
in the annual cycle for the subarea. Convective deepening
after June increases to a secondary maximum (73 m) in
September. Heating after that decreases the convective
mixing extent to 38 m in November. The convection due to
winter cooling deepens the mixing from December to a
maximum in February. The annual range of convective mixing
is about 55 m in the subarea.

The monthly mean MLD distribution exhibits a double
moded oscillation in the annual cycle. A maximum of 76 m
of mixed layer depth is observed during January. This is
followed by the spring heating from March resulting in a
decrease to an annual minimum of MLD (33 m) in May. The
mid-summer cooling during southwest monsoon deepens the
mixed layer to 73 m in August. The secondary warming from
August causes a minimum in October (36 m). Thereafter,
the winter cooling progressively deepens the mixed layer
depth from November to January. The mixed layer variation
observed in the present study for the subarea is similar
in respect of bimodality and occurrence of maxima and
minima discussed by Colborn (1975).

An examination of the distributional
characteristics of both wind mixing and convective
mixing curves for the annual cycle presented for this
subarea (Fig. 2.9) reveals the importance of buoyancy
fluxes in the annual cycle in controlling the effective
mixed layer. From January to May the depth of convective
mixing is more and closer to the actual MLD, and thereafter
upto August coinciding with it. The maximum difference
is about 26 m in March. From September to October
convective mixing is slightly more, differing from the
actual with a maximum difference of 22 m in October. The
wind mixing is less compared to the actual MLD and is
prominent and closer to it, only from June to October with
a minimum difference of 11 m in August.

2.2.4   Subarea 4 (Fig.2.9)

The wind induced turbulent mixing is significantly
higher after May until October. The maximum Mechanical
mixing is observed in August when the mixing extends to
a depth of about 41 m. Values of wind mixing are highly
insignificant ranging from 2 to 7 m in January - May and
October _ December. The annual variation of mechanical
mixing is about 40 m. Convective mixing reaches maximum
in February (about 73 m) decreasing to a minimum of 39 m
in June. A secondary maximum of about 71 m is reached
in August following net surface cooling. The secondary
heating after September causes a decrease in convective
mixing to 44 m. Winter convection is active from December-
January reaching maximum in February. The annual amplitude
of variation of convective mixing is 34 m.

Bimodal variation of the mean monthly MLD indicated in Fig.2.9 has a maximum of 64 m in February due to winter deepening. The spring heating reduces the MLD to about 39 m in May. The secondary deepening of the MLD occurs after May resulting in the maximum value of the layer during August (63 m). This deepening is almost equal in intensity to the winter deepening and may be due to the enhancement by the convergence of current owing to the presence of a major clockwise circulation in this area (Varadachari and Sharma, 1967). The secondary warming after August produces shallow mixed layers upto November with a minimum of about 42 m. Winter cooling further deepens the mixed layer to the maximum after January.

Convective mixing closely follows the annual cycle of observed MLD with coincidences in June and maximum differences upto 16 m in October in the subarea. The wind mixing drastically differs from the observed MLD and a minimum difference of about 39 m is observed only in July under intense summer monsoonal forces. The maximum difference between the wind mixing and observed MLD is about 58 m.

2.2.5 Subarea 5 (Fig.2.10)

From January to June and from October to November the wind mixing is indicated to be a minimum (about 2-4 m). The mixing due to turbulence is more during July-October under the southwest monsoon regime with a maximum of 28 m in August. The amplitude of annual variation in the wind mixing for the subarea is about 26 m.
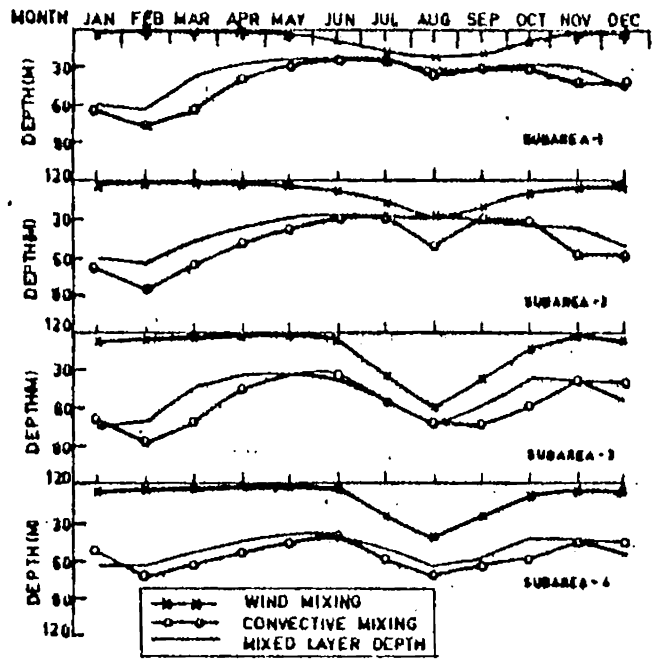
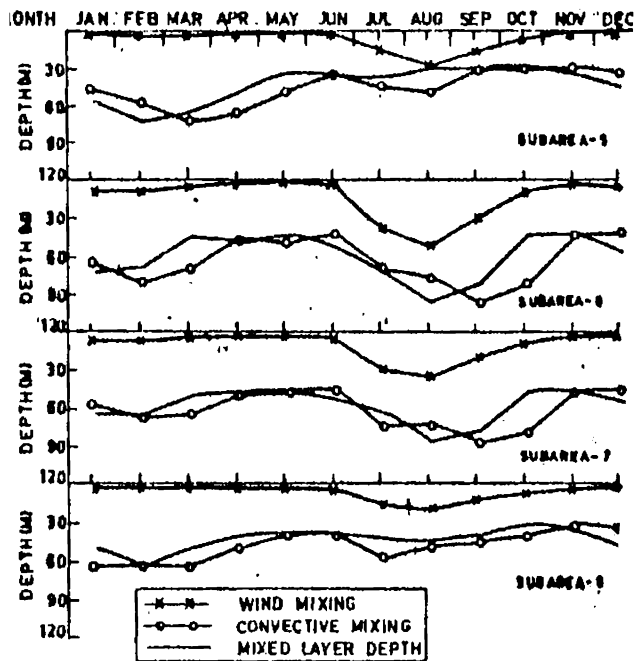FIG.2.9 ANNUAL CYCLE OF WIND MIXING, CONVECTIVE
MIXING AND MIXED LAYER DEPTH

FIG.2.10 ANNUAL CYCLE OF WIND MIXING CONVECTIVE
MIXING AND MIXED LAYER DEPTH

An annual maximum in the convective mixing is observed in March (73 m) with a decrease in June (34 m). The convection increases to 49 m in August. During the secondary heating season, mixing is further reduced in October. Convective deepening becomes more during winter reaching a maximum towards March. The annual variation in the convective mixing for the subarea is about 46 m .

The observed mean mixed layer depth follows as a mild bimodal variation in the annual cycle as a result of secondary shoaling and deepening effects due to the mid-summer cooling. Secondary warming produces no significant effect of decrease or increase in the MLD. The absence of a pronounced secondary deepening during June/July and shoaling in October, as in the case of subarea 2, can be explained only by processes of progressive upward movement of the thermocline observed in this area from June through November. Banse (1968) observed the presence of cool subsurface waters below 50 m during this period suggesting upwelling processes to be active at least upto that depth in the zone. Similar shoaling of thermocline penetrating the surface layer during the final stages of southwest monsoon along the Indian coastal zone from Indus river mouth, south of Bombay has been indicated by Colborn (1975). The annual maximum of MLD in the subarea is during winter with a value of 73 m in February. The spring heating reduces the layer to 34 m in March. Cooling in June/July deepens the MLD to 38 m. From August to October shoaling

of the surface mixed layer is observed upto about 27 m.
Winter deepening of MLD due to the net cooling is
observed from November to February. The annual range of
variation in MLD for the subarea is about 46 m .

In the annual cycle convective mixing values
are closer to the observed MLD with differences ranging
between 0-19 m. The wind mixing values are closer to the
observed values only during July-September, when actual
coincidence is observed in August. For most of the year
wind mixing depths are shoaler than the observed MLD with
the differences ranging from 21 to 69 m.

2.2.6   Subarea 6 (Fig.2.10)

The wind mixed layer computed for the subarea
shows a maximum value in August (52 m) and a minimum (2 m)
in October. Southwest monsoon winds mix surface layers
to the maximum. The mechanical mixing decreases in the
transitional period to reach a minimum in October. Mixing
due to the winds of northeast monsoon in winter is maximum
in January (about 9 m). The annual variation of mechanical
mixing is about 50 m in the subarea.

Convective mixing closely follows the annual monthly
mean MLD variation. Intense convection is observed in
February with values upto 80 m. During the heating season
the convective mixing values are reduced upto about 42 m
in June. Maximum convection is observed in September
(96 m). The annual range of variation is between 42-96 m.

The subarea is subject to the influence of the major anticyclonic circulation in the Arabian Sea during southwest monsoon and also a reversal of the system during late fall. The present study indicates the fact that the MLD ranges between 40-96 m following a bimodal oscillation. The mid-summer deepening of MLD is greater than that during winter as a result of enhancement by sinking due to convergence of currents in anticyclonic circulation system present during June-July. The earlier works of Wooster et al. (1967) and Colborn (1975) have documented similar observation for this area. The present analysis depicts a winter mixed layer of about 65 m in January/ February. From March onwards, spring heating lowers the mixed layer to about 42 m in May. Intense cooling of the surface layers during June/July results in entrainment mixing and deepening of the mixed layer supplemented by the convergence-induced sinking. Annual maximum of MLD (96 m) is observed in August followed by a mixed layer shoaling during the secondary warming period upto 41 m in November. Winter deepening starts in December and ends by January in the subarea. The annual variation in MLD for the subarea is about 55 m.

The difference between convective mixing and the observed MLD ranges between 0-38 m for the subarea. The convective mixing is decisive in fixing the MLD during much of the annual cycle. Wind mixing is found closer to the actual MLD only during June to August when the wind mixing is about 44 m less than the actual MLD.

2.2.7   Subarea 7 (Fig.2.10)

From June to October wind mixing is found
maximum under the influence of southwest monsoon. Maximum
wind mixing is observed in July (35 m). Wind mixing
values decrease from 6 m in February to about 2 m in May.

Mixing due to convection is maximum in February
(67 m). A decrease in convective mixing depth to about
44 m after spring warming occurs in June. This is
followed by the deepening of the layer to about 86 m
in September. The convective mixing shoals upto 44 m by
December. The range of convective mixing for the subarea
is 44-80 m.

The factors influencing MLD are almost the same
as in the case of subarea 6. Mixed layer variation in the
subarea exhibits pronounced bimodal oscillations in the
annual cycle. The maximum value of MLD (64 m)is observed
in January/February. Heating thereafter causes shoaling
of the mixed layer upto about 44 m. The mid-summer
cooling during June-July deepens the surface layer to an
annual maximum in August (about 86 m) as a result of
enhanced deepening by surface current convergence at that
time. The secondary warming produces shallow mixed layer
depths upto 44 m during November in the subarea.

The annual variation of the MLD for the subarea
is fully described by the convective mixing with difference
ranging from 0-32 m. Wind mixing is too shallow for the
entire annual cycle to have any agreement with the
observed MLD.

2.2.8   Subarea 8 (Fig. 2.10)

The coastal zones and southeast Arabian Sea
regions close to the Indian coast under the subarea are
influenced mainly by the changing circulation pattern
during the two monsoons in the Arabian Sea. Winter
deepening of MLD is maximum resulting in values of about
65 m in January-February. Though the winter deepening
is the result of cooling in other areas, in the present
analysis a cooling is not apparent in the subarea while
a decrease in the heating to minimal values are noticed.
(Fig. 2.10). As such, the increase in the MLD is the
result of decrease in heating during October-November and
further increase of the MLD to the maximum in February may
be attributed to the northward flowing currents of the
northeast monsoon (Fig. 3.1), which induce sinking in
the offshore waters though the winds are not augmenting
sinking. Works by Banse (1959), Rama Sastry and Myrland
(1959) and Ramamirtham and Jayaraman (1960) also indicate
upwelling upto September/October and sinking from November
to February. These observations have been confirmed by
Colborn (1975) who observed that dipping of thermocline
below mixed layer during January-February is related to
a zone of convergence between westerly flow due to
northeast monsoon drift and southeasterly flow of the
developing anticyclonic circulation in the Arabian Sea
during February. The present analysis also indicates a
decrease in MLD from March onwards due to the spring
heating upto about 39 m in May. Excess cooling occurs in

the beginning of southwest monsoon during June/July resulting in an increase of surface layer to about 45 m by August. The secondary deepening during this time is retarded in the subarea as a result of an upward shift of thermocline especially along the coastal zone due to the upwelling from March-April through September. The upwelling in this area commences from south to north along the coast (Colborn, 1975). Evidence is also available from the works of Raghavan (1969) who has presented satellite photographs in support of upwelling during September. Wooster et al. (1967) do not support an upwelling in this area as the winds during this time are not favourable for the phenomenon. But Sharma (1968) observed that the upwelling and sinking along the west coast of India are not only controlled by winds but also by the oceanic currents, playing a major role. But Shetye (1984) concludes that during April-October the coastal processes are generally controlled by local wind stress and the nature of surface current during this period is consistent with the classical model of a typical coastal upwelling. However, the present analysis supports the view that upwelling is due to the southerly flow set in by February-March changing to easterly and southeasterly upto September as a part of the major anticlockwise gyre present in the Arabian Sea during the period (Fig. 3.1). The upwelling is further enhanced by northerly components in the winds from August to September for the duration of the southerly

current (Fig 2.8 b). The MLD shoals during the secondary
warming period from September to November with a maximum
of 31 m, in October, though majority of the area especially

along the eastern boundary of the subarea is away and out of
the continental shelf   where   the upwelling and the
resulting shallow MLD can be upto 10-15 m at 10^0 N latitude
during September (Joseph and Durga Prasad, 1981). The
surface layer undergoes deepening during December-February
to the annual maximum. The annual range of mixed layer
in this area is 31-45 m.

Wind mixing is indicated to be highest during
southwest monsoon in the subarea with a range of 4-19 m
during June-September with a maximum occurring in August.
The minimum mechanical mixing is observed during March,
April and May and November/December (about 2 m). The
annual range in wind mixing is 2-19 m.

Convective mixing is maximum in February (about
64 m) and closely follows the actual MLD variation.
Mixing by convection is at a secondary minimum of 58 m
in June. The convective mixing varies with a difference
of 0-14 m while wind mixing has a range   38-62 m from
the observed MLD.

CHAPTER III

CHAPTER III

ADVECTION, CONVERGENCE/DIVERGENCE AND INTERNAL WAVES

Advection is the process by which heat is transported from one place to another. Advection of water due to wind and density currents plays an important role in deciding thermal structure profile in the upper layer and the MLD. The local exchange of heat altering the thermal structure, largely depends on the horizontal advection and diffusion of heat (Reed and Halpern, 1974). Joyce et al. (1980) observed that the dominant low frequency variability in the seasonal thermocline accounting to 60% of the observed temperature changes during JASIN experiment in north Atlantic was due to horizontal advection by currents. Vertical advection of cold waters during the upwelling period affects MLD especially in the coastal areas.

Divergence and convergence of waters due to surface currents cause vertical movements in MLD. Convergence causes sinking of the MLD and associated thermal and density structure while divergence causes upwelling or shoaling of MLD and associated structures (La Fond, 1954). Convergence/divergence can be semipermanent or vary at short time intervals with the periodicity of changes in surface wind and tides in an area. According to Mazeika (1960) each individual geographic area (of 5° or less square) possesses certain geographic characteristics which affect the formation of MLD and where permanent convergence

or divergence exists, these characteristics may be sufficiently strong to preclude conventional mixing processes. Apart from such extreme cases, local conditions due to changes in convergence/divergence will influence local MLD values.

Convergence/divergence can be estimated from local wind currents. But this method can be subjective (Laevastu and Hubert, 1965). A realistic approach is to derive the surface divergence from surface current data. The surface divergence is calculated following Hela (1954), reviewed by Laevastu and Hubert (1965).

Internal oscillations with periods ranging from about 10 seconds to months related to atmospheric pressure changes, current shears and tidal forces are found to influence time variations of MLD. The lower limit of the period of these oscillations is set by the Brunt-Vaisala frequency. Internal waves occur at the boundary between density layers and vary widely in amplitude and period (La Fond, 1954; Mazeika, 1960).

The annual variation of surface current speed, direction and its east-west and north-south components as well as surface current divergence for the 8 subareas of study are presented in this chapter. The characteristics of internal waves in the Arabian Sea are discussed only in respect to the time series data at S1 for a sample strength of 64 observations. Fig. 3.1 shows the monthly circulation pattern over the Arabian Sea after Varadachari and Sharma (1967).
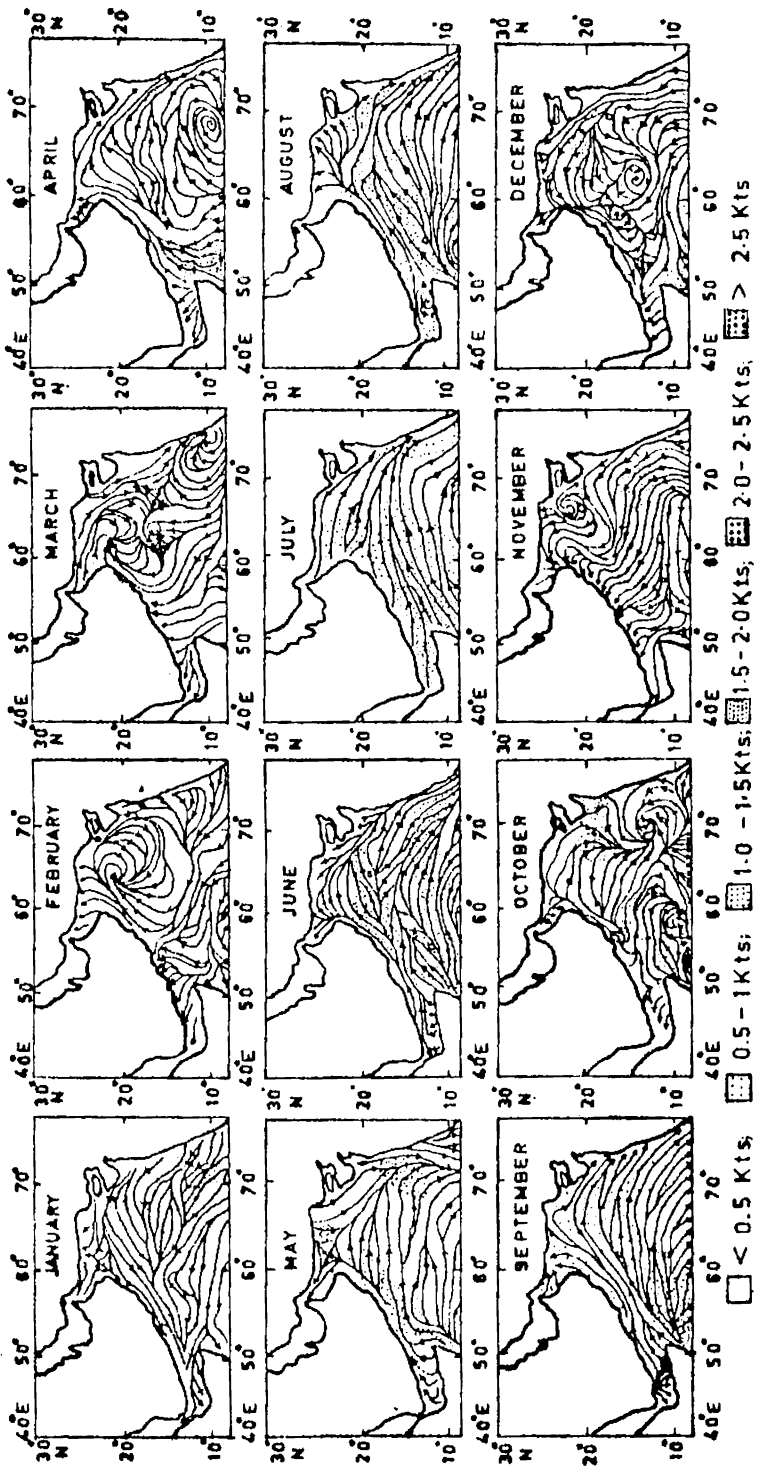
FIG. 3.1 MEAN SURFACE CIRCULATION IN THE ARABIAN SEA (AFTER VARADACHARI AND SHARMA, 1967)

3.1   Subarea 1 (Fig. 3.2)

3.1.1   Surface currents (Figs. 3.2 a to d)

Surface currents in the subarea at the mouth of Gulf of Oman is westerly during January with speeds upto 25 cm sec^{-1}.   During February a major easterly flow is apparent with diminished speeds. By March a southerly flow with speeds of about 14 cm sec^{-1} is present. In April current speeds are maximum (30 cm sec^{-1}) in the south-easterly direction. Currents with speeds 16-22 cm sec^{-1} continue to be present in the subarea during May-October. In October southwesterly currents with minimum speeds (about 13 cm sec^{-1}) are observed. The surface current speeds increase during winter due to the intensified westerly flow.

From an examination of the surface current components, easterly components are more apparent from April to October and from December to January while westerly components are dominant during January, March and November. The southward components are maximum during April and minimum during December.

3.1.2   Surface current divergence (Fig. 3.2 e)

Maximum negative values of surface divergence (about 40 units) are observed in January suggesting convergence and sinking for the surface mixed layer . A moderate positive value of surface divergence during February/March is followed by weak converging tendency in April. Upwelling tendency is indicated from May to July

reaching a maximum divergence in June (-25 units).
Convergence of the surface current from August to October
is conducive for sinking of the surface layer. The trend
is reversed in November with divergence at surface. But
increased convergence starts from December to January
during which the winter deepening of MLD is observed
(Fig. 2.9). This observed deepening may be the combined
result of sinking and cooling. A decrease in the surface
divergence during May/June is also supplemented by the
increased surface heat gain (Fig. 2.1 c) resulting in shoaling
tendency of MLD observed. The deeper layers observed
during August-October (Fig. 2.9) can be attributed to the
convergence apparent during this time.

The patterns observed especially of convergence
in December/January, divergence in February-March and
divergence in June-July and September-October are in
agreement with the earlier observations of Varadachari and
Sharma (1967).

3.2   Subarea 2 (Fig. 3.3)

3.2.1   Surface currents (Figs. 3.3 a to d)

The surface currents are southerly and generally
weaker near the Indus Cone and off Gujarat during January-
February (greater than 10 cm sec^{-1}). The flow changes to a
southeasterly direction from March to October attaining a
maximum speed in July (about 27 cm sec^{-1}). The wind speed
decreases in July (12 cm sec^{-1}) and increases to a second
peak in August (23 cm sec^{-1}). From November the wind speed

decreases with a mean southerly flow. The mean flow in
this area is fairly agreeable with the previous
observations (Varadachari and Sharma, 1967; Duing 1970),
except in January and December. This can be due to the
errors in averaging of sparse current data from mean 2^O
quadrangles from Wooster et al. (1967)for the subarea.

From February to October easterly components are
predominant while during November to January southerly
components are present.

3.2.2   Surface current divergence (Fig. 3.3 e)

Weak convergence (-4.9 units)is indicated in the
subarea from January to March. This is reflected in the
sinking tendency of MLD (Fig. 2.9) upto February.A strong
divergence is seen during April (26 units) as confirmed by
the circulation pattern during the period (Duetsches
Hydrographisches Institut, 1960). This is reflected in
shoaling of MLD observed upto May (Fig. 2.9). Convergence
is indicated from July to November with a maximum in August
(-32 units) which agrees with the observations of
Varadachari and Sharma (1967). A slight increase of MLD
(Fig. 2.9) from June to November is the consequence of the
convergence-induced sinking exceeding the shoaling effects
due to the secondary warming in September (Fig. 2.2 c).
Divergence is indicated in December which may oppose the
MLD deepening to a limited extent.

3.3   Subarea 3 (Fig. 3.4)

3.3.1   Surface currents (Figs 3.4 a to d)

This subarea in the western half of the central
Arabian Sea has strong average currents during May to
September (23-26 cm sec^{-1}) flowing in the easterly
direction. During October and November the mean currents
turn southeasterly and southerly with reduced speeds.
During winter months, the currents are southwesterly and
weaker. In February the surface current becomes stronger
(21 cm sec^{-1})in the southwesterly direction. During March-
April the currents again become weaker flowing towards south
and southwest.

Easterly components are present during January
and March-October while westerly components are present
from February to April. Northerly components are
prevalent during June-September, January-May and southerly
components are active during October-December. The
circulation pattern agrees with the results of Colborn,
(1975).

3.3.2   Surface current divergence (Fig. 3.4 e)

January is marked by convergence in the subarea
resulting in sinking of the surface layer which is
already deepened due to convective mixing during winter
cooling. The divergence of February is maximum (26 units)
and continues upto March. Sinking tendency for MLD is
indicated during April-July by the convergence with a

maximum in May (-19 units). The observed deepening of

MLD for the subarea (Fig. 2.9) during this month may be

the result of the net heat loss upto June supplemented by

the convergence upto July. This convergence is also seen

in the circulation pattern reported by Varadachari and

Sharma (1967). After a short spell of divergence in August

the convergence trend reappears again in September.

Divergent and convergent tendencies are alternatively

indicated from October to December. The weak divergence

in December is not sufficient to balance the convective

deepening of MLD during the month (Fig. 2.9).

3.4   Subarea 4 (Fig. 3.5)

3.4.1   Surface currents (Figs. 3.5 a to d)

The surface current direction in January is

southeasterly, with low speeds (less than 15 cm sec^{-1}).

The surface current becomes southwesterly in February

and stronger (22 cm sec^{-1}). The speed decreases in March

and again increases from April to June (22 cm sec^{-1}).

During April-May the currents are variable. By June the

current direction is set to northeasterly and remains so

till June. It becomes easterly/southeasterly in August-

October with a maximum surface speed (28 cm sec^{-1})in

August. From November the average current is westerly

with high speed in December (19 cm sec^{-1}).

Easterly components are predominant during

May to October while westerly components are dominant in

November-December and February (Fig. 2.9). During June-

July the northerly components are active and from January to

May and from August to November southerly components are predominant. The general pattern excepting for transitional periods agrees with that given by Varadachari and Sharma (1967).

3.4.2 Surface current divergence (Fig. 3.5 e)

The surface divergence indicated for January and February is not sufficient to shoal the MLD as the winter cooling and the convective deepening are stronger during this time (Fig. 2.9). The reversing trend in March also does not have any deepening effect as the spring heating and shoaling of MLD is already at the maximum, making the mixed layer shallow. The divergence indicated in April is also supplementing the shoaling of MLD upto May resulting from secondary warming. The maximum convergence in August (-13 units) coincides with the mid-summer deepening of MLD, when the effects of both cooling and convergence seems to be active during the month. The shoaling of MLD after September shows correlation with the maximum divergence (14 units) for the month. The low values of convergence estimated for October and November supplement the deepening of MLD due to cooling (Fig. 2.9). However, the divergence indicated during December is in contrast to the deep layers observed and hence may be erroneous due to the data scarcity. The surface divergence pattern is in agreement with the results of Varadachari and Sharma (1967) except for the period in December-January.
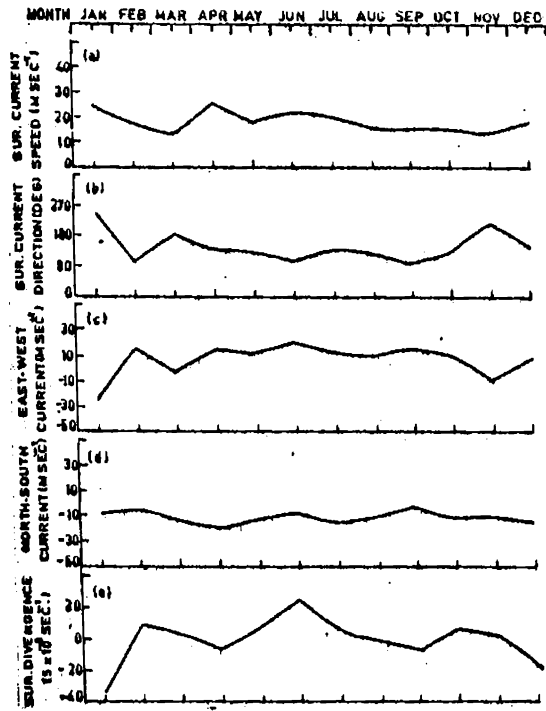
FIG.3.2 ANNUAL CYCLE OF (a) SURFACE CURRENT
(b) SURFACE CURRENT DIRECTION (c) E-W CURRENT
COMPONENT (d) N-S CURRENT COMPONENT AND
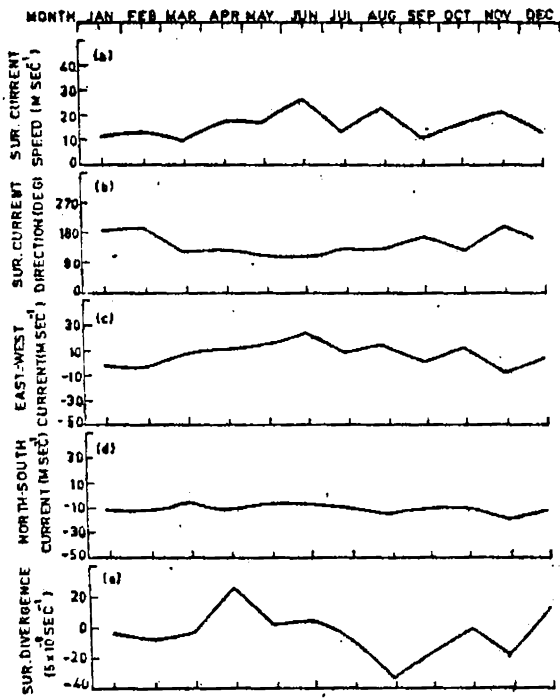(e) SURFACE DIVERGENCE (SUBAREA-1)

FIG.3.3 ANNUAL CYCLE OF (a) SURFACE CURRENT
(b) SURFACE CURRENT DIRECTION (c) E-W CURRENT
COMPONENT (d) N-S CURRENT COMPONENT AND
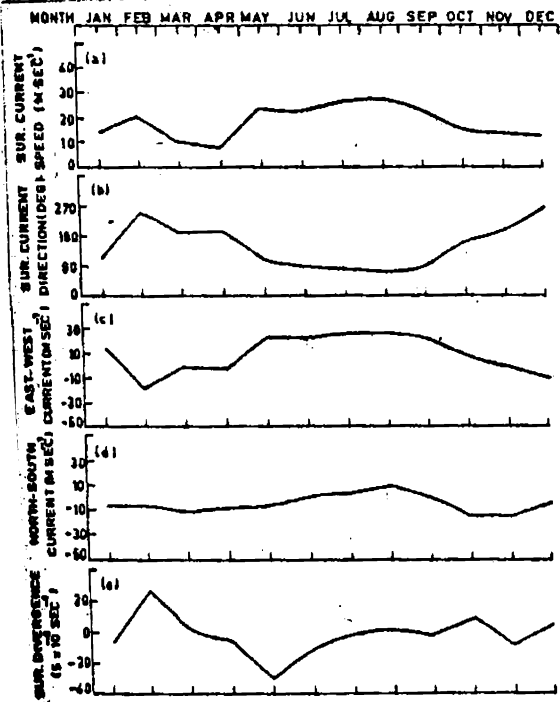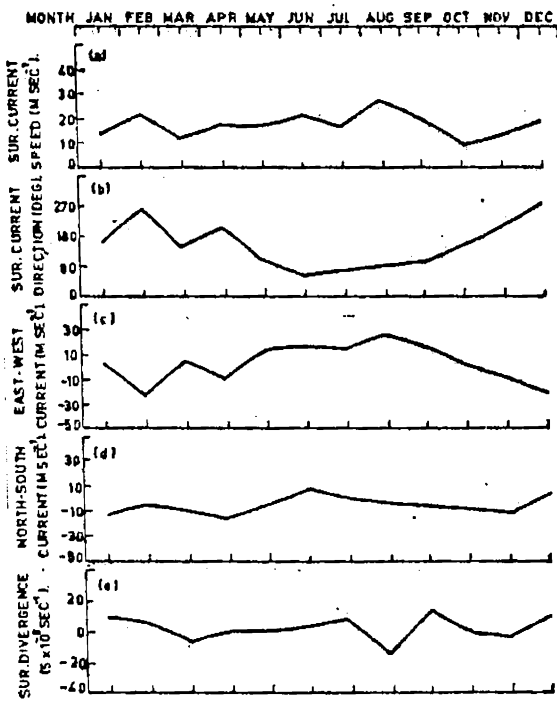(e) SURFACE DIVERGENCE (SUBAREA-2)

FIG.3.4 ANNUAL CYCLE OF (a) SURFACE CURRENT
(b) SURFACE CURRENT DIRECTION (c) E-W CURRENT
COMPONENT (d) N-S CURRENT COMPONENT AND
(e) SURFACE DIVERGENCE (SUBAREA-3)

FIG.3.6 ANNUAL CYCLE OF (a) SURFACE CURRENT
(b) SURFACE CURRENT DIRECTION (c) E-W CURRENT
COMPONENT (d) N-S CURRENT COMPONENT AND
(e) SURFACE DIVERGENCE (SUBAREA-4)

3.5   Subarea 5 (Fig. 3.6)

3.5.1   Surface currents (Figs. 3.6 a to d)

During January a weak westerly flow (13 cm sec^{-1}) is present which changes to southeasterly during February-March. The surface current speed increases from March. The current direction changes to southwesterly in May to southeasterly in June-September with maximum speed (30 cm sec^{-1}) in August. The surface currents weaken towards November through January. During November and December the surface current direction changes to southwesterly.

The variation of the current components indicates the prevalence of easterly component from February to March and June to September. Westerly component is apparent during November-January. Throughout the year only southerly component is observed in this area. The present observations on surface currents in this area closely resemble the patterns presented by U.S. Navy Hydrographic Office (1960).

3.5.2   Surface current divergence (Fig. 3.6 e)

From January to July divergence is indicated for the subarea with a maximum (about 13 units). Basil Mathew (1982) observed weak to moderate divergence in the same area except in April. The convergence and divergence are indicated in alternation from August to December. The divergence during January is not reflected in the deepening of MLD from November onwards in the subarea (Fig. 2.10).

Divergence from March to May supplements the shoaling
of the surface layer due to spring heating. Diminished
deepening of MLD during the mid-summer cooling in June/
July can be attributed to the divergence during this
month. Weak convergence in August observed in the present
study has not resulted in any increase of MLD because of
the counteracting influence of the secondary warming
during the month. However, Basil Mathew (1982) has
reported moderate upwelling in this area during this time.
A possible reason for this may be due to difference in
date sets and averaging. Secondary warming in unison
with divergence observed in September seems to cause
shoaling of MLD after November. Maximum convergence
indicated in December (about -10 units) coincides with
the deepening of MLD (Fig. 2.10). Divergence in September
and convergence in October observed in this area are also
apparent from the results of Varadachari and Sharma (1967).

3.6   Subarea 6 (Fig. 3.7)

3.6.1   Surface current field (Figs. 3.7 a to d)

Western areas of the southcentral Arabian Sea
falling under this subarea is characterised by
southwesterly and westerly flows during northeast monsoon
and northeasterly to easterly flows during southwest
monsoon period. Southwesterly flow in January becomes
weaker towards March and April(about 12 cm sec^{-1}) with
directions changing to southeasterly. The northeasterly
flow starts from June reaching a maximum (30 cm sec^{-1})

in July. A decrease in current speed from August to September is followed by a change in the current direction to southeasterly with very low speeds (less than 9 cm sec^{-1}) in October. Southwesterly currents attain maximum values (about 15 cm sec^{-1}) during December/January.

Easterly components are predominant during March to September while westerly components are active from October to December/January. Southerly components in the flow are observed during March-May and September-January and northerly components are observed during February and June-August. These observations are in general agreement with the pattern presented in the atlas of Deutsches Hydrographisches Institut (1960)except for March and April.

3.6.2 Surface current divergence (Fig. 3.7 e)

During January weak convergence is indicated resulting in the sinking of MLD during January due to winter cooling. Weak divergence is indicated in February. Convergence during March increases to moderately high values in April (-13 units). This may be due to the presence of the anticyclonic system in the central Arabian Sea by March (U.S. Navy Hydrographic Office, 1960). However, the MLD has not deepened significantly during this time. The divergence in May is reflected in shallower layers observed, though it may also be caused by net heating. From June to July high convergence is

correlated with maximum layer depths (Fig. 2.10). This

agrees with the observations by Bruce (1981) and Sastry

and Ramesh Babu (1979)of negative wind stress curl and

convergence. Moderate divergence in August increases

in September and is reflected in the shoaling of MLD.

This is also the result of the secondary warming. During

October and November weak convergence indicated has

agreement to the pattern discussed by Varadachari and

Sharma (1967), though a shoaling of MLD is observed during

this time in the present analysis due to positive heat

transfer. The weak divergence indicated in December also

is not reflected in the MLD value as it appears to be

mainly controlled by the convective process during this

time (Fig. 2.10).

3.7   Subarea 7 (Fig. 3.8)

3.7.1   Surface currents (Figs. 3.8 a to d)

The southeasterly flow indicated in January from

the present analysis for the subarea is not realistic. In

February southwesterly flow is present. Southeasterly and

southwesterly flow indicated in March and April respectively

are also indicated by Varadachari and Sharma (1967) and

may be explained as the irregular features of the

transitional months. The surface flow is mainly southeasterly

and easterly during March-October with maximum speeds

(41 cm sec^{-1}) in October. During November and December

the surface currents are northwesterly with moderate speeds

(about 20 cm sec^{-1}).

Easterly components are prominent during March
and May -October and westerly components in February,
April, November and December. Northerly components are
indicated only in December while for the rest of the year
southerly components are prevalent.

3.7.2 Surface current divergence (Fig. 3.8 e)

In January weak convergence is indicated. This
can also be associated with the sinking motion observed
in the offshore areas of southwest coast of India as a result
of convergence of westerly flowing northeast monsoon drift
and southerly flow in the beginning of formation of the
anticyclonic circulation (Colborn, 1975). The large MLD
values in January are in correlation with the convergence
and convective deepening during this month. However, the
persistence of a maximum MLD through February is not
explained by the divergence during this time. The divergence
observed in this subarea in February has also been reported
by Basil Mathew (1982). From March to April convergence
increases to moderate intensity (13 units), which closely
agrees with the convergence zone due to the presence of an
anticyclonic circulation (clockwise) formed in the subarea
during March/April (U.S. Navy Hydrographic Office, 1960;
Varadachari and Sharma, 1967). But shoaling of MLD during
this period is caused by the intense heating (Fig.2.7 c).
The weak convergence indicated in June/July in the present
study seems to augment the convective deepening during the
mid-summer cooling active by this time. The moderate

divergence appearing from August to September is reflected
in the shoaling of MLD. This shoaling is related to the
divergence of southerly flow in the area (Varadachari and
Sharma, 1967) similar to an upwelling motion, assisted by
the secondary warming during the period. In October a
weak convergence is present and it remains upto November,
though the secondary heating starting from August through
October is still active in shoaling the MLD against the
sinking influence of the convergence. The divergence
indicated during December is not supported by any evidence
in the present analysis as a thickening of MLD is observed
indicative of sinking during the month. This disparity
may be on account of the sparse current data set.

3.8   Subarea 8 (Fig. 3.9)

3.8.1   Surface currents (Figs. 3.9 a to d)

From February to October southeasterly flow is
indicated. Speeds are maximum in August (36 cm sec^{-1})
under the influence of southwest monsoon. During winter
speeds are stronger (28 cm sec^{-1}) in January. Flow
pattern agrees well with Varadachari and Sharma (1967)
except for December and January. Easterly and southerly
components show an extensive coverage in the annual cycle.

3.8.2   Surface current divergence (Fig. 3.9 e)

Weak to moderate convergence observed from January
to April is indicative of sinking during this period.
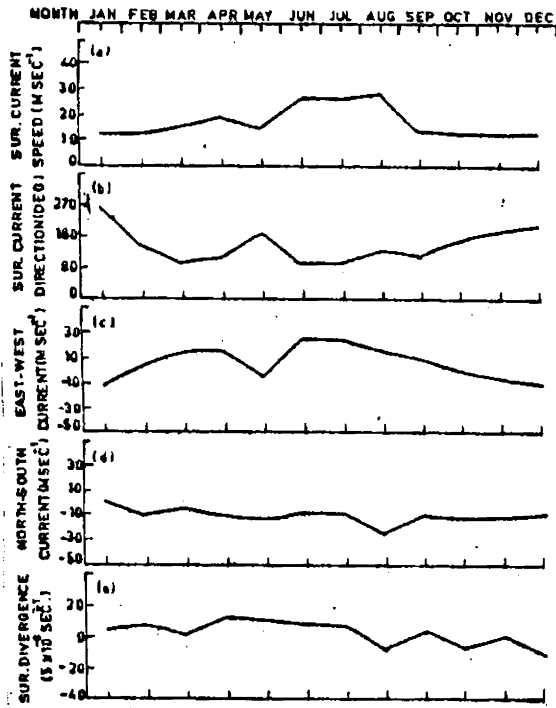However, deepening of MLD is reflected only upto February.

FIG. 3.6 ANNUAL CYCLE OF (a) SURFACE CURRENT
(b) SURFACE CURRENT DIRECTION (c) E-W CURRENT
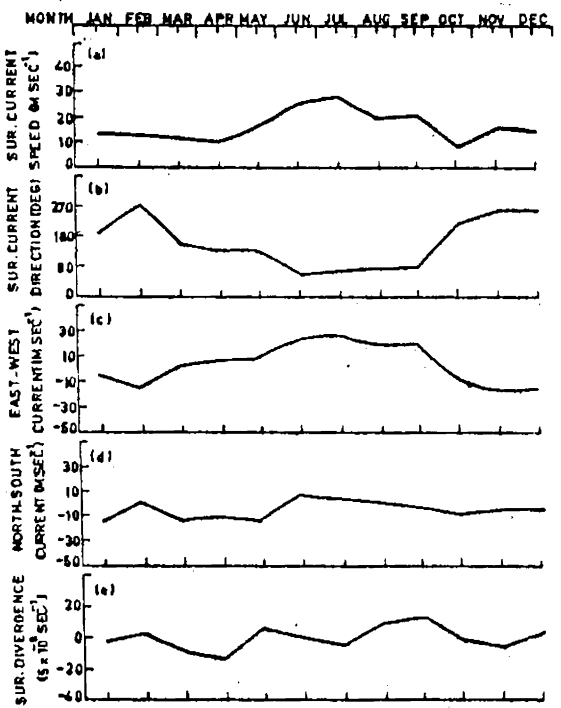COMPONENT (d) N-S CURRENT COMPONENT AND
(e) SURFACE DIVERGENCE (SUBAREA-5)

FIG. 3.7 ANNUAL CYCLE OF (a) SURFACE CURRENT
(b) SURFACE CURRENT DIRECTION (c) E-W CURRENT
COMPONENT (d) N-S CURRENT COMPONENT AND
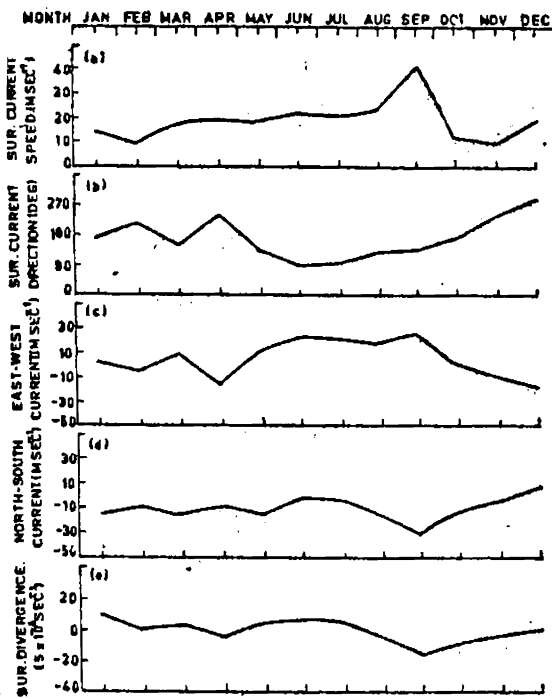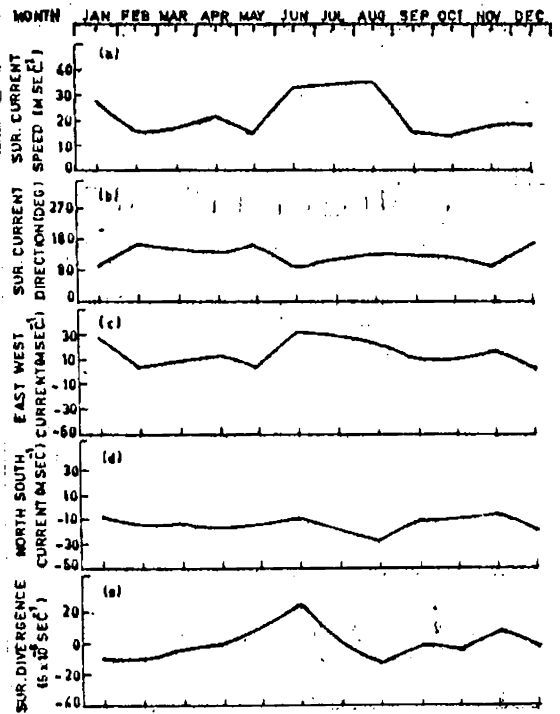(e) SURFACE DIVERGENCE (SUBAREA-6)

FIG. 3.8 ANNUAL CYCLE OF (a) SURFACE CURRENT
(b) SURFACE CURRENT DIRECTION (c) E-W CURRENT
COMPONENT (d) N-S CURRENT COMPONENT AND
(e) SURFACE DIVERGENCE (SUBAREA-7)

FIG. 3.9 ANNUAL CYCLE OF (a) SURFACE CURRENT
(b) SURFACE CURRENT DIRECTION (c) E-W CURRENT
COMPONENT (d) N-S CURRENT COMPONENT AND
(e) SURFACE DIVERGENCE (SUBAREA-8)

The reverse trend observed later indicates the dominant

influence of the net heating from February onwards

(Fig. 2.10). The moderate divergence indicated during

May-July with a maximum (about 25 units)does not

contribute to deepening of MLD till June. Moderate

convergence (-12 units) is found to act in unison with

the convective deepening (Fig. 2.10) from June to August.

The weak convergence apparent in the present analysis

from September to October is not reflected in the shoaling

of MLD observed during that period (Fig. 2.10). Basil

Mathew (1982)has reported similar moderate weak convergence

near the west coast of India derived from surface currents

during the period. The divergence indicated during

November does not seem to affect the layer as the observed

mixed layer deepening due to winter cooling is more.

A weak convergence is indicated during December which may

supplement the layer deepening in winter (Fig. 2.10). The

pattern of sinking due to convergence is also indicated

by the north flowing coastal currents in this area during

the month (Varadachari and Sharma, 1967).

3.9   Internal waves (Fig. 3.10)

The spectrum of the internal waves during the

southwest monsoon (June) periods in the central Arabian Sea

comprises several harmonic oscillations with periods ranging

from 6 hrs to 192 hours. Following Roberts (1975) they may

be categorised under two viz., short period (less than

12 hrs)and long period (greater than 12 hrs) internal waves.

SAMPLE STRENGTH = 64
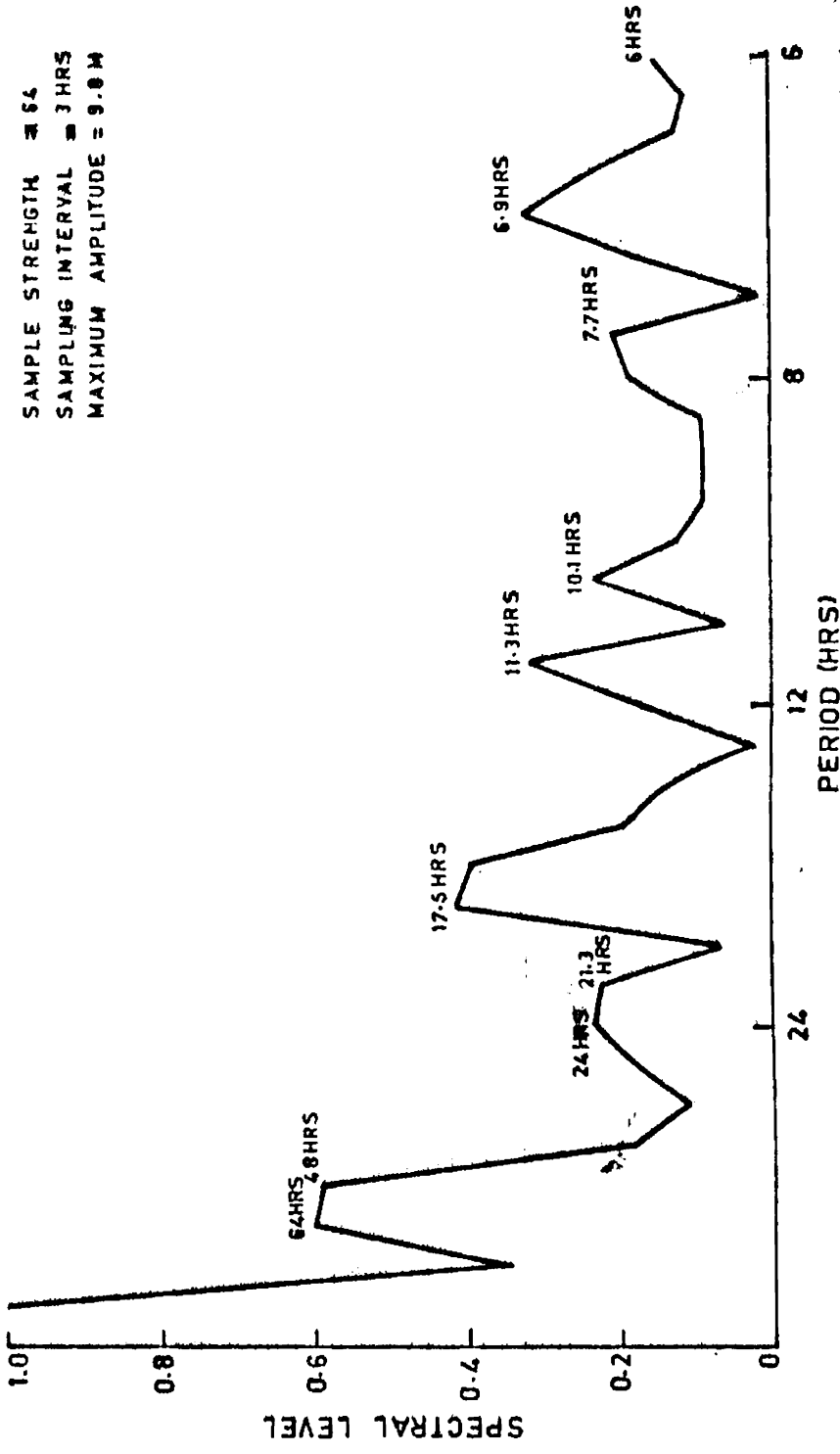SAMPLING INTERVAL = 3 HRS
MAXIMUM AMPLITUDE = 9.8 M

FIG. 3.10 SPECTRAL CHARACTERSTICS OF MIXED LAYER DEPTH OSCILLATION AT 10° 30'N, 66E

3.9.1   Short period internal waves

The predominant periods of the short period internal oscillations in MLD are around 6.9 hrs (maximum) amd 11.3 hrs with amplitudes around 3 m in the central Arabian Sea. The lower modes of short period internal oscillations have periods of 6 hrs, 7.7 hrs and 10.1 hrs with amplitudes between 1.5 m and 3 m. Using time series 3 hourly data sets, Ramam et al. (1979)reported short period oscillations with periods ranging from 5 to 11 hrs at a depth of 50-60 m in the central Arabian Sea during May-June with the internal wave height varying from 3 to 4 m (corresponding to amplitudes of 1.5-7 m). This agrees well with the present amplitudes of the short period internal oscillations in MLD. The variability of short period internal waves for the other months of the year is not available.

3.9.2   Long period internal waves

The long period components of MLD oscillations show increased amplitudes at the higher periods. The predominant peaks of energy occurs at harmonics with periods of 64 hrs (near inertial) 48 hrs, 24 hrs, 17.5 hrs and 16 hrs. The near inertial oscillations exhibit an amplitude range of about 6 m. The overall distribution of amplitude of the long period oscillations shows a range of 4-10 m. The range of amplitudes is of the same order of magnitude (4-5 m) of internal tides of both diurnal and semidiurnal periods (12 hrs and 24 hrs)reported by

La Fond and Rao (1954) in the Bay of Bengal.

The amplitudes inferred from the present study
fall within the range 1.5-10 m and a combination of one or
more of these components may occur simultaneously with
large amplitudes of layer depth.

The variability of internal waves is related to
the variability in the causative factors like wind and
air pressure fluctuation (Schott, 1971) and storms
(Pollard, 1972) and currents (Roberts, 1975) and bottom
irregularities. Seasonal and spatial variations of these
in the Arabian Sea have profound influence on the internal
oscillation which could not be examined from this data
set . However, under short time scales upto inertial
periods the MLD variability can be upto about $\pm$ 10 m
during the intense southwest monsoon regime over the mean
observed layer for a duration upto 8 to 10 hrs as observed
from this analysis.

CHAPTER IV

CHAPTER IV

SPATIAL AND SEASONAL VARIABILITY OF MIXED LAYER DEPTH

The variation of mixed layer depth (MLD) in the time and space domains is the result of combined action of many factors namely the heat exchange between the ocean and the atmosphere at the surface, lateral advection and subsurface mixing by wind/wave action and convection, convergence/divergence induced by oceanic currents, internal waves and the consequent vertical motions. As explained in chapter III, temporal and spatial variations of these factors have a profound influence on the variability of MLD in the ocean.

An analysis of the observed monthly variation of the MLD along selected longitudes, viz., 60° E, 65° E, 70° E and 75° E in the study area is presented in this chapter by means of latitude-time diagrams using data derived from Robinson et al. (1979) and the results are discussed. Seasonal (winter and pre-monsoon)distributions of wind speed, SST and MLD are presented for the northern Arabian Sea utilising data of OCEANAVEX. This presentation is substantiated also by 5 space sections of MLD in the northern Arabian Sea depicting the seasonal differences.

4.1   Meridional variation of MLD (Figs. 3.1 to 3.4)

4.1.1   January

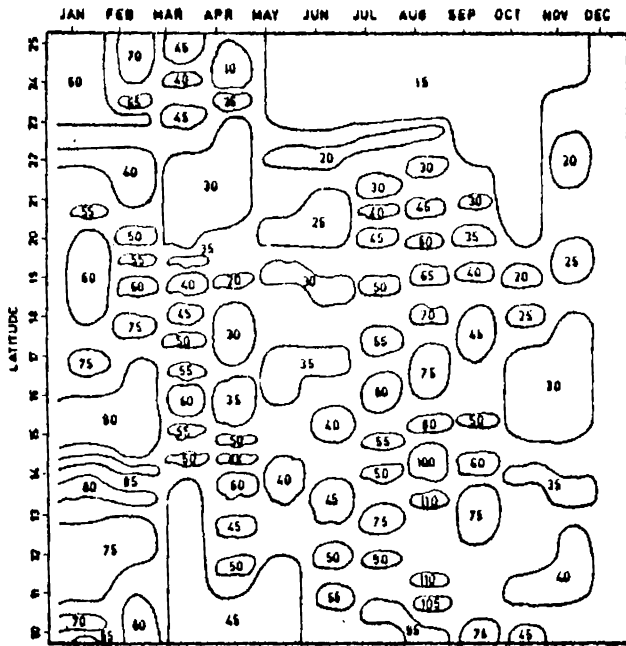Mixed layer depths of the order of 60 m are seen along 60° E (Fig. 3.1) in the northern latitudes near the

FIG. 4.1 Latitude–Time Diagram of Mixed Layer Depth (M) Distribution Along 60°E Longitude Between 10–25°N
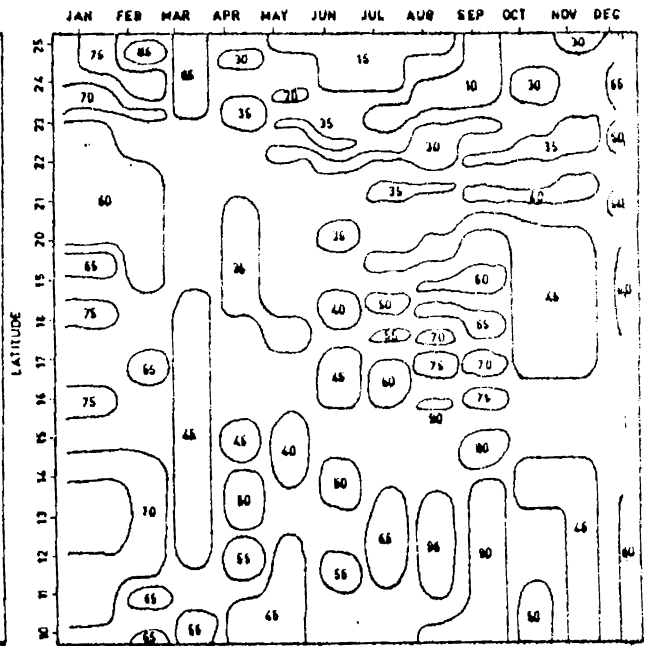

FIG. 4.2 Latitude–Time Diagram of Mixed Layer Depth (M) Distribution Along 65°E Longitude Between 10–25°N
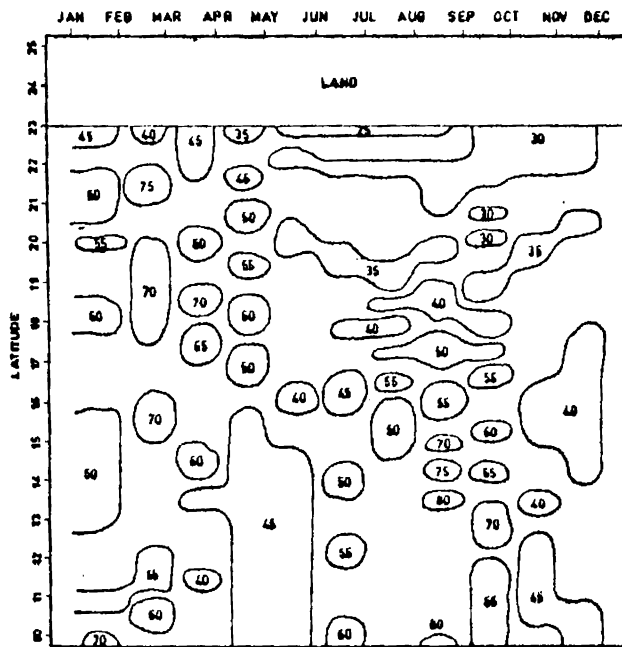

FIG. 4.3 Latitude–Time Diagram of Mixed Layer Depth (M) Distribution Along 70°E Longitude Between 10–23°N
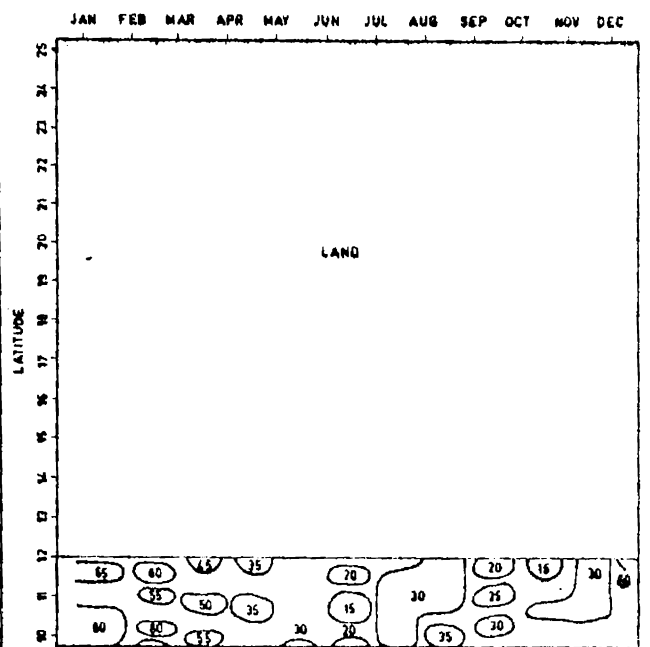

FIG. 4.4 Latitude–Time Diagram of Mixed Layer Depth (M) Distribution Along 75°E Longitude Between 10–12°N

Arabian and Oman coasts. Deeper mixed layers (about 90 m)found at the mouth of the Red Sea decrease southwards. The deeper values of the Arabian and Somali coasts reflects the winter convection though convergence of southeasterly and northeasterly flows in these areas during the month (Varadachari and Sharma, 1967) may supplement this.

Along 65° E (Fig. 3.2) deepest MLD (75 m) is observed at the northern end and between $15-18^{O}$ N in January as a result of the convergence present. The mixed layer shoals southwards probably due to the presence of weak anticlockwise vortices which are present during this time.

Along 70° E (Fig. 3.3) representing eastern section of the Arabian Sea shows deeper MLD upto 70 m towards north of 19° N latitude. Southwards the layer depth is 60 m or less upto 45 m.

Coastal areas of the southeast Arabian Sea represented by the section along 75° E between $10-12^{O}$ N latitudes (off Kasaragod to Cochin) show MLD range of 65-70 m.

4.1.2   February

Excepting the eastern longitude of 75° E, MLD distribution along all other longitudes of study shows an increasing trend or persistance in MLD in February. Along 60° E (Fig. 3.1) the northernmost latitudes show maximum

layer depth upto 70 m, which decreases between 18-22° N
with values ranging between 40-60 m. The winter maximum
of the eastern central Arabian Sea (90 m) due to a
convergence zone is retained throughout this month. MLD
decreases south of 18° N.

The meridional section along 65° E (Fig. 3.2)shows
a maximum MLD (85 m) between 24-25° N due to a convergence
zone inside an anticlockwise circulation which is beginning
to form in the month as evident from Fig. 3.1. The layer
shoals towards the lower latitudes between 22 to 19° N to
a minimum (60 m) and then a southward increase of MLD
around 65-70 m is observed upto 10° N.

Along the eastern meridian of 70° E (Fig. 4.3),
northern areas show a decrease in the MLD (60 m) near
Gujarat coast. However, southwards upto 15° N the MLD
is deeper ranging between 70-75 m and decreases farther
south.

Along the coastal zone represented by 75° E
longitudinal section (Fig. 4.4) off the west coast areas
from Kasaragod to Cochin (10-12° N) MLD range between
60-65 m.

4.1.3   March

All meridional sections (latitude-time diagrams)
indicate a decrease in mixed layer depth due to the spring
heating beginning in March. Along 60° E (Fig. 4.1) MLD
ranges between 30-45 m in the northernmost latitudes near
Iran and Gulf of Oman indicating a southward downslope of

the mixed layer surface. This may be attributed to the
presence of an anticyclonic circulation system in the
Arabian Sea whose periphery coincides with the northern
areas with easterly currents causing coastal divergence.
The layer depth increases southward to a maximum of 60 m
around 15° N and then decreases to 45 m at the southern
boundary of the study area. Decrease in slope towards
south and north of 15° N in the MLD suggests a convergence
around 15° N during March.

Along 65° E (Fig. 4.2) MLD variation from $10-25^O$N
ranges between 55-45 m showing a minimum range of variation
across the latitudes during this month. This suggests the
stable formation of the flow pattern without any lateral
reversals of current due to interplay of smaller circulatory
vortices.

The meridional section along 70° E shows (Fig.4.3)
shallower layers of Gujarat upto 45 m. Towards south MLD
increases to a maximum of 75 m around 18° N. This can be
the result of the convergence induced by the anticyclonic
gyre centred in the Arabian Sea during this time. The mixed
layer decreases further southward to about 40 m near 12° N
and then increases to about 60 m around 10° N, showing a
wavy pattern induced probably by a secondary anticyclonic
cell around 10° N (Varadachari and Sharma, 1967).

Near shore waters (meridional section along 75° E)
exhibit MLD range of 50-55 m between 10-12oN latitude
(Fig. 4.4).

4.1.4   April

The effect of spring heating is maximum during this month with shallow surface layers in the annual cycle. The general flow characteristics indicated are northeasterly, easterly and southeasterly north of 15° N latitude. Along the western boundary of the study area (Fig. 4.1) meridional variation of the MLD is less southwards upto 17° N with values ranging between 20-30 m. The mixed layer upsloping south and north of 14° N suggests a trough centred at this latitude due to the presence of the anticyclonic (clockwise) circulation in the area.

Along the central longitude of 65° E (Fig. 4.2) northern areas have minimum MLD possibly due to the divergence of coastal flow with easterly components. A southward increase in the MLD reaching a maximum(about 60 m) between $13-14^O$ N latitudes is followed by a decrease southward upto 45 m towards the boundary of the study area. A trough in the topography of mixed layer surface induced by a clockwise circulation around the area is indicated along this section also.

The MLD is minimum of about 35 m off Gujarat along 70° E (Fig. 4.3). Southwards the mixed layer increases to reach a maximum of 60 m around 18° N and then it decreases southwards towards the boundary of the study area.

Coastal distribution of MLD along 75^ON(Fig.4.4) between $10-12^O$ N latitudes shows a value of about 35 m.

4.1.5   May

The distribution of MLD along 60° E (Fig. 4.1) suggests the beginning of shoaling tendency of MLD to 15 m in the northern areas of Iran/Pakistan and Gulf of Oman. The MLD increases uniformly towards south with a maximum (45 m) occuring around 10° N.

Along 65° E (Fig. 4.2) shallowest surface mixed layer of 15-20 m is observed at the northernmost latitudes between 20-25° N. A gradual increase of the MLD southwards upto about 55 m is indicated.

The meridional distribution of the MLD along the eastern section of 70° E (Fig. 4.3) exhibits a similar north-south downsloping from about 25 m at 23° N to 45 m between 10-15° N. The downsloping of MLD southwards suggests that the major flow is easterly which is in agreement with the flow pattern presented by Wooster et al. (1967) for the area.

The coastal section along 75° E (Fig. 4.4) shows MLD around 40 m for the areas off Kasaragod and Cochin.

4.1.6   June

In the western Arabian Sea during this month (along 60° E represented by Fig. 4.1) the meridional distribution of the MLD reflects the influence of southwest monsoonal current regime. The significant feature is the northsouth downsloping of the mixed layer surface with about 15 m off Iran/Pakistan and Gulf of Oman, 35 m off

Arabian coast and 55 m towards the southern end of the study area.

The central meridional section along 65° E (Fig.4.2) also presents a similar pattern as that of the western section with a north-south downsloping of the MLD ranging from 15 m at the north to 55 m at the south.

Along 70° E (Fig. 4.3) slightly greater MLD of about 25 m is observed at the northern latitude near Pakistan and Indian coastal zone. The mixed layer increases southward to 45 m around 16° N with a further increase upto 60 m at about 10° N.

Near the west coast of India along 75° E (Fig.4.4) between 10° and 12° N a shallowing tendency of the MLD (upto 20 m) from the deeper values during April and May is observed in the coastal zone. This reflects the upwelling tendency of the coastal waters along the western section as observed by Colborn (1975) and Banse (1968). However, intense upwelling due to shoaling of isotherms are restricted only to the continental shelf zone of less than 300 km width (Shetye, 1984).

4.1.7   July

The distribution of MLD along the eastern boundary of the study area represented by 60° E (Fig. 4.1) displays marked change induced by the southwest monsoonal force active during the period. In the northern latitudes between 23-25° N the mixed layer is shallower indicating current-induced divergence of the surface water along the

northern Arabian Sea coastal zones near Iran/Pakistan and
Gulf of Oman by an easterly flow.   The surface divergence
in this area is also indicated by the prevailing surface
wind system blowing towards northeast (Wooster et al., 1967) .
A southward increase in the mixed layer progressively to
about 60 m around 15° N and 75 m around 12° N is observed.
Mixed layer deepening upto 95 m is noticed around 10° N.
Though the intensification of any anticyclonic system is
not apparent during this month in the central or southern
Arabian Sea, the location of the deeper mixed layer
coincides with a convergence indicated by Varadachari and
Sharma (1967).   Layer deepening due to extensive monsoonal
cooling and resulting convective turn over to a maximum by
50 m in the southcentral Arabian Sea for a duration of
5 weeks has been reported by Rao et al. (1981).

Along the central section of 65° E (Fig. 4.2), due
to the effect of wind and current induced divergence ,
shallower MLD (15 m) is indicated to prevail during this
month also.   Southward increase in MLD due to the major
easterly flow in the Arabian Sea becomes more
(60-65 m) as a result of excessive cooling in the central
and southcentral Arabian Sea during this month.

The eastern section of 70° E (Fig.4.3) shows an
increase in the MLD from June to July upto about 25 m
suggesting the effect of mid-summer cooling.   The mixed
layer increases southward to about 60 m around 15° N.

The coastal zone off Kasaragod to Cochin along
75° E (Fig. 4.4) experiences a dip in the MLD to 30 m
showing a cessation of the shoaling tendency observed
during June . Colborn (1975) observed a secondary
deepening in MLD in July-August especially in the areas
far south and west, which agrees with the present analysis.

4.1.8   August

Along the western boundary of the study area
represented by 60° E (Fig.4.1) the areas near Iran/Pakistan
coast have shallower MLD (15 m). Towards the central
Arabian Sea MLD deepens to values of 70-80 m. The MLD
is deepest at the southern extent of the section where
values upto 110 m are observed. As in the case of the
previous month the deeper values at the southern end are
due to the excess surface cooling by net heat loss and
advection (Sastry and D'Souza, 1970).

The meridional distribution of MLD along 65° E
(Fig.4.2) displays a general dip to deeper depths due to
the effect of mid-summer cooling acting to deepen the surface
layer by increased convection. Northern areas have a
lower surface layer of about 15-20 m while southwards the
layer is deeper ranging from 45 m at 20° N to 95 m at
12° N. Overall effect of the prevailing southwest monsoon
winds causing increased evaporation and cloudiness thereby
cooling the surface layer is apparent.

The eastern section along 70° E (Fig.4.3) shows
the persistence of the layer depth at the same level as

that of the previous month (about 25 m) in the northern

areas off Indus River mouth and Gujarat. Cessation of

the upwelling tendency observed during the previous

monsoonal months for these northern latitudinal areas

is indicated from the latitude-time diagram. Towards

south the MLD increases to about 80 m at the boundary of

the study area which is the maximum due to the layer

deepening during the month.

The coastal section along 75° E (Fig. 4.4)suggests

a similar tendency of cessation of the deepening processes

at the end of the southwest monsoon.

4.1.9   September

During this month shallow layers upto 15 m is

present from 25° N to 22° N along 60° E (Fig. 4.1) showing

the effect of upwelling near the coasts off Iran/Pakistan,

Gulf of Oman and Arabia (Quraishee, 1984). The MLD

ranges from 50 m at 15° N to about 75° N at the southern

limit of the study area.

The central section along 65° E (Fig.4.2) shows the

areas along the eastern half of the Pakistan coast having

slightly deeper mixed layers (about 20 m) indicating the

beginning of a deepening motion attributable to sinking.

Quraishee (1984) observed the deepening due to the cross-

wind orientation of the coast and the presence of mesoscale

anticlockwise eddies near eastern part of the Pakistan

coast. However, sinking motion in this area may be due to

the continuation of the mid-summer cooling and the resulting convective deepening. South of 20°N latitude the mixed layer is deeper upto 90 m near the southern limit of the study area.

The eastern Arabian Sea section along 70° E (Fig. 4.3) exhibits similar characteristics of deepening of MLD as in the previous month towards the northern latitudes where a layer depth upto 30 m is observed. From 18 to 15° N the mixed layer ranges between 40-65 m.

Along the coastal zone between 10° - 12° N (Fig.4.4) the MLD is found to vary between 20-30 m. The upwelling influence observed in the previous month is indicated to persist.

4.1.10 October

The month of October marks the beginning of transition period from the southwest to the northwest monsoon and the secondary warming due to the clearer skies and reduced upward moisture flux results in the shoaling of MLD in a significant portion of the western Arabian Sea. Shoaling of MLD due to the secondary warming makes the mixed layer shallower upto 15 m between $21-25^{\circ}$N. The shoaling effects due to the upwelling along the western portion of the Pakistan coast is probably due to the coastal current divergence at the periphery of the anticyclonic flow present during this time(U.S. Navy Hydrographic Office, 1960). The MLD shows an increase southward to about 30 m at 15° N and 45 m at the end of the study area.

In the central Arabian Sea along 65° E (Fig.4.2)
MLD in the northern area off the Pakistan (eastern) shelf
exhibits sinking characteristics as a result of a probable
wind induced deepening along the eastern coastal zone.
Shoaling effect of mixed layer due to secondary warming
observed in the southern areas is masked in this zone
by wind induced divergence. MLD shows increasing tendency
(upto 45 m) between 17 to 20° N. The surface layer remains
almost same southwards upto the limit of the area.

Along 70° E (Fig. 4.3) offshore areas in the
north near Gujarat and the Indus Delta shows a persistence
of MLD from the previous month (30 m). A southward
increase in the MLD is weak ranging from 30-45 m. The
shallowing effect of the MLD in the southern areas can
be related to the secondary warming during the month.

Along the coastal section off the west coast of
India between 10-12° N (Fig. 4.4) the MLD exhibits
deepening trend indicative of the coastal convergence and
sinking due to the northerly and northeasterly surface
currents prevailing during the month as part of the newly
formed cyclonic (anticlockwise) circulatory system in the
southcentral Arabian Sea (U.S. Navy Hydrographic Office,
1960).

4.1.11 November

The western section along 60° E (Fig. 4.1)
indicates the beginning of sinking/deepening of MLD in
the northern areas off the Arabian Coast and the Gulf of

Oman, but retaining the shallow mixed layers of 15 m at the northern most areas off Iran/Pakistan. The changed wind pattern causes sinking near the Arabian coast and the Gulf of Oman while western Pakistan coasts experience a shoaling of mixed layer. South of 19° N the features are almost similar to that of the previous month.

Along 65° E (Fig. 4.2) northern areas experience deepening of the MLD between 22-25° N. South of this, MLD ranges between 45-50 m upto the southern boundary. Shoaling of MLD evident in the southern areas is probably induced by the divergence of northeast monsoon drift in the area (Colborn, 1975).

The eastern section along 70° E (Fig. 4.3)exhibits sinking tendency in the mixed layer between 20-25° N, which is mainly due to the net cooling during winter. The MLD variation in this area is between 30-35 m. Towards south the variation in the layer depth is very much weak between 40-45 m.

The coastal section between 10-12° N (Fig. 4.4) displays the presence of shallow mixed layer off the coastal zone from Kasaragod to Cochin.

4.1.12   December

Winter deepening due to convection is active during this month as indicated by the western section along 60° E (Fig. 4.1). Near the northern latitudes the MLD is about 45 m off the coast of Iran/Pakistan and increases afterwards

to about 50 m off the Arabian coast. Southwards the layer depth increases.

Along 65° E (Fig. 4.2) MLD is about 55 m in the northern areas and increases southward to about 60 m upto the southern limit of the study area.

Eastern Arabian Sea area represented along 70° E (Fig. 4.3) also shows a northsouth range of 45-50 m in the MLD from the coastal zone off Gujarat and Indus Delta to about 11° N.

The coastal section between 10-12° N (Fig. 4.4) exhibits deeper mixed layer during the month (60 m).

4.2   Seasonal variability of MLD in the northern Arabian Sea

The BT data along with the surface meteorological information on wind speed, SST and MLD collected during OCEANAVEX (1973-74) have been analysed and presented in the form of seasonal charts for discussion under 2 climatic regimes namely winter (December, January and February) and pre-monsoon (March, April and May)(Figs. 4.5 to 4.10). The seasonal variability of MLD is also discussed with the aid of four space sections (Figs.4.11 to 4.16)depicting winter and pre-monsoon distributions.

4.2.1   Winter (December, January and February) (Figs. 4.5,4.7&4.9)

During the season,winds (Fig. 4.5) are mainly northerly with easterly components in the northeastern part and weak westerly components in the northwestern

part of the Arabian Sea (India Meteorological Department, 1975). Strongest winds are observed off the coasts of Bombay and Gujarat with maximum values of mean wind speeds upto 20 kts. Off the northern Arabian coasts wind speeds are moderately high while off the Iran coast winds are weaker.

The SST distribution during winter (Fig.4.7) shows a warm temperature cell off Bombay around 26° C with the temperature decreasing to about 24° C off Gujarat. A cold cell centred around 23° C is found off Iran and Pakistan at the mouth of Gulf of Oman.

The MLD (Fig. 4.9) generally shows an increasing trend from about 120 m at the mouth of the Gulf of Oman to about 140 m off Iran reaching a maximum value around 190 m off Pakistan indicating a trough like feature. The configuration of MLD resembles a dome centred around 110 m between $23-24^O$ N and $61-64^O$ E off the Arabian coast. Towards north the variation of mixed layer is from 60 to 110 m. There is an extensive ridge between $20-23^O$ N and $61-65^O$ E with a minimum of 50 m at the centre. Another trough with a maximum layer of 70 m at the centre is located between $21-22^O$ N and $61-62^O$ E. Off Gujarat ($20-22^O$ N and $67-70^O$ E) an extensive trough with central values of layer depth upto 120 m are observed. Off Bombay a trough with a central deep layer upto 100 m is found with shallower layers (about 70 m) on the periphery.
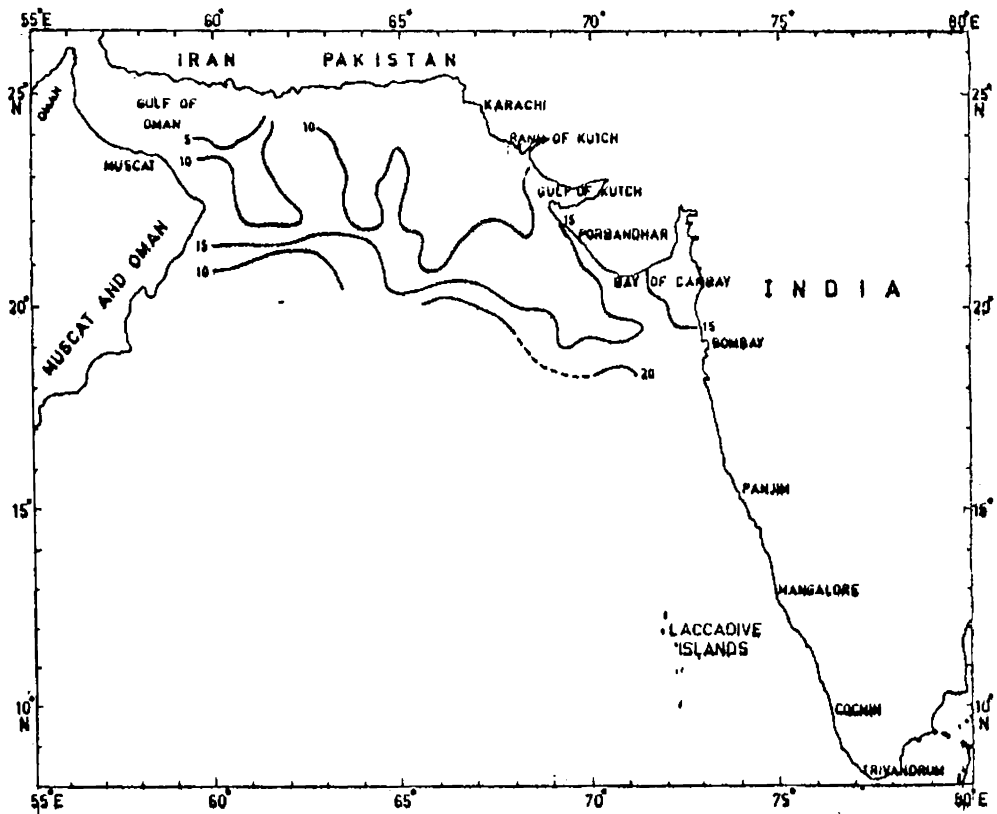
FIG.4.5 WIND SPEED (IN KNOTS) DISTRIBUTION IN THE NORTHERN ARABIAN SEA
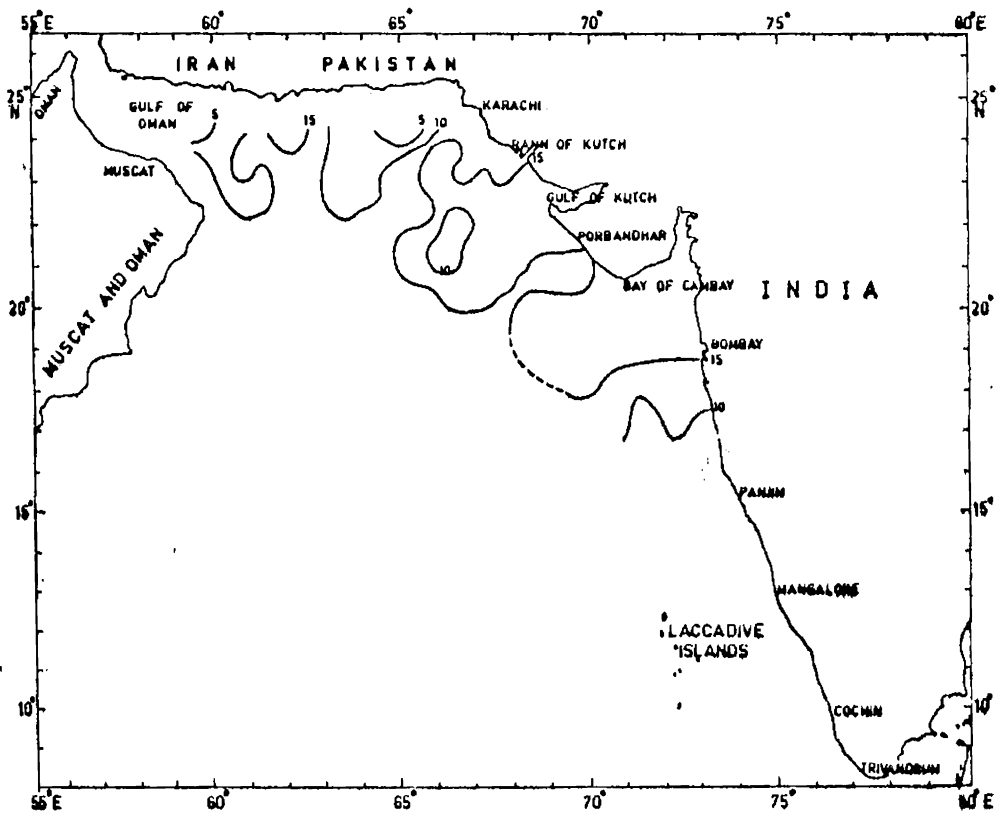DURING WINTER (DECEMBER, JANUARY AND FEBRUARY)

FIG.4.6 WIND SPEED (IN KNOTS) DISTRIBUTION IN THE NORTHERN ARABIAN SEA
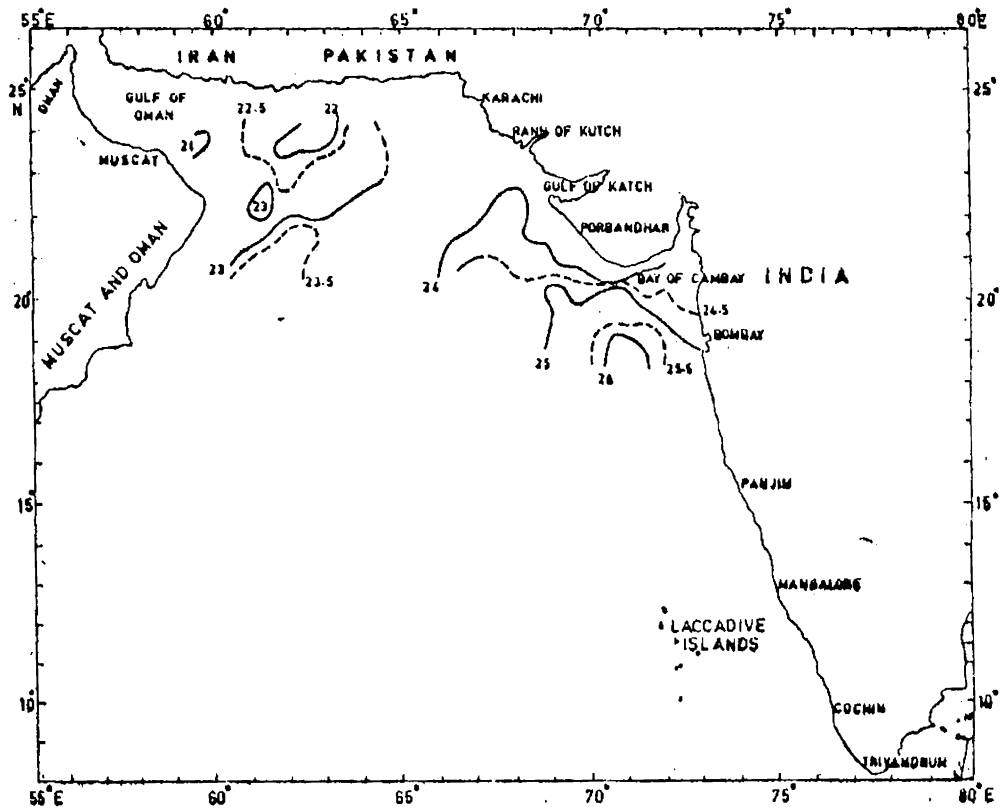DURING PRE-MONSOON (MARCH, APRIL AND MAY)

FIG. 4.7 SEA SURFACE TEMPERATURE (IN DEGREES CELSIUS) DISTRIBUTION IN THE NORTHERN ARABIAN SEA
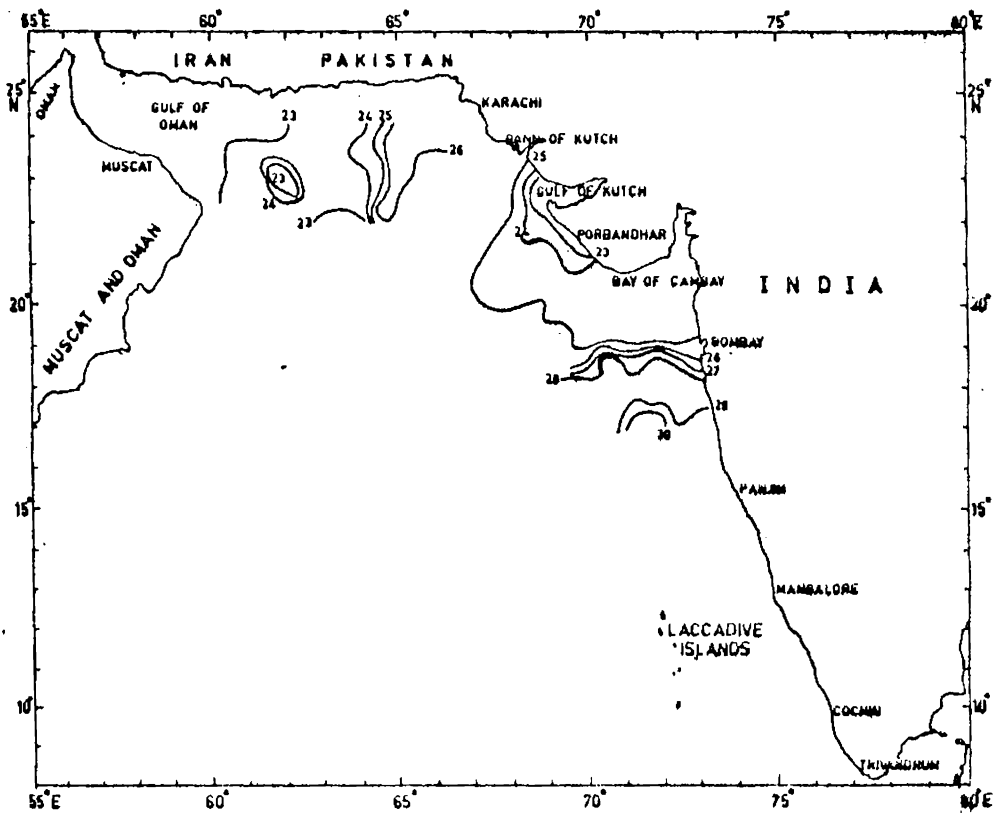DURING WINTER (DECEMBER JANUARY AND FEBRUARY)

FIG. 4.8 SEA SURFACE TEMPERATURE (IN DEGREES CELSIUS) DISTRIBUTION IN THE NORTHERN ARABIAN SEA
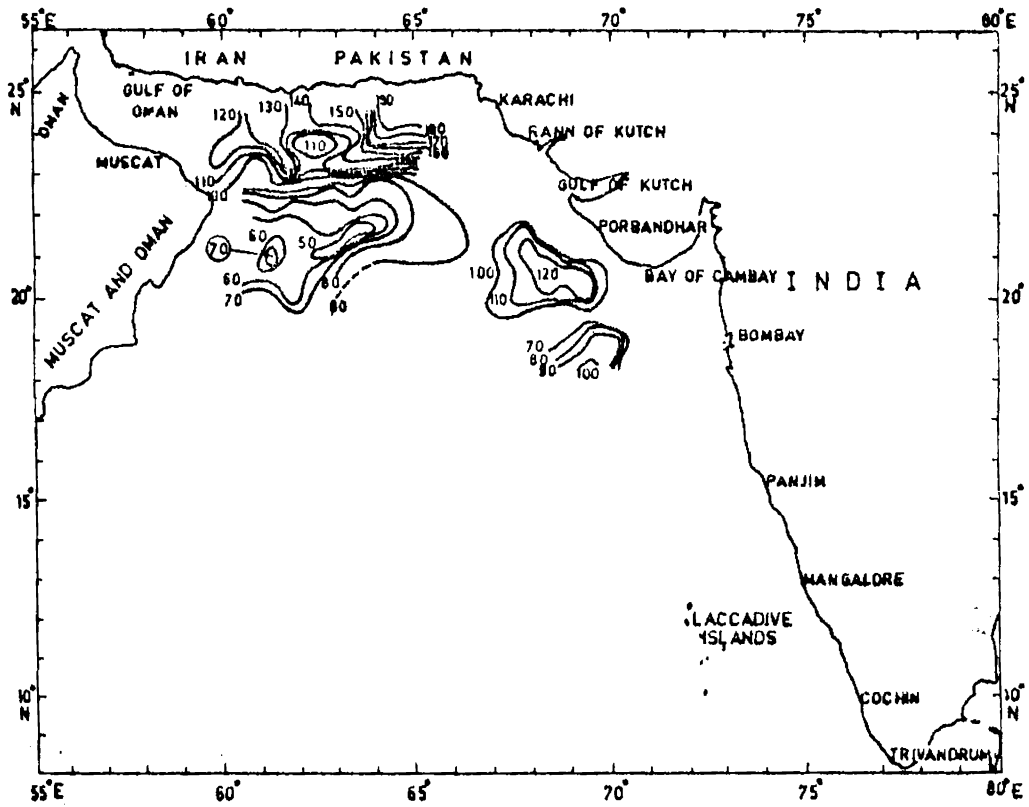DURING PRE-MONSOON (MARCH APRIL AND MAY)

FIG.4.9 MIXED LAYER DEPTH (IN METERS) DISTRIBUTION IN THE NORTHERN ARABIAN SEA DURING WINTER (DECEMBER, JANUARY AND FEBRUARY)
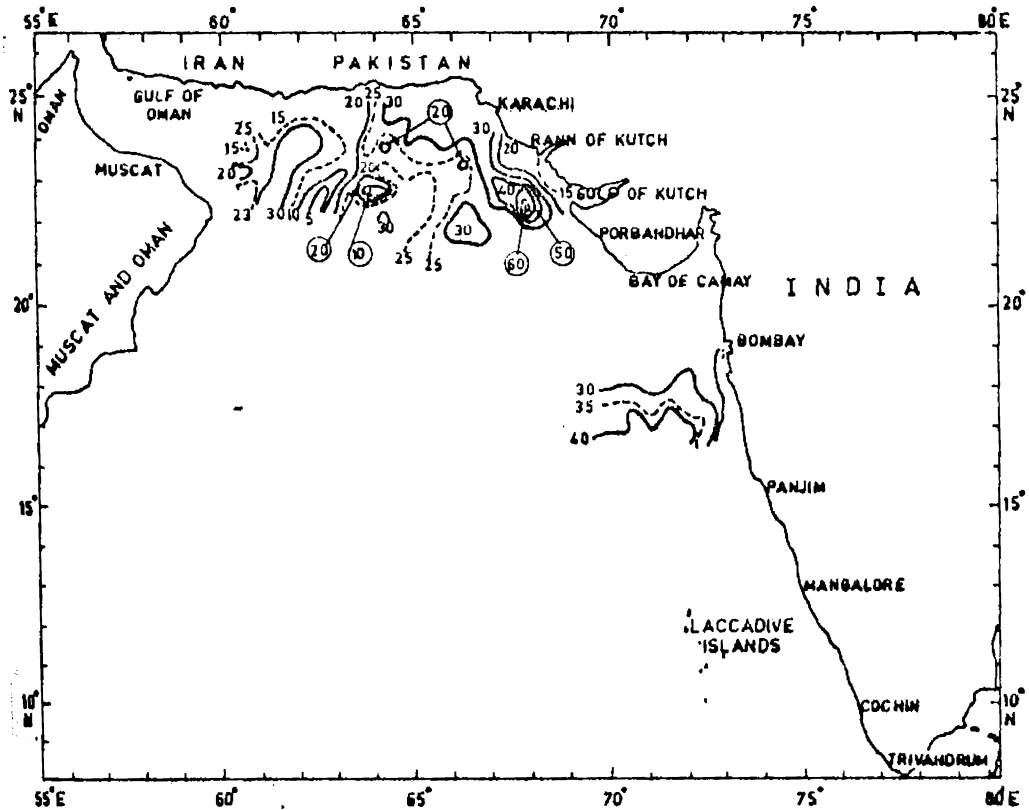

FIG.4.10 MIXED LAYER DEPTH (IN METERS) DISTRIBUTION IN THE NORTHERN ARABIAN SEA DURING PRE-MONSOON (MARCH APRIL AND MAY)

The MLD distribution with a ridge or dome in
the northern Arabian Sea, Gulf of Oman and off Iran/
Pakistan bears a close correlation to the cyclonic
(anticlockwise) circulation existing from December to
January inducing divergence as seen from Fig. 3.1 (after
Varadachari and Sharma, 1967) and from Knox and Anderson
(1985). Divergence is also evident by the cold water cell
at the mouth of Gulf of Oman observed in the present study.
The near coastal troughs off Gujarat and Bombay will have
more relevance to convergence caused by anticyclonic
system under formation in February.

4.2.2   Pre-monsoon (March, April and May)(Figs.4.6,4.8 &4.10)

The premonsoon period is characterised by low
mean wind speeds blowing mainly from west with southerly
and northerly components over most of the northern Arabian
Sea area (India Meteorological Department, 1975). The mean
wind speeds (Fig. 4.6) are maximum off Bombay, in the Bay
of Cambay and off Gujarat ranging between 10-15 kts. In
the northwestern portion, minimum speeds of 5 kts are
observed.

The sea surface temperature is warmer (Fig. 4.8)
especially towards the southern part of the observational
area. Off Ratnagiri,the sea surface temperature is as
high as 30° C as a result of spring heating. Northward
decrease of temperature with a sharp lateral gradient
perpendicular to the coast, south off the Bay of Cambay
is observed. Off Gujarat and the Rann of Kutch, coastal

waters are with low temperature (about 23° C) and an
offshore increase in temperature is indicated. At the
mouth of Gulf of Oman surface water temperatures are low
with a cold water cell centred around 23° C. The north-
western portion has higher temperatures from 24 to 26° C
with an east-west gradient.

MLD distribution in the northern Arabian Sea
during premonsoon (Fig. 4.10) is characteristic with
shallower values as a result of spring heating. At the
mouth of Gulf of Oman the layer increases from 15 m at
the north to 30 m at South , adjacently forming an
extensive trough with a central value of MLD of 30 m
between 22°-24° 30' N and $61-63^O$ E. East of this the
mixed layer topography indicates domes centred at 5 and
10 m, the latter being pronounced between $22-23^O$ 30' N and
63° 30' - $64^O30'$ E. The offshore variation of MLD near
Pakistan coast shows a west to east range of 20-30 m.
Near the west coast off Gujarat mixed layer is shallow
(50 m). There is an offshore trough of mixed layer
topography near the west coast of Gujarat which is centred
around 60 m. In the near shore waters off Bombay and
Ratnagiri MLD increases from 20-40 m offshore. However,
in the offshore waters the gradient changes into a north-
south slope with deeper layers to the north.

The MLD distribution during premonsoon suggests a
correlation to the net heat exchange and circulation. At
the mouth of Gulf of Oman the extensive trough with deeper
surface layer coincides with the area of cold cell whereas

the warmer zone off the west Pakistan coast and off
Gujarat with an upslope is only indicative of the
influence of the strengthening anticyclonic flow in the
area with southerly coastal flow (Wooster et al., 1965).
The same explanation can hold good for the offshore slope
of MLD. A thickening of the surface layer off Saurashtra
(Gujarat) prior to monsoon was also noticed by Banse (1968)
off Bombay. The trough of MLD with a southward upslope
coincides with the southward increasing surface temperature
gradient which could be explained only by the presence of
the periphery of smaller anticyclonic circulation systems
in the area. A similar anticyclonic (clockwise) secondary
circulation formed southwards during March is indicated in
the charts of U.S. Naval Hydrographic Office (1960). The
present indication of a local cell can only be explained
by the northward extension or shift of a similar clockwise
eddy.

Fig.4.11 shows the plan of sections along which
seasonal variability of MLD is presented.

4.2.3   Section A1A2 along 23°45'N, off Oman (Fig.4.12)

During winter, MLD around 120 m at 60°E shoals to
100 m near 61°E and then dips towards deeper layers of
about 145 m beyond 61°30' E. The mixed layer shoals after
this to about 115 m. In the central part of the northern
Arabian Sea the mixed layer variation is less significant.
During premonsoon mixed layer is shallow ranging from 20-30 m.
There is a minimum difference of 120 m between the winter
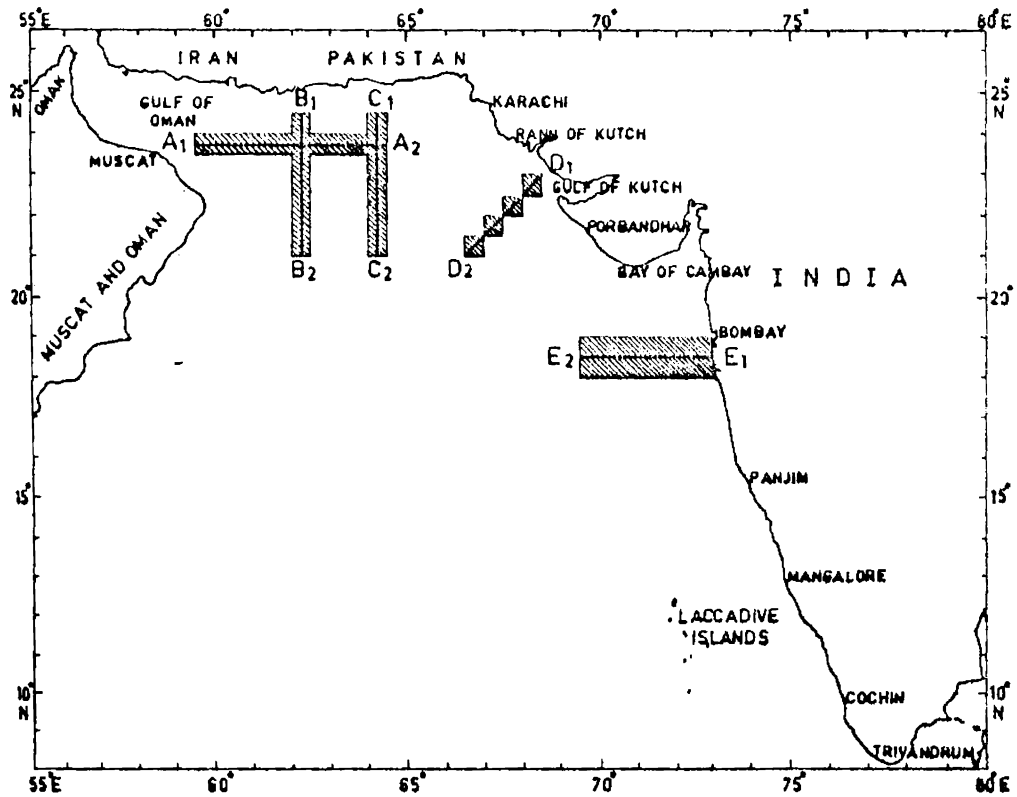and premonsoon layers observed along the section.

FIG. 4.11 SECTIONAL PLAN OF MEAN MIXED LAYER DEPTH DISTRIBUTION
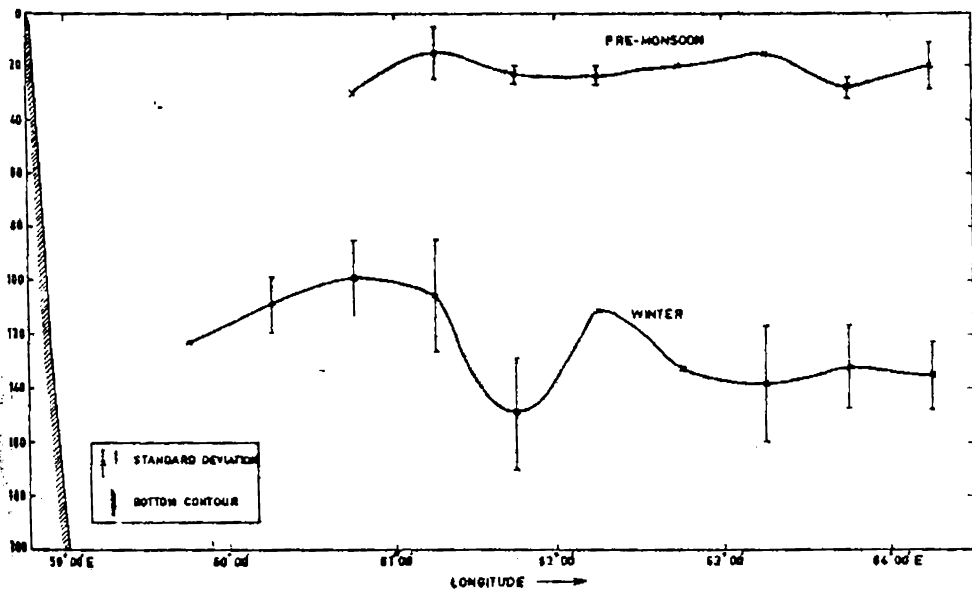IN THE NORTHERN ARABIAN SEA

FIG. 4.12 MEAN MIXED LAYER DEPTH DISTRIBUTION-SECTION $A_1 A_2$ ALONG 23° 45N (OFF OMAN)

4.2.4   Section B1B2 along 62°15'E (Fig. 4.13)

During winter the northsouth section on the western side of the northern Arabian Sea indicates an upslope of the MLD from north to south suggesting the influence of the general westerly flow in the area during winter. During premonsoon, mixed layer is shallower ranging from 5 to 20 m. The difference between the mixed layer depths during winter and premonsoon is about 125 m.

4.2.5   Section C1C2 along 64° 15'E (Fig. 4.14)

MLD slopes down northwards from a shallow depth of 60-80 m between 21-22° N to approximately 195 m off the Pakistan coast at about 24° N during winter. This slope is also indicative of the general westerly flow during the season. During premonsoon the shallower MLD along the section ranges between 10-30 m. The MLD difference between the 2 regimes is about 175 m.

4.2.6   Section D1D2 (off Kutch) (Fig. 4.15)

As there is no coverage of winter period along the section, only premonsoon distribution of MLD is presented. This section clearly shows the dip in MLD offshore from the shallow coastal values of around 25 m to 60 m and shoaling up of the mixed layers in the northwesterly direction to about 30 m. The dip in the MLD indicates a section through the trough of MLD formed possibly due to the presence of anticyclonic eddy near the coast.
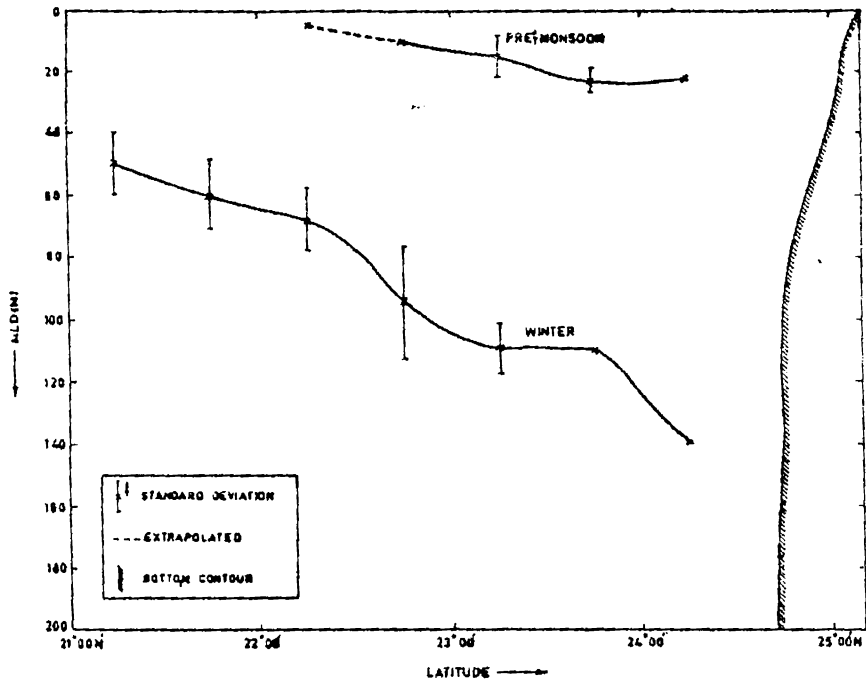
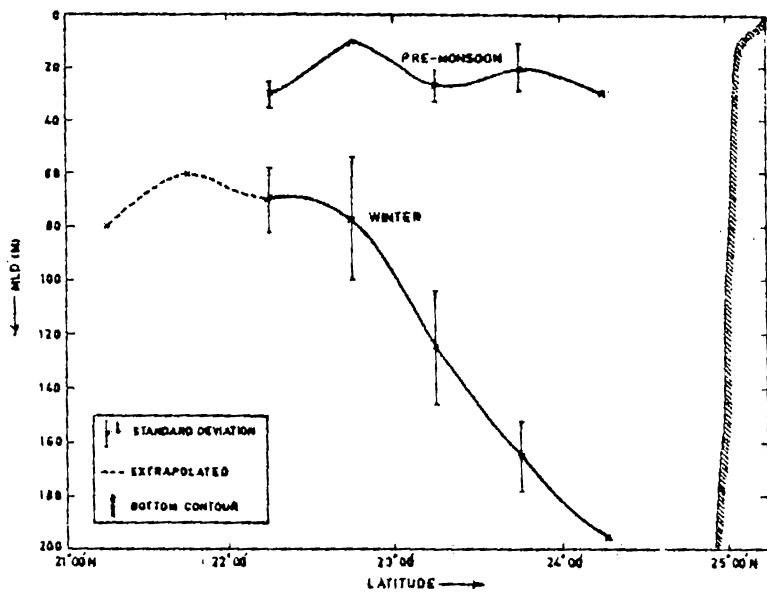FIG. 4.13 MEAN MIXED LAYER DEPTH DISTRIBUTION - SECTION B_1 B_2 ALONG 62° 15'E

FIG. 4.14 MEAN MIXED LAYER DEPTH DISTRIBUTION - SECTION C_1 C_2 ALONG 64° 15'E
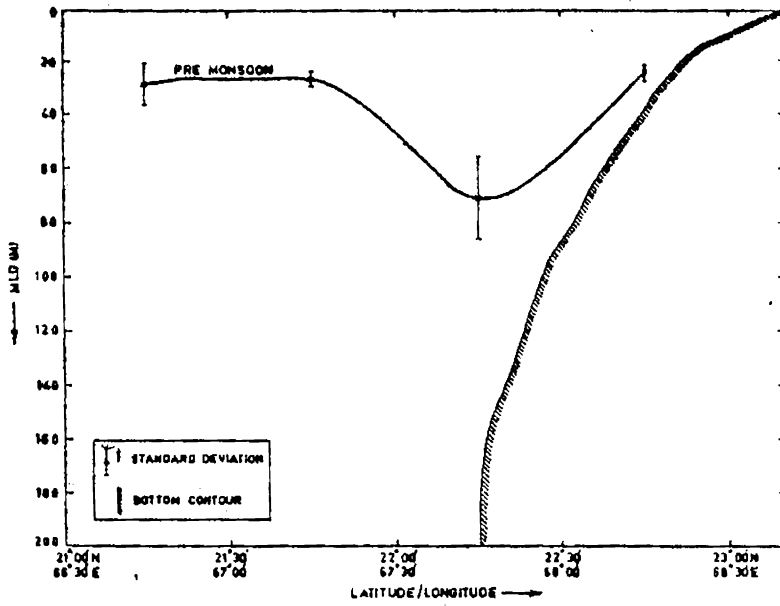
FIG. 4.15 MEAN MIXED LAYER DEPTH DISTRIBUTION SECTION D₁ D₂ (OFF KUTCH)
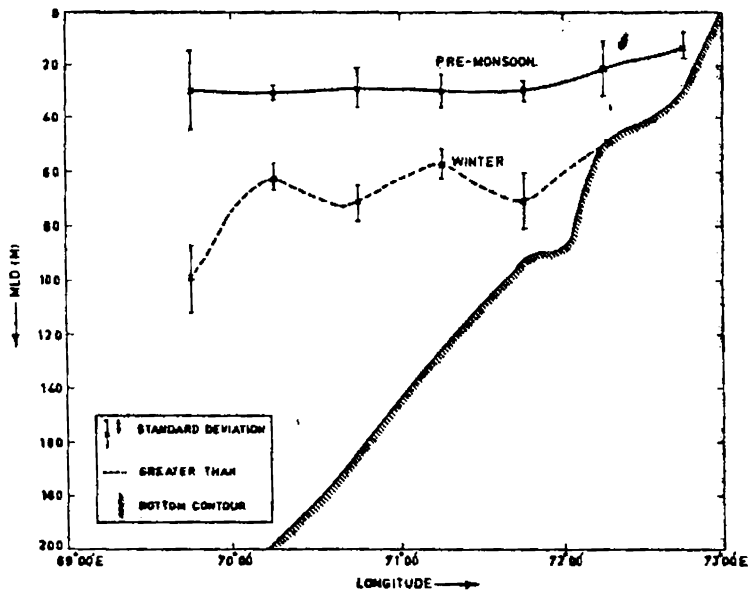
FIG. 4.16 MEAN MIXED LAYER DEPTH DISTRIBUTION-SECTION E₁E₂ ALONG 18°30′N (OFF KONKAN COAST)

4.2.7 Section E1E2 along 18°30'E (off Konkan coast)
       (Fig. 4.16)

The winter variation of the MLD indicates near

shore values ranging between 70-80 m which drops down

to about 100 m at about 200 nm from the coast. The

upward sloping of the mean mixed layer near the coast

can be explained only by the presence of southerly coastal

flow during the season. Such a flow is apparent only

from February as indicated by Varadachari and Sharma

(1967). During premonsoon the mixed layer is shallower

with coastal values upto 10-15 m increasing offshore to

a maximum of about 30 m. The maximum difference between

the two seasons in the MLD is about 70 m. The gentle

downward slope of MLD off the coast suggests the presence

of the southerly flow which is also present during March

to May.

CHAPTER V

CHAPTER V

PREDICTIVE CHARACTERISTICS OF THE MIXED LAYER DEPTH

On account of the relevance of mixed layer depth (MLD) to applications in fisheries, naval warfare and planetary boundary layer modelling, it is pertinent to evolve techniques of forecasting MLD from easily observable data such as, wind and air/sea temperatures. A number of one dimensional models have been developed to give time dependent estimates of the surface mixed layer depth using parameterisation of surface fluxes of heat, momentum (wind stress) and buoyancy. The model developed by Kraus and Turner (1967) does not take into account horizontal motion (advection) and assumes that kinetic energy is generated at surface, a constant fraction of which is used for entrainment across the interface below the mixed layer. Their expression for potential energy does not take into account frictional dissipation. Giesler and Kraus (1969), Denman (1973), Niiler (1975) and Kim (1976) have developed variants of Kraus-Turner model. Niiler (1975) showed that turbulent kinetic energy (considered earlier by Denman (1973)) dominated the energy generated by the mean shear which was taken into account by Pollard et al. (1975) for mixing a day or more. Gill and Turner (1974) pointed out that the convective release of turbulent energy is essential in addition to the energy generated by wind stress. Kim (1976) generalised the Kraus-Turner model to include both wind generated and convective release of turbulent energy

isolating non-penetrative and penetrative convection depending upon the magnitude of surface cooling. These models failed to predict the features of the thermocline and also the variation of MLD above it, over longer periods. This shortcoming arises out of ignoring advection effects in the models.

A simple one dimensional scheme is evolved incorporating methods of Laevastu and Hubert (1965) and James (1966) to give short term prediction of the MLD in deeper and shallow zones where advection effects can be assumed negligible. Earlier evaluation of this model using data from coastal waters off Cochin (Joseph, 1980) indicated that for short term predictions upto 6-10 hrs the error between the predicted and observed values of MLD was small and within the variability of diurnal and semidiurnal internal oscillations in the sea,even though advection effect had not been considered. In the present study, this scheme is evaluated for predicting MLD at the deep water station S1 ($10^{o}30'$ N,66°E and 2000 m depth) and at the shallow water station S2 ($10^{o}15'$ N,$75^{o}48'$ E and 200 m depth). In the first case 3 hourly BT and salinity data along with the meteorological data collected on board R.V. PRILIV from 7 to 19 June 1977 (92 observations) during Monsoon-77 programme, are utilised . In the second case BT and salinity data along with meteorological data (near-hourly) collected on board M.V. PRASIKSHANI on 19 January 1983 are utilised.

5.1   Description of the scheme

In a slab (continuous density model) of sea water, the change in temperature in the slab is effected mainly through the top surface of the mixed layer. Considering the lateral heat advection to be negligible, heat budget at the surface can be written as,

$$Q_N = (Q_s - Q_r - Q_b - Q_e - Q_h) \quad \ldots \ldots \quad (5.1)$$

where Q_N = the net heat gain at the surface

Q_s = incoming solar and sky radiation

Q_r = reflected radiation at the surface

Q_b = back radiation (long wave)

Q_e = evaporative/condensation heat transfer

Q_h = sensible heat transfer.

The incoming solar and sky radiation is evaluated following Lumb (1964),

$$Q_0 = 1.93 \sin\alpha \ (0.61 + 0.2 \sin\alpha) \quad \ldots \ldots \quad (5.2)$$

where Q_0 = clear sky radiation in cal cm^{-2} min^{-1}

α = solar altitude in degrees.

A correction introduced by Reed (1977) is applied to obtain an equation for insolation for cloudy sky.

$$Q_S = Q_0 \ (1 - 0.62 \ C + 0.0019 \ \bar{\alpha}) \quad \ldots \ldots \quad (5.3)$$

where Q_S = insolation under cloudy conditions in cal cm^{-2} min^{-1}

C   = cloud cover in tenths

$\bar{\alpha}$ = noon solar altitude in degrees.

It appears appropriate to use the above formula suggested for higher values of cloudiness in the tropics and subtropics.

The reflected radiation is calculated using relationship after Laevastu and Hubert (1965),

$$Q_r = \frac{3Q_S}{\bar{\alpha}} \qquad \dots (5.4)$$

where Q_r = reflected radiation in cal cm^{-2} min^{-1}.

Following Laevastu and Hubert (1965), the back radiation (long wave) is obtained as,

$$Q_b = \left(\frac{297 - 1.867\,T_S - 0.95\,U}{1440}\right)(1 - 0.765\,C) \quad ..(5.5)$$

where Q_b = back radiation in cal cm^{-2} min^{-1}

T_S = sea surface temperature in degree centigrade

U = relative humidity in percentage .

Following James, (1966) the evaporative loss is calculated.

$$Q_e = 2.46\,(0.26 + 0.04W)\,(E_w - E_a) \text{ for } E_w \gtrsim E_a \quad ..(5.6)$$

where Q_e = evaporative loss in cal cm^{-2} hr^{-1}

W = wind speed in knots

E_w = saturated vapour pressure at sea surface in millibars

E_a = vapour pressure in the air in millibars.

The sensible heat loss Q_h is obtained from

$$Q_h = 1.5 \ (0.26 + 0.04 \ W)(T_s - T_a) \quad \text{for} \ T_s \geqslant T_a \qquad \ldots (5.8)$$

where Q_h = sensible heat loss in cal $\text{cm}^{-2} \ \text{hr}^{-1}$

   T_a = air temperature in degree centigrade

   When $T_s < T_a$, a modified equation can be used.

$$Q_h = 0.036 \ W \ (T_s - T_a) \qquad \ldots \ldots \qquad (5.9)$$

5.1.1   Positive heat transfer

The change in temperature ΔT in a layer of thickness L due to heat transfer Q over a time step Δt is given by ,

$$\frac{\Delta T}{\Delta t} = \frac{QA}{100 \ C_p \rho L} \qquad \ldots \ldots \qquad (5.10)$$

where   T = the change in temperature in degree centigrade

   Q =   the net heat gain at the surface
         in cal $\text{cm}^{-2} \ \text{min}^{-1}$

   A = percentage absorption of heat for the layer

   C_p = specific heat of sea water
         (taken as 0.955 cal $\text{g}^{-1 \text{o}}\text{C}^{-1}$)

   L = thickness of the layer in centimetres

   ρ = the density of sea water in g cm^{-3}

When the heat transfer from air to sea is positive at the surface, absorption of heat takes place in the surface and subsurface layers.

If Q_0 is the initial heat energy available at the top of layer thickness L and Q_L the heat energy available

at the bottom of the layer after absorption within the thickness, the ratio of the heat energy at the top to that at the bottom of the layer is obtained by,

$$\frac{Q_0}{Q_L} = e^{-kL} \qquad \qquad \text{.... (5.11)}$$

where Q_0 = heat gain at the top of the layer in cal

Q_L = heat available at the bottom of the layer in cal

k = extinction coefficient

L = layer thickness in centimetres.

Depending on the optical characteristics of water masses, extinction coefficients have been classified by Jerlov (1951). Tables 5.1 and 5.2 are based on these data, reproduced after Laevastu and Hubert (1961), giving percentage absorption values for different water masses and depths.

Heating of the layers is considered taking into account first the net heat gain available at the surface of the different layers from surface to 150 m namely 2.5, 5, 10, 20, 30, 40 , 50, 75, 100 and 150 m by distributing the net heat gain available at the surface to the different subsurface layers using the appropriate percentage absorption values obtained from Table 5.2. Using equation 5.10, change in temperature at the respective levels is calculated and the change in the thermal structure due to positive heat transfer is accounted.

TABLE 5.1

OPTICAL WATER MASSES (AFTER LAEVASTU AND HUBERT,1965)

Category No.	Optical water mass	Characteristics	Colour (Forel scale)
1	Oceanic, clear	"Old" clear oceanic waters in productive areas (especially in low latitudes)	0 - 2
2	Oceanic, normal	Medium-productive oceanic waters in medium and low latitudes	2 - 5
3	Oceanic, turbid and coastal, clear	High productive oceanic areas, especially during plankton bloom. Tropical coastal waters, especially over sheep shelves	5 - 8
4	Coastal, normal	Normal, medium-productive coastal waters and waters over shallow shelves	8 - 10
5	Coastal, turbid	Estuarine and coastal waters during intensive plankton bloom and waters close to the coast where much sediment has been whirled up by wave action	>10

TABLE 5.2

ABSORPTION OF TOTAL ENERGY (%) IN VARIOUS LAYERS OF THE SEA
(AFTER LAEVASIU AND HUBERT, 1965)

Layer in metres from surface	Optical water mass				
	1	2	3	4	5
0 - 2.5	71.4	78.2	84.8	89.6	95.1
2.5- 5	6.8	9.1	8.1	6.5	4.0
5 - 10	7.2	7.2	4.7	3.2	0.9
10 - 20	6.6	3.7	2.0	0.6	
20 - 30	3.0	0.9	0.3	0.1	
30 - 40	1.3	0.5	0.1		
40 - 50	1.1	0.2			
50 - 75	0.9	0.1			
75 - 100	0.6				
100 - 150	0.1				

5.1.2 Wind/turbulent (mechanical) mixing

Mechanical mixing is the result of wind and wave action causing turbulent mixing and drift currents. Wind mixing does not elways produce deeper layer depths. The effect of wind mixing is to redistribute the heat gain by the surface layers. As the mixing is inversely proportional to the stability of the water column it is desirable to introduce stability factor while considering the wind mixing (James, 1966). However, in the present schedule both shallow and deep water thermal structures are found to have deeper mixed layers with negligible stability in the surface few metres, and hence the stability effect is ignored. Following Laevastu (1960) who assumed that mixing ceases where the diameter of the orbital path is less than 10cm, and the depth of wind/wave mixing is calculated as

$$D_M = 12.5 \, H_s \qquad \qquad \dots \quad (5.12)$$

where D_M = depth of wind mixing in metres

   H_s = significant wave height in metres.

The significant wave height is obtained from a relationship (Laevastu and Hubert, 1965).

$$H_s = \frac{0.0008 \, W^2 \quad 50 + (T_W - T_a)}{(1 + \frac{5 \, W}{F}) \, (1 + \frac{W}{3 \, t})} \qquad \dots \quad (5.13)$$

where   W = wind speed in m sec^{-1}

   T_W = sea surface temperature in degree centigrade

   T_a = air temperature in degree centigrade

F = fetch in kilometres

t = duration in hours

The wind mixed layers thus obtained are adjusted such that equal areas of heating and cooling with respect to the initial structure are obtained by the new position of the wind mixed layer in the final structure.

5.1.3 Negative heat transfer and convective mixing

In case of negative heat transfer (heat loss) from the surface, the increase in surface density will induce convective mixing and the depth of convective mixing is calculated from the relationship given by James (1966),

$$D_C = \left(D_0^2 + \frac{2 \, Q_L}{C_p \, \rho \, \Delta T} \right)^{\frac{1}{2}} \qquad \ldots\ldots (5.14)$$

where D_C = convective mixing depth in metres

D_0 = initial MLD in metres

Q_L = heat loss for the period of forecast in cal

C_p = specific heat of sea water in cal $g^{-1} \, {}^o C^{-1}$

ρ = average density of sea water in the mixed layer in g cm^{-3}

ΔT = average gradient of temperature in 30 m below MLD.

Heat loss for the time interval of forecast is calculated from the heat budget equation using inputs from observations at the beginning of the interval and the layer deepening is calculated.

5.1.4   Salinity effects

The salinity effects are assumed minimal and
negligible . Hence,only temperature gradient is considered
for stability in both cases as applicable to isohaline
condition. However, average salinity data are used to
compute density for using in equations 5.10 and 5.14
following standard equations given by National Oceanographic
Data Centre (1974).

5.1.5   Advection and convergence/divergence

Horizontal and vertical advection becomes relevant
only when wind currents of long duration and intensity are
present. Geostrophic currents are semi-permanent and do
not affect the thermal structure. Hence the final layer
depth is computed assuming no advection. As a result,
the effect of convergence/divergence due to the horizontal
currents are also not taken into account in the present
scheme.

5.1.6   Internal waves

The effect of internal waves is to generate
periodic functions of MLD. The predicted MLD is assumed
to be the average on which internal wave amplitude is
superimposed to give the current position. However, in
the evaluation, the predicted values of MLD are without
the internal wave amplitudes.

5.1.7   MLD prediction routine

For the deep station S1,92 vertical thermal
structures beginning at 1355 hrs on 7th June 1977 and

ending at 0200 hrs (IST) on 19th June 1977 along with

data on wind, sea surface temperature, dry and wet bulb

temperatures and cloudiness are utilised for the prediction

run. For the shallow station S2, 21 vertical thermal

structures beginning at 1015 hrs (IST) and ending at

2130 hrs (IST) on 9th January 1983 along with the

supplementary meteorological observations as in the deep

water case are utilised. In each prediction run the

first thermal structure is initialised from the observed

and MLD and SST are predicted at the end of the time step.

The thermal structure is again initialised from the

observed for prediction of the structure after the next

time step and the process is repeated till the end of the

series. In this manner forecast runs were made for

3 hourly and 6 hourly steps for both deep water and shallow

water cases. In each case the predicted values of SST

and MLD are compared with the observed values.

5.2   Deep station S1 (10°30'N, 66°E)

5.2.1   Observed characteristics (Figs.5.1 and 5.2)

Deep station S1 is in the central Arabian Sea·
The observed variations in the air-sea transfer parameters,
MLD with the associated thermal structure and the average
salinity profile for the period from 1355 hrs (IST) on
7 June to 0200 hrs (IST) on 19 June 1977 are presented
in Figs. 5.1 and 5.2.

The general distribution of wind (Fig.5.1) during the period
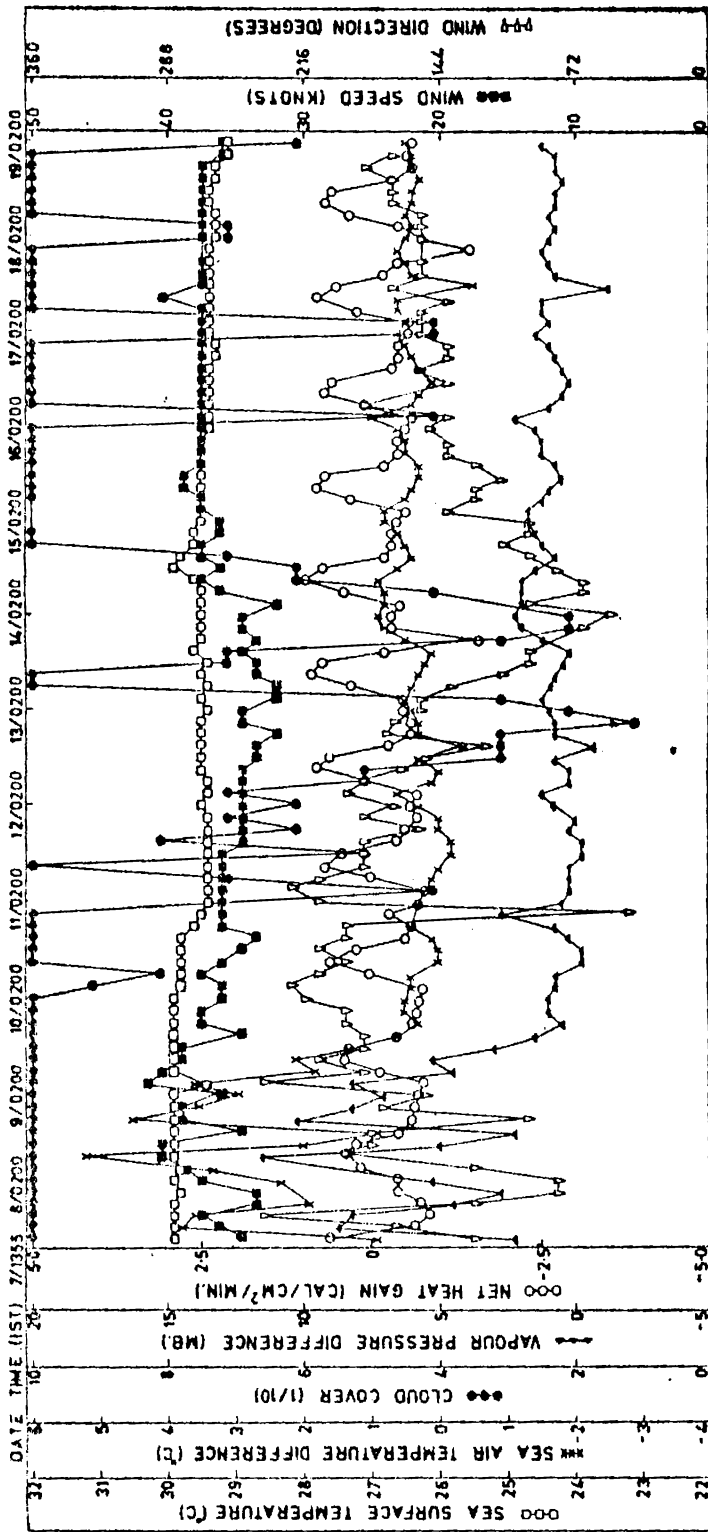was predominantly easterly with speeds ranging from 12 to

FIG. 5.1 OBSERVED TIME VARIATION OF AIR-SEA TRANSFER PARAMETERS DURING JUNE 1977 AT 10°30'N, 63°E

32 kts in the beginning, decreasing to nearly 15 kts by 10 June and then stabilising around 25 kts towards the end of the series between 16 - 19 June, 1977.

The net heat gain variation (Fig.5.1) exhibited cyclic changes with maximum values ranging from 0.23 to 0.36 cal cm^{-2} min^{-1} occurring between 1100 to 1400 hrs (IST) in the beginning of the run upto 10 June and afterwards increasing to values between 0.6 - 0.8 cal cm^{-2} min^{-1}. A further increase to 0.7 cal cm^{-2} min^{-1} was observed after 12 June. The night time cooling ranged between -0.4 and -0.9 cal cm^{-2} min^{-1} through out the period. Vapour pressure difference was positive and showed variation in the beginning between about 2 to 11 mb upto 9 June and then decreased to lower values ranging between -1.7 and 1.5 mb till the end. Till 10 July the sky was overcast and after that the cloudiness decreased upto 14 July. Sky was overcast again towards end of the period. The sea surface temperature was higher in the beginning (29.8° C) which progressively decreased from 11 July reaching the lowest (28.9° C) towards the end as a result of cooling in the central Arabian Sea (Rao et al., 1981). The corresponding sea-air temperature was positive throughout the period ranging from 0 - 3.5° C.

The observed MLD variation (Fig.5.2a) shows a progressive increase of average MLD towards the end of a 11 day period from 40 m to about 75 m which corresponds to a progressive cooling period in the area. The MLD variation is superimposed by the internal oscillation of
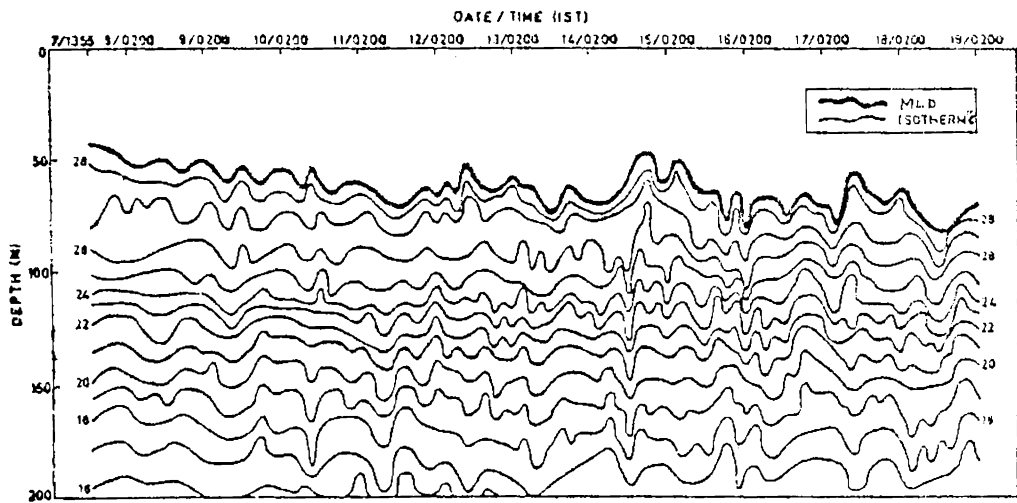
(a)
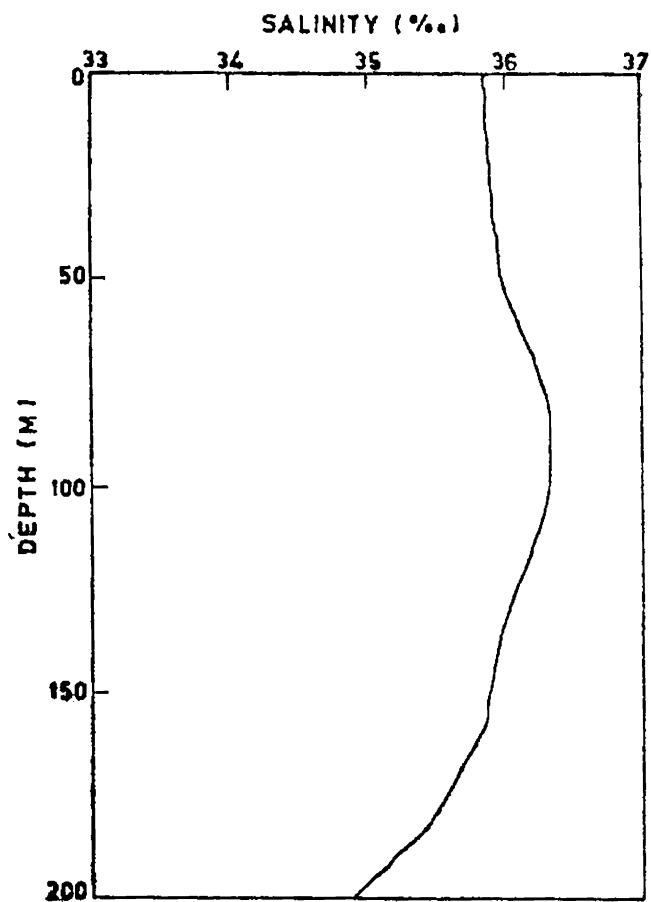
(b)

FIG. 5.2 (a) TIME SECTION OF OBSERVED MIXED LAYER DEPTH
AND ASSOCIATED THERMAL STRUCTURE (b) AVERAGE SALINITY
PROFILE DURING JUNE 1977 AT 10°30'N, 66E

predominantly 6 and 10 hrs period with a maximum

amplitude of about 10 m. The below layer gradient in

thermocline exhibited similar amplitudes of oscillation,

but the gradient thickness does not change throughout

even after the MLD deepens.

The observed average salinity structure (Fig.5.2b)

for the period of observation at the deep station shows

vertical positive gradients of 0.13 ppt in 50 m (0.003 ppt

in 10 m) upto a depth of 50 m. There is a subsurface

maximum corresponding to 95-100 m (36.35 ppt). Between

50-100 m and 100-150 m,the salinity gradient is approximately

0.027 ppt in 10 m, positive and negative respectively.

Below this the gradient is negative and more.

5.2.2   Station constants

For the deep water station a fetch of 1000 km is

taken for calculating the wind mixing. Average duration of

12 hrs is considered for the average winds of the same

duration. The subsurface radiation absorption (percentage)

appropriate for different levels was based on the optical

water mass type 1 representing "oceanic, clear" (Tables

5.1 and 5.2).

5.2.3   Results and discussion (Figs. 5.3 to 5.10)

Figs. 5.3 to 5.10 presents the characteristics of

the predicted SST and MLD for 3 hourly and 6 hourly

intervals.

5.2.3.1 3 hourly series

The 3 hourly prediction run initialised at 1355 hrs

(IST) on 7 June (Fig. 5.3) shows a night cooling in excess

of the observed by having predicted SST values lower by around 1°C for each diurnal cycle. A positive difference (increase) of predicted SST from the observed in the afternoon hours on 8, 9 , 10 and 14 June with a maximum difference of about 0.5° C is noticed. The excess cooling has resulted in corresponding deeper MLD. Similarly shoaling of MLD occurs whenever SST increase is noticed. Maximum difference of MLD coincides with shoaling events due to afternoon increase in SST on 10, 14 and 15 and 17 June upto about 30 m from the observed.

Figs. 5.4 and 5.5 presents the error evaluation of the 3 hourly run. In about 61.4% of the intervals the difference between predicted and observed SST is within 0.5° C (Fig. 5.4). The difference increase to $0.6 - 1.0^{\circ}$C for 37.4% of the intervals. For about 1.2% intervals the difference is highest between $1.1 - 1.5^{\circ}$ C. Fig. 5.5 shows the corresponding error evaluation for MLD. The difference in MLD between the predicted and observed is upto 5 m for 54% of the intervals while for 28.6% of the intervals the difference is between 6 - 10 m. Higher differences in MLD ranges from 8% of the intervals having differences between 11 - 15 m, 4.6% having 16 - 20 m, 3.8% with 21 - 25 m and 1% with 26 - 30 m.

A comparison of the wind mixing and convective mixing computed for 3 hourly run is presented in Fig.5.6. Till the end of the prediction the wind mixing length is less throughout the run by 5 - 50 m than the convective mixing which is closer to the predicted. The
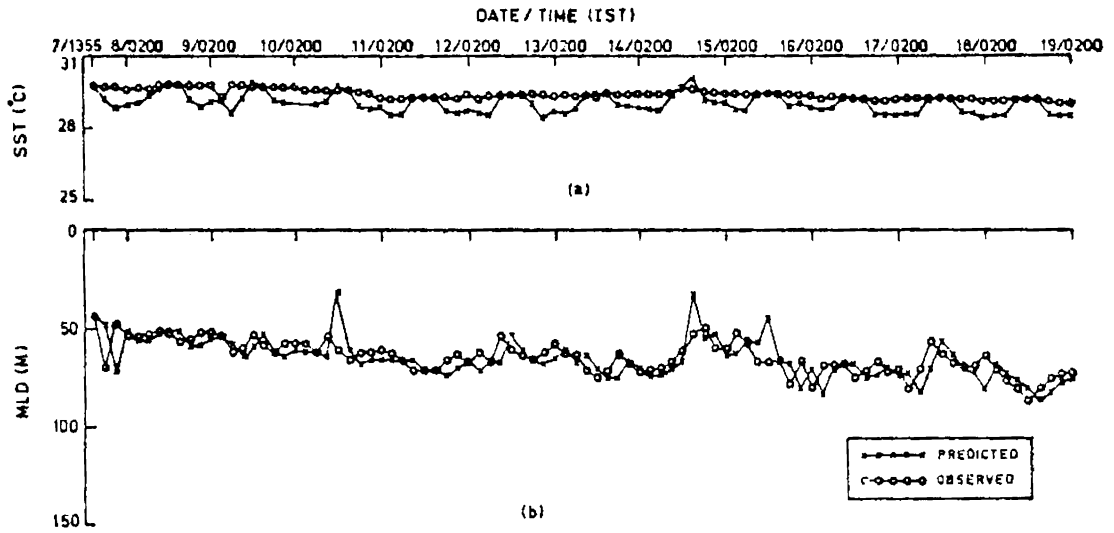
7/1355 8/0200 9/0200 10/0200 11/0200 12/0200 13/0200 14/0200 15/0200 16/0200 17/0200 18/0200 19/0200

(a)

(b)

PREDICTED
OBSERVED

FIG 5.3 COMPARISON OF PREDICTED AND OBSERVED (a) SEA SURFACE TEMPERATURE AND (b) MIXED LAYER DEPTH FOR 3 HOURLY TIME STEPS DURING JUNE 1977 AT 10°30'N, 66°E

FIG 5.4 DIFFERENCE BETWEEN PREDICTED AND OBSERVED SEA SURFACE TEMPERATURE (°C) FOR 3 HOURLY TIME STEPS AT 10°30'N, 66°E

FIG 5.5 DIFFERENCE BETWEEN PREDICTED AND OBSERVED MIXED LAYER DEPTH (m) FOR 3 HOURLY TIME STEPS AT 10°30'N, 66°E

DATE / TIME (IST)

7/1355 8/0200 9/0200 10/0200 11/0200 12/0200 13/0200 14/0200 15/0200 16/0200 17/0200 18/0200 19/0200

WIND MIXING
CONVECTIVE MIXING

FIG 5.6 COMPARISON OF WIND AND CONVECTIVE MIXING DEPTHS FOR 3 HOURLY TIME STEPS DURING JUNE 1977 AT 10°N, 66°E.

anomolous increase in wind mixing from 2000 hrs on 13

June to 1100 hrs (IST) on 14 June and from 2300 hrs (IST)

on 17 June to 0800 hrs (IST) on 18 June are only due to

errors in the wind force introduced by gaps in wind data

on 13 June (2005 hrs, IST) and on 17 June (2300 hrs, IST).

5.2.3.2 6 hourly series

The result of the 6 hourly prediction run

initialised at 1355 hrs (IST) (Fig. 5.7) shows that the

predicted cooling was in excess by maximum 1.5° C upto

16 June. But from 0200 hrs (IST) on 17 June to 0600 hrs

(IST) on 18 June, the predicted SST is lower by more than

3° C which corresponds to the error in wind forcing and

the resulting errors in heating due to the gaps in wind

data on 17 and 18 June, referred earlier. The predicted

SST is slightly in excess of the observed by about 0.1 to

0.5° C on 13, 14, 15, 16, 18 and 19 June. Predicted MLD

is closer to the observed with differences ranging from

0 to 25 m, except for great differences in deepening

corresponding to the gaps on wind data on 17 and 18 June.

Histograms (Figs. 5.8 and 5.9) present the error

evaluation for the prediction run with 6 hourly time steps.

The difference between predicted and observed SST is upto

0.5° C for 54% of cases and $0.6 - 1^{\circ}$ C for 34.2% cases,

between $2.6 - 3.0^{\circ}C$ for 3.8% cases and between $3.6 - 4^{\circ}C$

for 1.8% cases. The difference in MLD between the

predicted and observed is upto 5 m for 32.8% cases, 6 - 10 m

for 38.2% cases, 11 - 15 m for 13.4% cases, 16 - 20 m

for 4% cases, 21-25 m for 2% cases and 26 - 30 m for

DATE / TIME (IST)
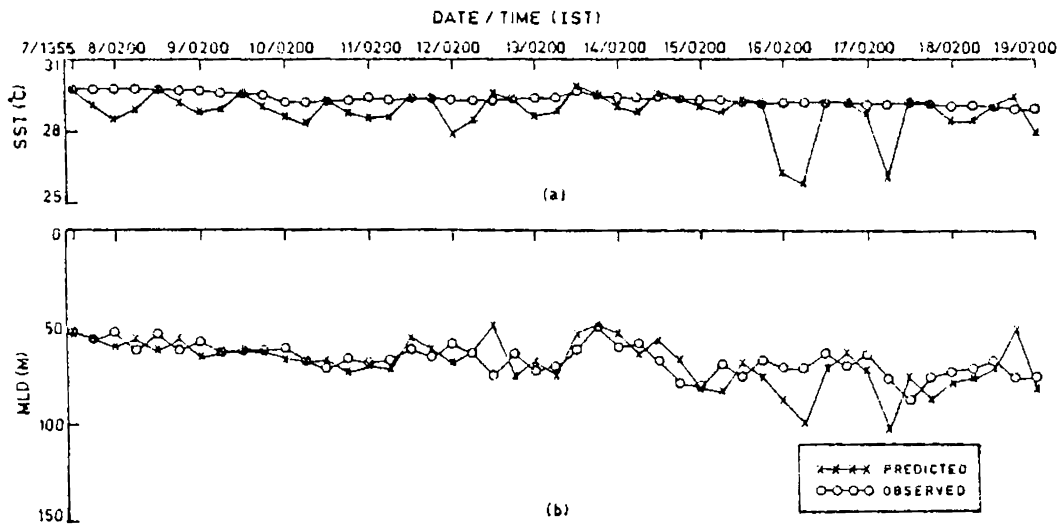
FIG.5.7 COMPARISON OF PREDICTED AND OBSERVED (a) SEA SURFACE TEMPERATURE AND
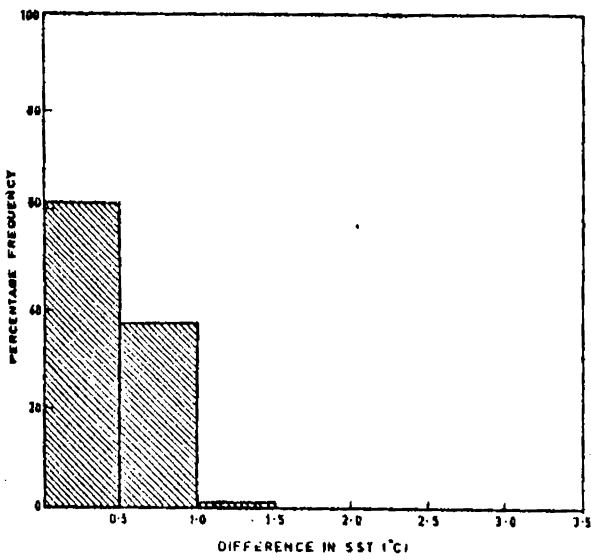(b) MIXED LAYER DEPTH FOR 6 HOURLY TIME STEPS DURING JUNE 1977 AT 10°30'N, 60°E

FIG.5.8 DIFFERENCE BETWEEN PREDICTED AND OBSERVED
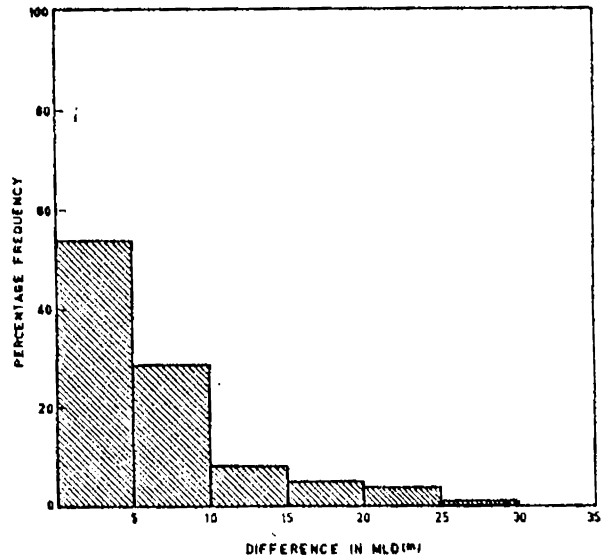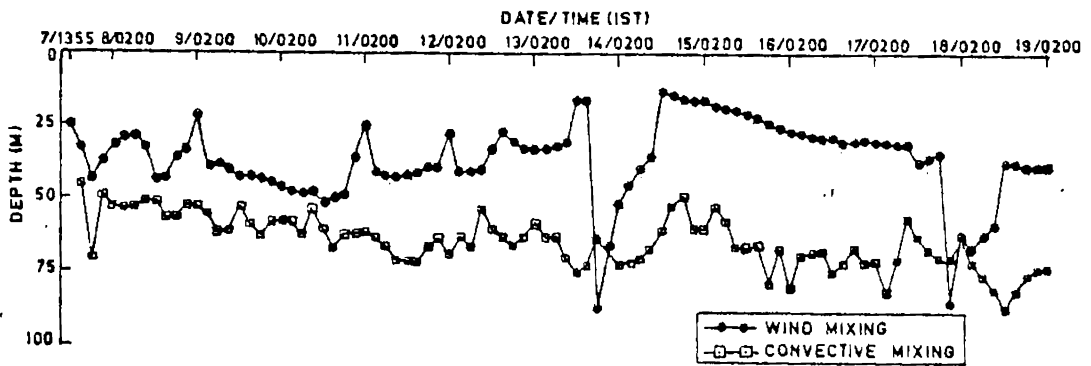SEA SURFACE TEMPERATURE (°C) FOR 6 HOURLY
TIME STEPS AT 10°30'N, 66°E

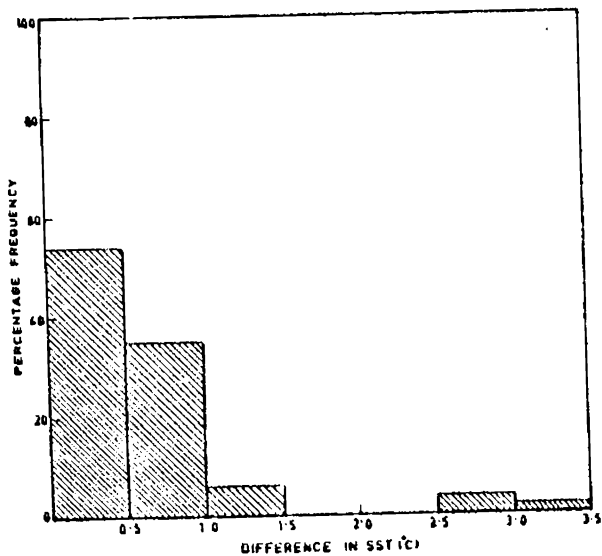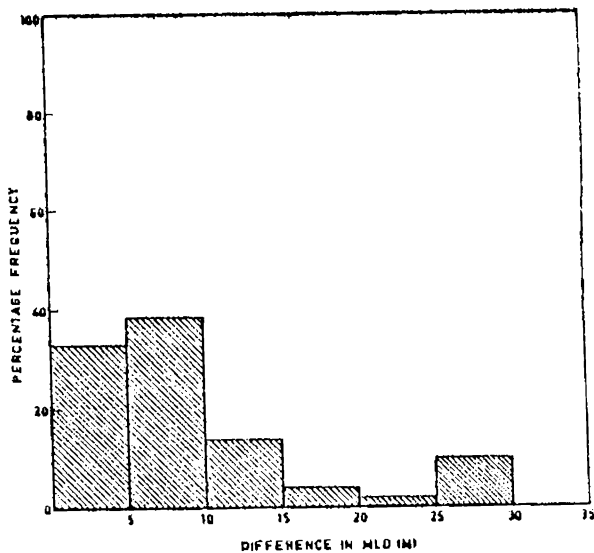FIG.5.9 DIFFERENCE BETWEEN PREDICTED AND OBSERVED
MIXED LAYER DEPTH (M) FOR 6 HOURLY TIME STEPS
AT 10°30'N, 66°E
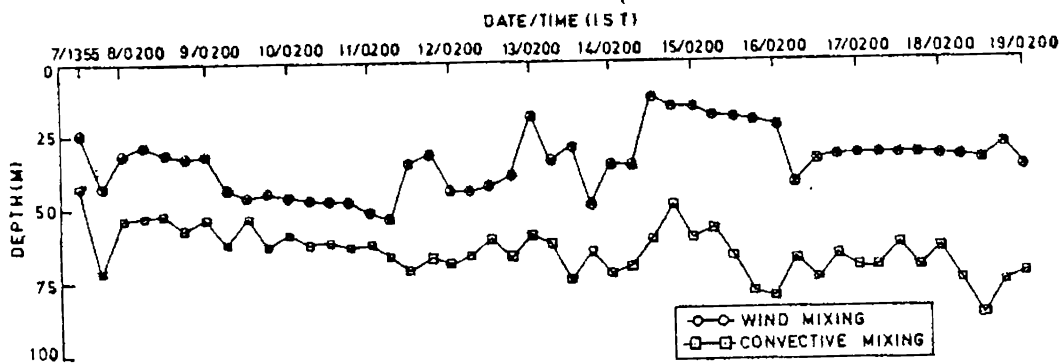
FIG.5.10 COMPARISON OF WIND AND CONVECTIVE MIXING DEPTHS FOR 6 HOURLY TIME STEPS DURING
JUNE 1977 AT 10°N, 66E.

A comparison of the wind mixing and convective mixing for 6 hourly time steps is presented in Fig.5.10. The wind mixing shows shallower extent with a difference from convective mixing ranging from 8-15 m. The convective mixing is closer to the predicted throughout the run.

5.3   Shallow station S2 ($10^{o}15'N$, $75^{o}48'E$)

5.3.1   Observed characteristics(Figs. 5.11 and 5.12)

This station is in the continental slope off Cochin and the evaluation period represents the winter regime. The observed variation in the air-sea transfer parameters and the MLD with the associated thermal structure and average salinity structure are presented in Figs. 5.11 and 5.12.

The distribution of air-sea transfer parameters(Fig.5.11) from 1015 hrs (IST) to 2115 hrs (IST)on 19 January 1983 at the shallow site is presented in Fig. 5.11. The wind speed ranges from 0 to about 5 kts for the entire duration. The wind direction was predominantly southeasterly, but changing to southerly towards the end with a short spell of northeasterly weak winds during 1600-1800 hrs (IST).

The net heat gain is positive from 1015 hrs (IST) to 1600 hrs (IST). The negative phase of cooling is prevalent from 1600 hrs (IST) upto 2150 hrs (IST) till the end of the duration. The maximum heat gain was at the beginning from about 1030 hrs (IST) (nearly 1.2 cal cm^{-2} min^{-1}) and maximum cooling was towards the end of the duration
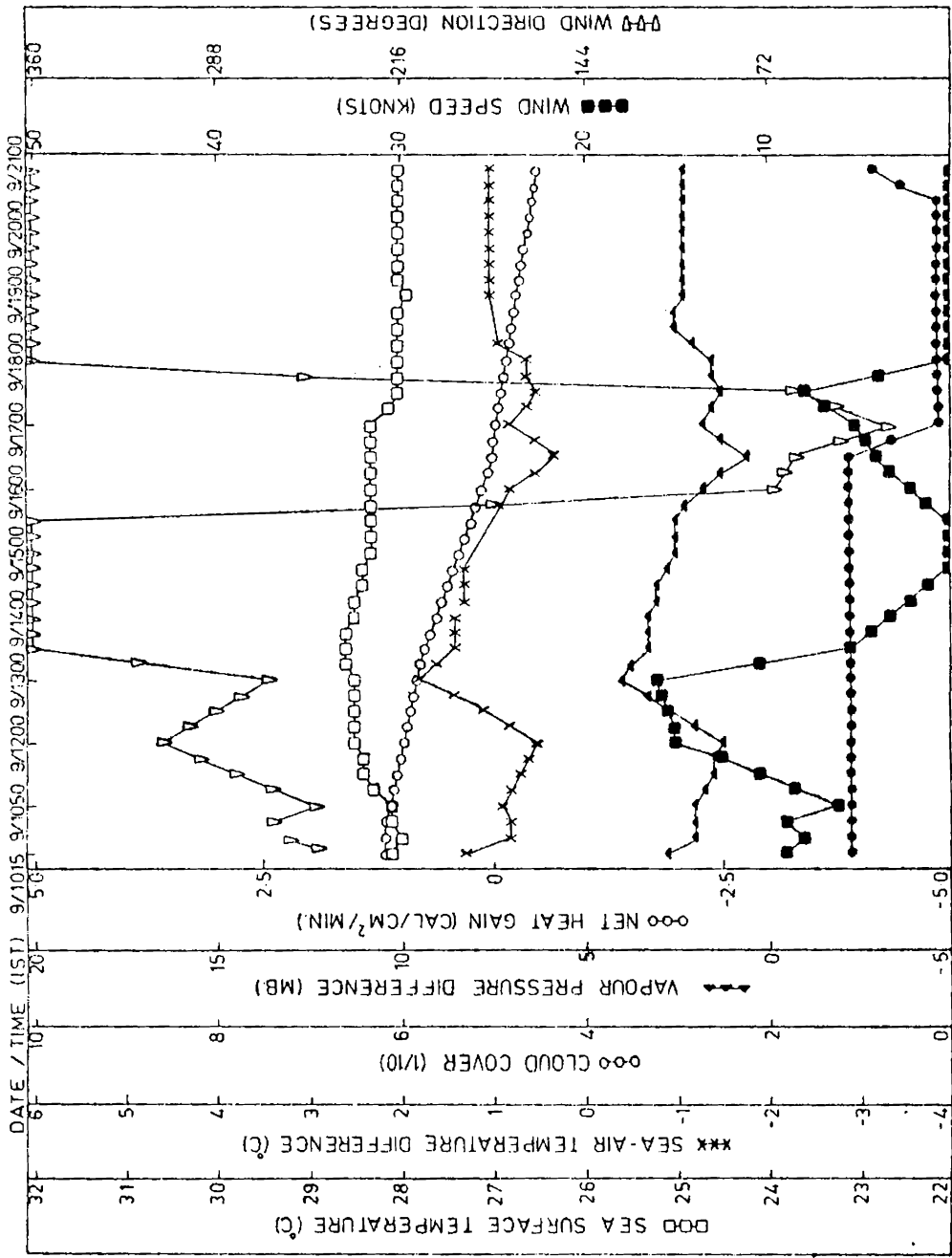
FIG. 5.11 OBSERVED TIME VARIATION OF AIR-SEA TRANSFER PARAMETERS DURING JANUARY 1983 AT 10°15'N, 75°48'E

at around 2130 hrs (IST) (nearly -0.2 cal cm^{-2} min^{-1}).

Variation of vapour pressure difference from sea surface

to air shows a range between 0-3 mb. Cloud cover was very

low between 0 - 1 (one tenth) for the duration. The sea-air

temperature difference was positive (0 - 1.5°C) indicating

the sensible heat loss. The temperature of sea surface

was highest (28.6°C) at around 1350 hrs (IST), which decreased

to a minimum (28°C) from 1700 to 2130 hrs (IST).

The MLD (Fig. 5.12a) varied from about 70 m at

1030 hrs (IST)to shallower depths of 60 m at 1445 hrs (IST)

and 1600 hrs (IST). This was followed by a deepening to

the previous depth and then back to a shallowest position

of 58 m by about 1800 hrs (IST). The layer further deepened

to the end of the observation period. The oscillations

in the MLD during the length of the observation are related

to periods of about 3 and 6 hourly durations with average

amplitudes of 5-12 m. The thermal gradients below the

mixed layer show an average range from about 4°C/10 m

in the beginning to 2.5°C/10 m afterwards.

The observed average vertical salinity structure

(Fig.5.12b) at the shallow station indicates a slight negative

gradient upto 30 m (about 0.03 ppt in 10 m). From 30 to

75 m the salinity increases to a subsurface maximum

35.62 ppt) with a gradient of 0.3 ppt in 10 m. The salinity

change is very weak between 100 and 150 m. From 150 m to 180 m

the gradient is negative and more (0.2 ppt in 10 m).

DATE / TIME (IST)

(a)
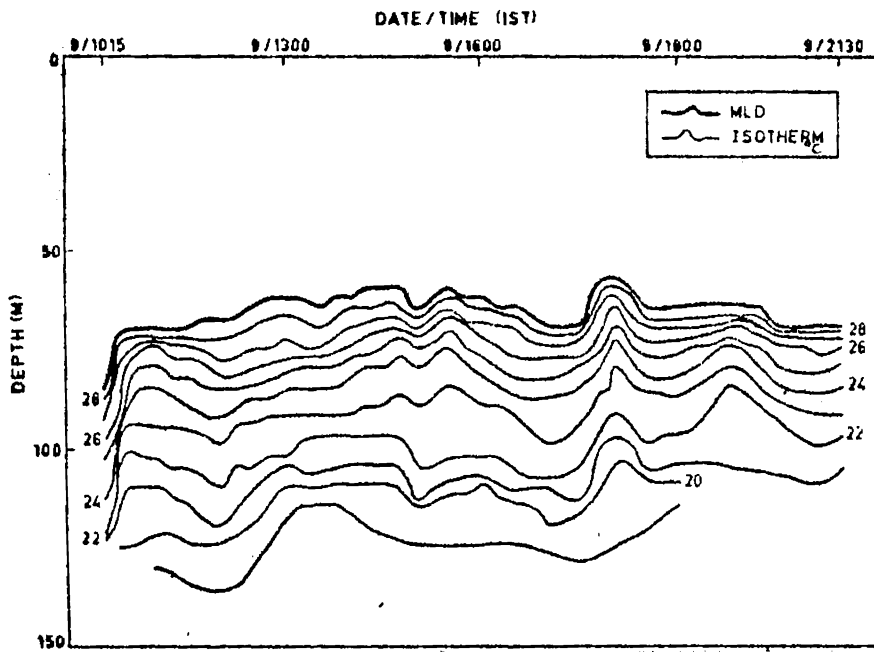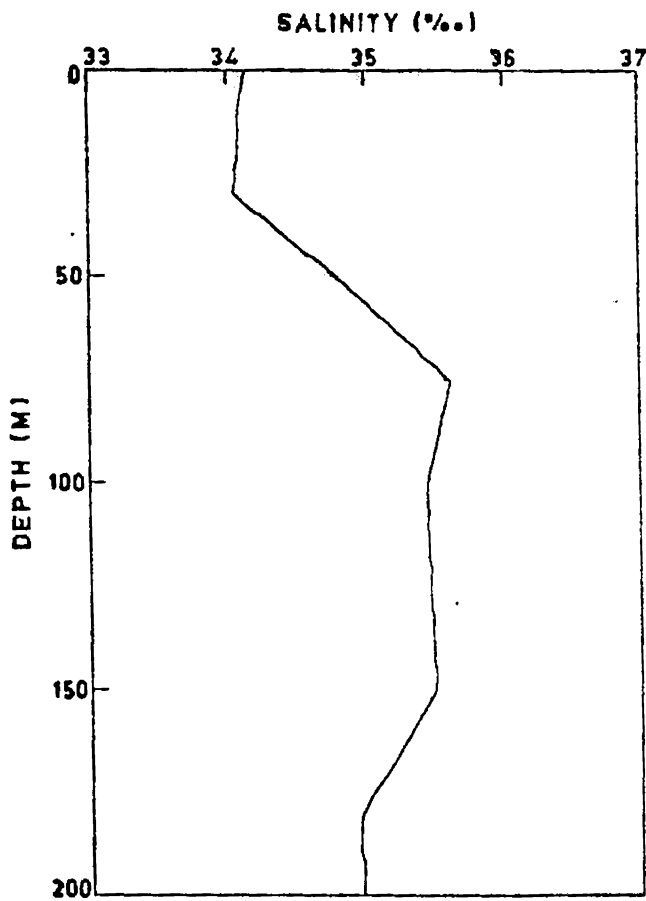
SALINITY (‰)

(b)

FIG. 5.12 (a) TIME SECTION OF OBSERVED MIXED LAYER
DEPTH AND ASSOCIATED THERMAL STRUCTURE
(b) AVERAGE SALINITY PROFILE DURING JANUARY 1983
AT 10° 15'N 75° 48'

5.3.2   Station constants

For the shallow station a fetch of 35 km is used with 12 hourly average wind speeds for wind mixing calculations. Percentage absorption values for different levels relevant to type 4 "Coastal, normal" water mass (Tables 5.1 and 5.2) are used for obtaining the temperature changes due to heating.

5.3.3.   Results and discussion

The results of the prediction run for the 3 hourly and 6 hourly time steps at the shallow station are presented in Figs. 5.13 to 5.20.

5.3.3.1 3 hourly series

Predicted SST is slightly less (Fig. 5.13) in the beginning at 1300 hrs (IST) which becomes more than the observed with increasing difference at 1600 hrs (IST). The difference in predicted MLD remains the same, but the values become less than observed towards the end. The predicted MLD is deeper with a difference of 25 m from the observed at 1300 hrs (IST) which decreases to nil at 1600 hrs (IST). At 1900 hrs (IST) the predicted MLD is slightly less by about 5 m and towards the end the difference disappears.

Figs. 5.14 and 5.15 present the error evaluation of SST and MLD between the predicted and observed situations, for 3 hourly time steps. For 66% cases the difference in predicted SST from the observed is upto 0.5° C and for 34% cases the difference ranges between $0.6 - 1^{\circ}C$. For predicted

FIG. 5.13 COMPARISON OF PREDICTED AND OBSERVED (a) SEA SURFACE
TEMPERATURE AND (b) MIXED LAYER DEPTH FOR 3 HOURLY TIME
STEPS DURING JANUARY 1983 AT 10°15'N 75°48'E

FIG 5.14 DIFFERENCE BETWEEN PREDICTED AND OBSERVED
SEA SURFACE TEMPERATURE (C) FOR 3 HOURLY
TIME STEPS AT 10°15'N, 75°48'E.

FIG 5.15 DIFFERENCE BETWEEN PREDICTED AND OBSERVED
MIXED LAYER DEPTH(M) FOR 3 HOURLY TIME STEPS
AT 10°15'N, 75°48'E

FIG 5.16 COMPARISON OF WIND AND CONVECTIVE MIXING DEPTHS FOR 3 HOURLY
TIME STEPS DURING JANUARY 1983 AT 10°15'N, 75°48'E

MLD the difference is upto 5 m in 77% cases and 21-25 m
for the rest.

A comparison of wind and convective mixing values
(Fig. 5.16) indicates wide difference between both ranging
from about 22 m to 50 m. The low wind mixing profiles are
due to the low wind forcing and the predominence of
convective mixing is indicated for the predicted MLD.

5.3.3.2 6 hourly series

Fig. 5.17 presents the distribution of the predicted
and observed SST and MLD resulting from the prediction run
for 6 hourly time steps at the shallow station. The
predicted SST is slightly more than the observed for the
first interval. The difference increases to 1600 hrs (IST)
when predicted SST values are lower and the trend remains
somewhat same till 1900 hrs (IST). The trend changes
reversing the difference towards the end of the series.
The predicted MLD shows maximum difference of about 20 m
at 1300 hrs (IST) when the predicted MLD is deeper. The
predicted layer coincides with the observed at 1600 hrs
(IST). The predicted layer depth is shallower by about 5m
at 1900 hrs (IST) and the difference vanishes towards the
end.

The error in prediction for 6 hourly time steps
at the shallow station is presented in Figs. 5.18 and
5.19. For equal numbers of 6 hourly intervals (50% each)
the difference between the predicted and observed SST is
upto 0.5^{o} C and $0.6 - 1^{o}C$ respectively. The difference

between the predicted and observed MLD is upto 5 m for
50% cases. However, for the other 50% cases,the difference
is between 16-20 m.

The wind mixing is shallower than the convective
mixing for the 6 hourly series at the shallow station
(Fig. 5.20). This difference is maximum in the beginning
(about 80 m) and decreases to near 70 m at the end. The
wind mixing decreases from 70 m in the beginning to about
5 m at the end. The predicted convective mixing shows a
decrease towards the end while the maximum negative heat
transfer and observed MLD for the same period (Figs.5.11
and 5.12) are suggestive of convective deepening. This
contrast in the predicted shallowing of the MLD is due to
the perturbation of the internal oscillation making the MLD
input at 1630 hrs (IST) shallower upto about 60 m. This
results in the deepening of predicted MLD due to negative
heat transfer to an extent less than the observed deepening.

5.4   Conclusions

The predictive scheme which does not take into
account advection and salinity effects is found to be
sensitive to both wind forcing and heating. In fact the
model equations used   predict more cooling and corresponding
deepening of MLD during night time. The prediction run for
3 hourly and 6 hourly time steps is more sensitive to the
wind forcing which may result in errors due to data gaps.
However, the differences are found to be well within the
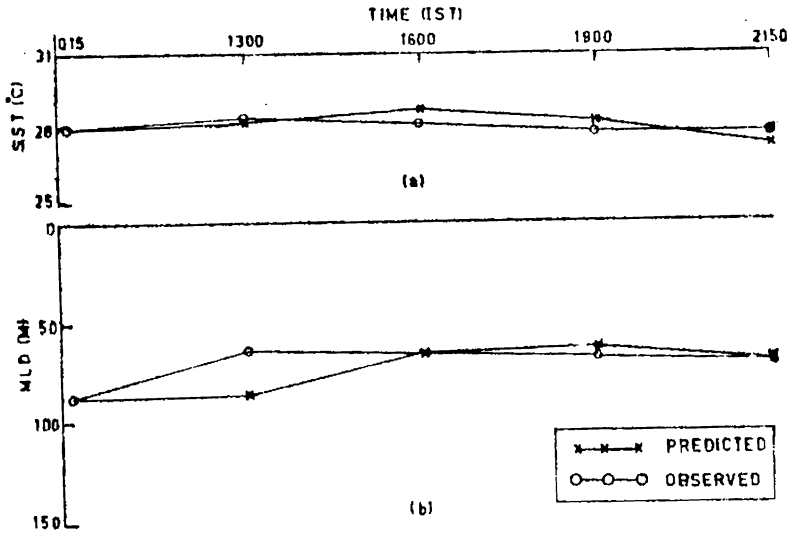range of internal wave variability in the Arabian Sea

TIME (IST)
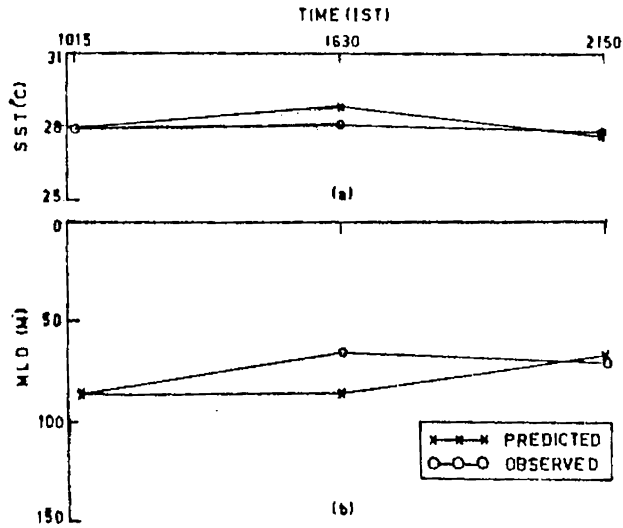
FIG. 5.17 CAMPARISON OF PREDICTED AND OBSERVED
(a) SEA SURFACE TEMPERATURE AND
(b) MIXED LAYER DEPTH FOR 6 HOURLY TIME
STEPS DURING JANUARY 1983 AT 10°15'N, 75°48'E
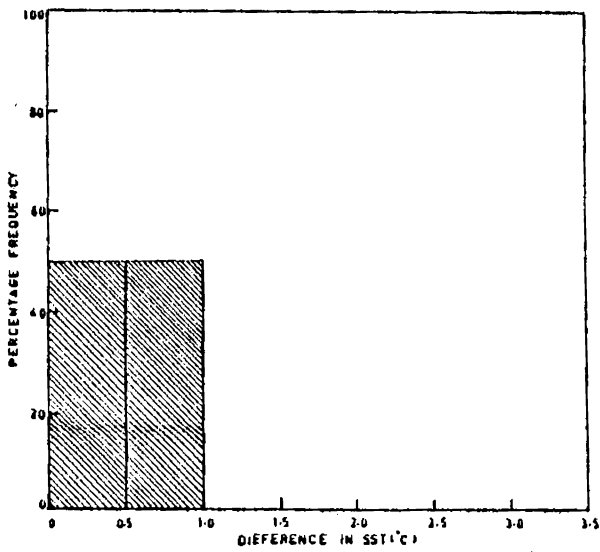
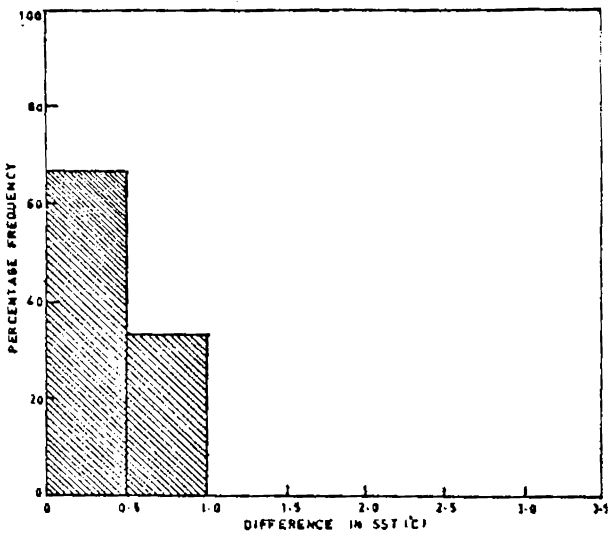FIG. 5.18 DIFFERENCE BETWEEN PREDICTED AND OBSERVED
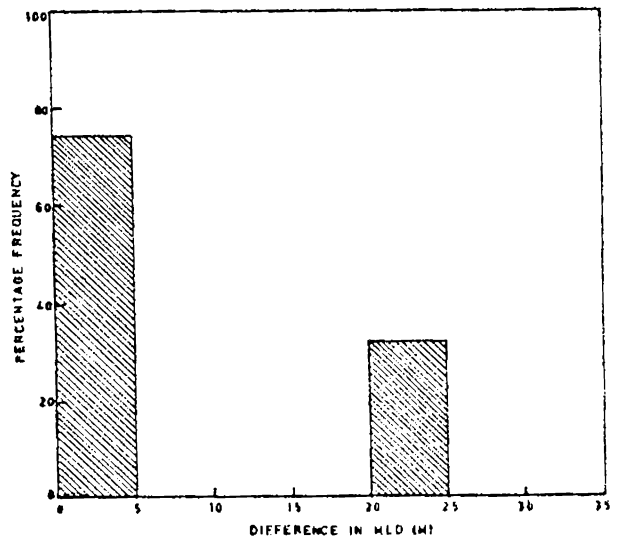SEA SURFACE TEMPERATURE (°C) FOR 6 HOURLY
TIME STEPS AT 10°15'N, 75°48'E.
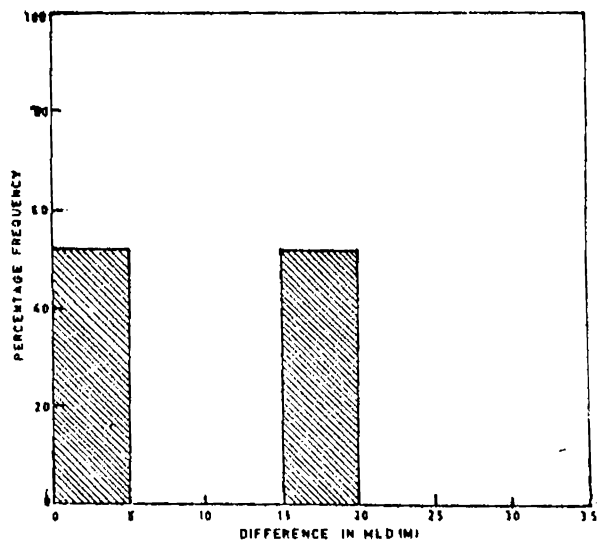
FIG. 5.19 DIFFERENCE BETWEEN PREDICTED AND OBSERVED
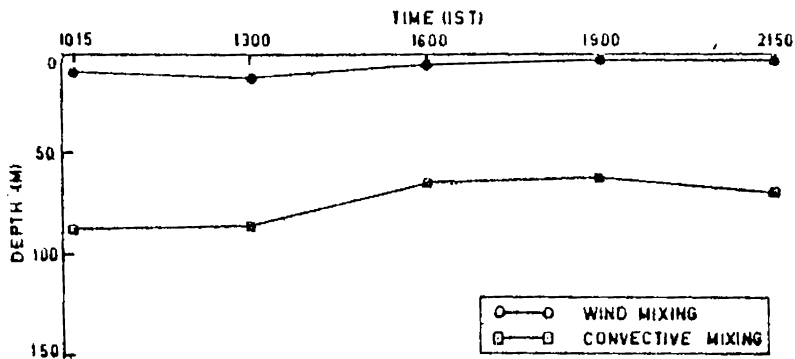MIXED LAYER DEPTH (M) FOR 6 HOURLY TIME STEPS
AT 10°15'N, 75°48'E
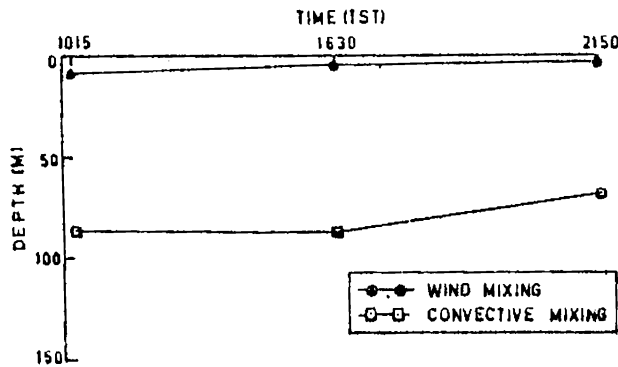
FIG 5.20 COMPARISON OF WIND AND CONVECTIVE MIXING DEPTH
FOR 6 HOURLY TIME STEPS DURING JANUARY 1983 AT
10°15'N, 75°48'E

and within the limits imposed by this, the scheme is satisfactory for predicting short term variations from 3-6 hrs in the deep site during June (southwest monsoon) and in the shallow site during winter regime.

As the MLD parameterisation is based on the average criterion of Wyrtki (1971) the scheme is unable to take into account the formation of transient thermoclines. The use of averaged fluxes for (3 hourly and 6 hourly)predicting the SST and MLD may result in the excess cooling and heating and corresponding deepening or shoaling of MLD as has been observed by Elsberry et al. (1984) who omitted advective and salinity effects in their one dimensional model for short time scale. The non-inclusion of salinity effects in accounting stability during turbulent and convective mixing can be a set back for cases where sharp salinity gradient exists (Miller, 1976).

CHAPTER VI

CHAPTER VI

SUMMARY AND CONCLUSIONS

This thesis is the result of an elaborate study on the mixed layer depth (MLD) and the various oceanic environmental factors controlling it in the Arabian Sea examining its predictability on annual and short term basis. To accomplish this, the study area between $10^O - 25^O$ N latitudes and $60^O - 75^C$ E longitudes in the Arabian Sea is divided into 8 subareas of 5° quadrangles. The distribution of monthly means of the surface wind field, net heat exchange and sea surface temperature (SST) over each subarea in the annual cycle is examined. The corresponding wind (mechanical) and convective mixing values are computed and presented along with the observed mean MLD for the subareas in the annual cycle. Effects of advection due to surface currents and surface divergence (convergence and divergence) for these subareas are examined for correlating the MLD variations. A representative time series data from typical deep water station under southwest monsoonal forcing is analysed for the spectral components to estimate the amplitude perturbations on the mean MLD variation.

The spatial variability of MLD is examined along four selected longitudes depicting the monthly variations. The spatial distribution of MLD is also examined in relation to the wind speed and SST distribution in the northern Arabian Sea under two climatic regimes viz., winter (December, January and February) and premonsoon (March, April and May).

Finally, the short term predictability of MLD and SST is examined by evaluating a one dimensional prediction scheme, using only surface exchanges of momentum by wind and heat transfer, neglecting advection and salinity effects on stability for two stations, one deep and the other shallow in the Arabian Sea.

The average distribution of the surface wind field analysed in the present study indicates the dominance of southwest monsoonal wind forcing both by duration and severity. The southwesterly winds are observed to be established by May, persisting through September. Even in May and September, at the beginning and end of the southwest monsoon, average wind speeds over significant areas exceed the maximum speed observed at the height of the northeast monsoon. In contrast, the northeast monsoon winds are weaker and pronounced during November-January, though in some areas of the central Arabian Sea, this period is from November to March. The present analysis has indicated that the wind speeds generally increase from coastal zones towards the central oceanic area during both monsoons in the Arabian Sea.

The monsoon-controlled Arabian Sea exhibits unique characteristics of bimodality in the annual signals of net heat transfer, SST and MLD. The strong periodic upwelling and mid-summer surface layer cooling are distinctive features modifying the annual variations of these parameters.

Annual cycle of net heat transfer examined for each subarea in the Arabian Sea reveals double maxima corresponding

to heating in April/May and secondary warming in August/
September. The heating generally starts in February and
lasts till June in the northern Arabian Sea while it lasts
upto May in the central and southern Arabian Sea. The spring
and summer heating is maximum in the northern areas (about
120 W m^{-2}) whereas it is minimum off the southwest coast
of India (about 80 W m^{-2}). The secondary warming at the end
of the southwest monsoon starts generally in August and
continues upto November except in the southwest coast of
India. The secondary warming results from the reduction
in the latent heat loss due to a reversal in the vapour
pressure gradient after the onset of southwest monsoon and
increase in radiation due to a reduction in cloudiness. The
minima in net heat transfer corresponding to the cooling
occur in December/January and June/July.

The winter cooling has lower intensity in the central
and southern subareas (about -8 W m^{-2}) to -15 W m^{-2}) while
higher values (-40 W m^{-2} and more) are observed in the
northern subareas. In the subarea near the southwest coast
of India, net heat transfer is positive after July without
any interruption of winter cooling (negative heat transfer),though
the positive heat transfer progressively decreases to a minimum in
December (about 10 W m^{-2}), as revealed by the present study.
mid-summer cooling results from increase in evaporation
and reduction in incoming radiation due to cloudiness,
supplemented by cold advection and upwelling in the Arabian
Sea. The surface cooling in July is less (-13 W m^{-2} to
-30 W m^{-2}) in the northern Arabian Sea. The mid-summer
cooling is intense and more than the winter cooling in most

of the areas in central and southern Arabian Sea

$(-50 \text{ W m}^{-2} \text{ to } -70 \text{ W m}^{-2})$.

The study of SST variation reveals a bimodal seasonal cycle whose response is found to lag by 1-2 months behind the net heating with respect to the peaks. The annual range in SST variation is more in the northern parts $(4^{\circ}C)$ and less towards central $(3^{\circ}C)$ and southern parts $(2^{\circ}C)$. In the present analysis, excepting the coastal areas of southwest coast of India during upwelling season, SST maxima and minima have generally coincided with MLD shoaling and deepening respectively.

The analysis of mean distribution of MLD over the annual cycle for the 8 subareas in the present study reveals a variability of about 20 - 100 m in the Arabian Sea, whereas closer averaging used for the study on seasonal variability has revealed a higher range of 5 - 195 m. The effect of complete reversal in the atmospheric and oceanic circulation along with bimodal characteristic of heating has given the MLD a bimodal pattern of annual variation, evident in the present analysis for majority of the subareas, excepting northern and east coastal areas where a unimodal trend is apparent. MLD deepens during winter and mid-summer cooling (December-February and July-September). In the northern and eastern coastal areas, the secondary deepening in mid-summer is supressed due to coastal divergence and upwelling processes. Shoaling of MLD takes place due to net heating at surface during March-June and August-October. On the basis of 5° quadrangle averages, northern areas show shallower MLD

(20 - 30 m) compared to the central and southern areas
(33-44 m) due to the difference in heating. The mid-summer
deepening in MLD is pronounced in the northern, western
and central Arabian Sea, whereas winter deepening is
significant in all subareas. The shoaling of MLD in
September/October is of equal intensity as that during
April/May in most of the areas except near the southwest
coast of India, where MLD shoals up to a greater extent
during this time under the influence of upwelling. Winter
deepening of MLD ranges between 65-76 m based on 5° average
data, the lower values corresponding to eastern coastal
areas and higher values corresponding to northern and
central areas.

Utilising the mean wind field and net heat transfer
cycle analysed for the subareas, the mechanical and
convective mixing values computed indicate that convective
mixing closely describes the annual cycle of MLD in all the
subareas while wind mixing seems significant only during
July-September (22-52 m). The mechanical mixing due to
wind exhibits an annual range of 1 - 60 m with low values
in the northern and eastern coastal areas and high values
in the central Arabian Sea. The difference between the
mean observed MLD and the wind mixing during the period of
intense wind force (July-September) ranged between 8-44 m.
The convective mixing, on the other hand, shows difference
from the observed MLD (0-35 m) mainly during the heating
periods (March-May and September-October).

The average advection examined for the subareas indicates only the response of the surface circulation to the changing monsoonal systems. From December to February, the surface currents are westerly and northwesterly in the northern and central subareas. In the eastern coastal subareas northerly or northwesterly flow is indicated. From March to October southerly/southwesterly and south-easterly flows are prevalent in the Arabian sea. Maximum surface current speeds occur during May-September (16-40 cm sec^{-1}) in the Arabian Sea with higher speeds occurring along western and eastern coastal zones. The currents are weaker during winter under the influence of northeast monsoon. The direct impact of advection is examined only from the derived surface divergence pattern for the subareas.

Convergence and divergence seems to enhance or supress the processes of shoaling or deepening due to heating and cooling in the annual cycle. In most of the subareas in the Arabian Sea, deepening of MLD due to winter cooling in January is found to be augmented by convergence, inducing sinking. The maximum deepening in MLD due to mid-summer cooling in July-September in the majority of subareas, is found to be enhanced by surface convergence (upto -35 units). Similarly the shoaling of MLD during March-May in a significant portion of the Arabian Sea is found supplemented by divergence causing upwelling (upto about 20 units). For the long term predictive characteristics, the differences in MLD from wind and convective mixing could be reasonably reduced by quantitatively

incorporating the convergence and divergence effects, as examined in the present study.

FFI analysis of the spectrum of internal oscillations sampled at 3 hourly intervals for 192 hours from the deep station in the central Arabian Sea during southwest monsoon implies that amplitude perturbations of the order of 1.5-3 m in the short period (less than 12 hrs) and 4-10 m in the long period (greater than 12 hrs)domains are possible over the mean MLD predicted for an area in the central Arabian Sea. However, these amplitudes can increase due to overlapping of the component amplitudes.

The spatial variability of MLD examined along four meridional (60°, 65°, 70° and 75° E longitudes) time sections suggest the influence of reversals in the circulation pattern. During December-February, MLD topography indicated is of dome shape, especially along the western longitudes in the study area due to the presence of cyclonic circulation (anticlockwise) with shallow MLD (40-60 m) around 18°-22° N latitudes, with higher values (75-90 m) north and south of it. The pattern is very vague in the eastern section. From March to October, a southward downsloping of MLD surface is apparent along all meridional - time sections, suggesting the presence of a major anticyclonic (clockwise) and easterly flow. The slope is maximum along the western longitudes in August with 10 m at 25° N to 115 m at 10-11° N. This deepening of MLD in the central and western zones in the study area during June-August is the result of cooling and convergence

causing entrainment mixing at the base of MLD. At the same time eastern coastal zone between $10^{\circ}-15^{\circ}$ N experiences shoaling of MLD (15-30 m) due to upwelling, induced by southerly coastal flow and enhanced by weak longshore components of wind. The upwelling effects are also indicated in the coastal zone off Pakistan/Iran/Gulf of Oman(upto 50 m of MLD) during this time, as a result of wind/current divergence. The transition months of March and October/November are characterised by little changes in the slopes of MLD along the meridional sections.

The seasonal variability of MLD in relation to wind speed and SST based on $\frac{1}{2}^{\circ}$ averaged data has revealed differences in the patterns during winter and premonsoon regimes. During winter, SST distribution in the northern Arabian Sea is characterised by warm cell (around 26°C) off Bombay and cold cell (around 23°C) off Pakistan/Iran coasts, which coincide with corresponding trough of MLD (around 100 m) indicating anticyclonic eddy and dome of MLD (around 110 m) indicating a cyclonic eddy respectively during the period. The deepest MLD (greater than 190 m) is observed in the northeastern portion off Karachi. The overall pattern during winter suggests that a mean cyclonic circulation in the northern Arabian Sea is embedded with anticyclonic eddies off Bombay and Gujarat and cyclonic eddy in the northeastern portion of the study area.

During the premonsoon regime a warm cell of SST (around 30°C) off Bombay coincides with a trough of MLD (around 40 m) due to an anticyclonic eddy in the area.

Presence of cold cells (around 23°C) is found related to the dome of MLD (around 10-20 m) in the centre of northern Arabian Sea area, due to a cyclonic eddy. Similarly extensive trough of MLD at the mouth of Gulf of Oman (around 30 m) and off Kutch (around 50 m) are found related to anticyclonic eddies. These observations point out the importance of eddies especially in the northern and eastern coastal zones in the study area, interacting with the MLD variability in space and time domains.

The winter regime presents deep MLD and premonsoon shallow in the northern Arabian Sea. Zonal section off Oman shows a range of 20-145 m in MLD between the two regimes, while the meridional sections indicate a variability of 5-190 m.

A one dimensional prediction scheme evolved from Laevastu (1965) and James (1966) for use with readily available parameters of wind and air-sea temperatures, with its assumption of no advection and salinity gradients has worked well to predict MLD variability on short term basis upto 6 hrs within the range of variability of internal waves. This scheme parameterisis the MLD changes due to absorption of surface heat energy, mixing by wind and convection. Prediction evaluation at 3 hourly intervals it the deep station in June in the Arabian Sea shows MLD ifferences upto 5 m and 6-10 m in 54% and 29% cases espectively while SST differs upto 0.5°C in 61% cases. hourly predictions at the deep station indicate MLD ifferences upto 5 m and 6-10 m in 33% and 38% cases

respectively and SST differences upto 0.5°C in 54% cases.
3 hourly predictions at the shallow station during January
showed MLD differences upto 5 m in 77% cases and SST
differences upto 0.5°C in 66% of cases . In the case of
6 hourly predictions at the shallow station, MLD differs
upto 5 m in 50% cases and SST upto 0.5°C in 50% cases
respectively. Maximum differences in MLD of 25 m and SST
of 1.5°C were observed for deep station while respective
differences in shallow station were 20 m and 1°C. From
the evaluation it is also observed that for the southwest
monsoon cooling and winter regimes the predicted MLD closely
follows the convective mixing forecasts, while wind mixing
is shallower in both deep and shallow water cases.

The model however suffers from the set back that
due to the assumption of average 3/6 hourly fluxes of wind
and heat energy, the model equations seem to over predict
cooling and deepening of MLD during night. Similarly, it
predicts slightly excess   heating and shoaling of MLD in
the afternoon hours. The scheme is also not capable of
predicting transient thermoclines in the MLD, as it treats
MLD as a single slab by definition.

In conclusion, long term predictions of MLD can
be improved by incorporating the effects of advection,
convergence/divergence in addition to the momentum and
heat transfer processes. Short term predictions could be

reasonably made,using one dimensional scheme of the
present study upto 6 hours. For better results, integral
models using grid data of temperature, salinity and
currents to evolve advective influences are suggested.

REFERENCES

REFERENCES

Banse, K., 1959: On upwelling and bottom trawling off
        the west coast of India. J. Mar. Biol. Ass.
        India, 1, 33-49.

Banse, K., 1968: Hydrography of the Arabian Sea shelf
        of India and Pakistan and effects on demersal
        fishes. Deep-Sea Res., 15, 45-79.

Banse, K., 1980: Upsloping of isotherms on the continental
        shelf off Goa and Bombay in June 1967. J. Mar.
        Biol. Ass. India, 14, 344-356.

Basil Mathew, 1982: Studies on upwelling and sinking in
        the seas around India. Ph.D. Thesis, University
        of Cochin, 159 pp.

*Berliand, T., 1960: Metodika climatologicheskih raschetov
        radiatsii, Meteorologia i Hydrologia, 6, 9-16.

Bruce, J.G., 1968: Comparison of near surface topography
        during the two monsoons in the western Indian
        Ocean. Deep-Sea Res., 15, 665-667

Bruce, J.G., 1981: Variations in the thermal structure
        and wind field occurring in the western Indian
        Ocean during monsoon. Naval Oceanographic Office
        Report TR-272, 171 pp.

Budyko, M.I., 1974: Climate and Life. Academic Press, 508 pp.

Bunker, A., 1976: Computations of surface energy flux and
        annual sea-air interaction cycles of the North
        Atlantic Ocean. Mon. Wea. Rev., 104,1122-1140.

Busch, N.E., 1977: Fluxes in the surface boundary layer
        over the sea. Modelling and Prediction of the
        Upper Layers of the Ocean, E.B. Kraus, Ed.,
        Pergamon Press, 72-91.

Colborn, J.G., 1975: The Thermal Structure of the Indian
         Ocean. Int. Indian Ocean Expedition Oceanogr.
         Monogr., No.2, University Press of Hawaii,173 pp.

Colon, J.A., 1964: On interactions between the southwest
         monsoon current and the sea surface over the
         Arabian Sea. Indian. J. Meteor. Geophys., 15,
         183-200.

*Darbyshire,J., 1959: A further investigation of wind
         generated waves. Dtsch. Hydrogr. Z, 12, 1-13.

Darbyshire, M., 1967: The surface waters off the coast
         of Kerala, South West India. Deep-Sea Res.,
         14, 295-320.

Das,V.K., A. Gouvia and K.K. Varma, 1980: Circulation and
         water characteristics on isanosteric surfaces in
         the Northern Arabian Sea during February-April.
         Indian J. Mar. Sci., 9, 156-165.

Davis, R.E.,R.A. De Szoeke and P. Niiler, 1981: Variability
         in the upper ocean during MILE, Part II :
         Modelling the mixed layer response. Deep-Sea Res.,
         284, 1453-1475.

Defant, A., 1961: Physical Oceanography, Vol. I, Pergamon
         Press, New York, 729 pp.

Denman, K.L., 1973: A time dependent model of the upper
         ocean. J. Phys. Oceanogr.3, 173-184.

Denman, K.L. and M. Miyake, 1973: Upper layer modification
         at ocean station 'Papa' : Observation and
         simulation, J. Phys. Oceanogr., 3, 185-196.

Deutsches Hydrographisches Institut, 1960: Monaskarten
         fur den Indischen Uzean, Pub. No. 2422, Hamburg.

De Szoeke, R.A., 1980: On the effects of horizontal
         variability of wind stress on the dynamics of the
         ocean mixed layer. J. Phys.Oceanogr. 10, 1439-1454.

De Szoeke, R.A., and P.B. Rhines, 1976: Asymptotic
        regimes in mixed layer deepening. J. Mar. Res.,
        34, 111-116.

Duing, W., 1970: The Monsoon Regime of the Currents in the
        Indian Ocean, International Indian Ocean Expedition
        Monograph No.1, East-West Center Press, Honolulu,
        105 pp.

Duing, W., and A. Leetma, 1980: Arabian Sea cooling: a
        preliminary heat budget. J. Phys.Oceanogr.,
        10, 302-312.

Duing, W., R. Molinari and J.C. Swallow, 1980: Somali Current:
        evolution of surface flow, Science, 209, 588-589.

*Ekman V.W., 1905: On the influence of earth's rotation on
        ocean currents. Ark. f. Math. Astron. Och.Fysik.,
        2152 pp.

Elsberry, R.L., and N.T. Camp, 1978: Oceanic thermal response
        to strong atmospheric forcing. Part I: Characteristics
        of forcing events. J. Phys. Oceanogr.,8,206-214.

Elsberry, R.L., and S.O. Raney, 1978: Sea surface temperature
        response to variations in atmospheric wind forcing.
        J. Phys. Oceanogr., 8, 881-887.

Elsberry, R.,S.A.Sandgathe and F.J. Winninghoff, 1984:
        Short-term oceanic response predicted by a mixed
        layer model forced with a sector atmospheric
        model, J. Phys. Oceanogr., 14, 79-91.

Foster, T.D., 1965: Onset of convection in a layer of fluid
        cooled from above. The Physics of Fluids. 8, 1770-1774.

Gargett, A.E.,T.B. Sanford and T.R. Osborn, 1979: Surface
        mixing in the Sargasso Sea. J. Phys.Oceanogr.,
        9, 1090-1111.

Garwood, R.W., Jr., 1977: An oceanic mixed layer model
        capable of simulating cyclic states. J. Phys.
        Oceanogr. 7, 455-468.

Geisler, J.E., and E.B. Kraus, 1969: The well mixed
        Ekman boundary layer. Deep-Sea Res., 16,73-84.

Gill, A.E., and A.J. Clarke, 1974: Wind induced upwelling,
        coastal currents and sea level changes. Deep-Sea
        Res., 21, 325-345.

Gill, A.E., and J.S. Turner, 1976: A comparison of seasonal
        thermocline models with;observation. Deep-Sea Res.,
        23, 391-401.

Gonella, J., 1971: A local study of inertial oscillation in
        the upper layer of the ocean. Deep-Sea Res., 18,
        775-788.

Gregg, M.C., H. Peters, J.C. Wesson, N.S. Oakley and T.J.Shay,
        1985: Intensive measurements of turbulence and shear
        in the equatorial under current. Nature, 318,
        140-144.

Halpern, D., S.P. Hayes, A. Leetma, D.V. Hansen and
        S.G.H. Philander, 1983: Oceanographic observations
        of the 1982 warming of the tropical eastern Pacific.
        Science, 221, 1173-1175.

Hastenrath, S., and P.J. Lamb, 1979: Climatic Atlas of the
        Indian Ocean. Part I: The Surface Climate and
        Atmospheric Circulation, Part 2:The Oceanic Heat
        Budget. University of Wisconsin Press, 116 and
        110 pp.

*Hela, I. 1954: The surface current field in the western
        part of the North Atlantic. Bull. Mar. Sci. Gulf
        Caribb., 3, 241-272.

India Meteorological Department, 1975: Meteorological
        Observations recorded on board I.N.S. DARSHAK
        during special survey cruise, 29 pp.

Ivanoff, A., 1977: Oceanic absorption of solar energy.
        Modelling and Prediction of the Upper Layers of
        the Ocean, E.B. Kraus, Ed., Pergamon Press, 47-71.

James, W.J., 1966: Ocean Thermal Structure Forecasting.
ASWEPS Manual Sp-105, 5, U.S. Naval Oceanographic
Office, Washington D.C., 217 pp.

Jayaraman, R., and C.P. Aravindakshan Nair, 1960:
Hydrography of the Laccadives off-shore waters
J. Mar. Biol. Ass. India, 2, 24-34.

Jenkins, G.M., and D.G. Watts, 1968 : Spectral Analysis and
its Applications, Holden-Day, San Francisco, 525 pp.

Jerlov, N., 1968: Optical Oceanography. Elsevier, 194 pp.

Joseph, M.G., 1980: Evaluation of a scheme of forecasting
ocean thermal structure during SUMET-80 off Cochin,
Part II, Thermal characteristics off Cochin during
SOMET-80 NPOL RR 6/80, 7 pp.

Joseph, M.G.and N. Durga Prasad, 1981: Oceanographic features
off Cochin and the west coast upto Trivandrum with
special reference to sound velocity characteristics
during SEILAZ -80, NPOL RR 3/81, 9 pp.

Joseph, P.V. and P.V. Pillai, 1986: Air sea interaction
on a monsoonal scale over north Indian Ocean -
Part II : Monthly mean atmospheric and oceanic
parameters during 1972 and 1973, Mausam, 37, 139-168.

Joyce, T.M., R.H. Kase and W. Zenk, 1980: Horizontal
advection of temperature in the seasonal thermocline
during JASIN 1978. J. Phys. Oceanogr. 10,1686-1690.

Kantha, L.H., 1977: Note on the role of internal waves
in the thermocline erosion. Modelling and Prediction
of the Upper Layers of the Ocean, E.B. Kraus, Ed.,
Pergamon Press, 173-177.

Katsaros, K.B., W.G., Liu, J.A. Businger and J.E. Tillman,
1977: Heat transport and thermal structure in the
interfacial boundary layer measured in an open tank
of water in turbulent free convection. J. Fluid.Mech

131

Kim, J.W., 1976: A generalised bulk model of the oceanic
        mixed layer. J. Phys. Oceanogr. 6, 686-695.

Kitaigorodskii, S.A. 1960: On the computation of the thickness
        of the wind mixing layer in the ocean. Izv. Akad.
        Nauk. S.S.S.R. Geophys. Ser. 3, 425-431.

Kitaigorodsky, A.N.and Y.Z. Miropolsky, 1970: On the theory
        of open ocean active layer, Izv. Akad. Nauk. S.S.S.R.
        Atmos. Ocean. Phys., 6, 97-102.

Knox, R.A. and D.L.T. Anderson, 1985:Recent advances in the
        study of the low-latitude ocean circulation, Prog.
        Oceangr., 14, 259-317.

Kondo, J., Y. Sasano and T. Ishii , 1979: On the wind
        driven current and temperature profiles with diurnal
        periods in the oceanic planetory boundary layer.
        J. Phys. Oceanogr. 9, 360-372.

Koninklijk Nederlands Meteorologisch Institut, 1952:
        Indische Ocean Oceanographische on Meteorologische
        gegevens, Publ. No. 135, 33 pp, 24 charts.

Kraus, E.B., and J.S. Turner, 1967: A one dimensional
        model of the seasonal thermocline, II, The general
        theory and its consequences. Tellus, 19, 98-106.

Kraus, E.B., (Ed), 1977: Modelling and Prediction of the
        upper Layer of the Ocean. Pergamon, 325 pp.

La Fond, E.C., 1954: Environmental factors affecting the
        vertical temperature structure of the upper layers
        of the sea. Andhra University Ser. 49, University
        Memoirs in Oceanography, 1, 94-101.

La Fond E.C., and C. Poornachandra Rao, 1954: Vertical
        oscillations of tidal periods in the temperature
        structure of the sea. Andhra University Ser.49,
        University Memoirs in Oceanography, 1, 109-116.

*Laevastu, T., 1960: Factors affecting the temperature of the surface layer of the sea. Soc. Sci. Fenn., Comm. Phys. Math. 25, 136 pp.

Laevastu,T., and W.E. Hubert, 1965: Analysis and prediction of the depth of the thermocline and near surface thermal structure. FNWC. Techn. Note,No.10.

Laevastu, T., and I.Hela, 1970: Fisheries Oceanography. Fishing News (Books) Ltd, London, 238 pp.

Levitus, S., 1982: Climatological Atlas of the World Ocean. NOAA Prof. Paper 13, U.S. Govt. Printing Office, Washington, D.C., 173 pp.

Liepper, D.F., 1967: Observed Ocean Conditions and hurricane Hilda, 1964, J. Atm. Sci., 24, 182-196.

Linden P.F., 1975: The deepening of a mixed layer in a stratified fluid. J. Fluid. Mech. 71, 385-405.

Longuet-Higgins, M.S., and J.S. Turner, 1974: An 'entraining plume' model of a spilling breaker.J. Fluid. Mech. 63, 1-20.

Lumb, F.E., 1964: The influence of clouds on hourly amounts of total solar radiation at the sea surface. Quart. J. Roy. Meteorol. Soc.90, 43-56.

Lumby, J.R., 1955: The depth of the wind produced homogenous layers in the ocean. Fish. Invest.Lond.Ser. 2 2, 12 pp.

Madsen, O.S., 1977: A realistic model of the wind induced Ekman boundary layer. J. Phys. Oceanogr.1, 248-255.

Marchuk, I.G., V.P. Kochergin, V.I. Klimok and V.A. Sukhorukov, 1977: On the dynamics of the ocean surface mixed layer. J. Phys. Oceanogr. 7, 868-875.

Matsuike, K.T. Morinaga and S. Sasaki, 1970: The optical
        characteristics of the water in the three oceans,
        part IV. J. Oceanogr. Soc. Japan, 26, 52-60.

Mazeika, P.A., 1960: Prediction of the thermocline depth.
        U.S. Naval Oceanographic Office, TR-104, 79 pp.

Mc Alister, E.D., and W. Mc Leish, 1969: Heat transfer
        in the top millimeter of the ocean. J. Geophys.
        Res., 15, 577-598.

Meehl, G.A., 1984: A calculation of ocean heat storage
        and effective ocean surface layer depth for the
        northern hemisphere. J. Phys. Oceanogr. 14, 1747-1761 .

Mellor, G.L., and P.A. Durbin, 1975: The structure and
        dynamics of the ocean surface mixed layer. J.Phys.
        Oceanogr. 5, 718-728.

Miller, J.R., 1976: The salinity effect in a mixed layer
        ocean model. J. Phys. Oceanogr. 6, 29-35.

Miropolsky, Y.Z., 1970: Non stationary model of the wind-
        convective mixing in the ocean. Izv. Atm. and Ocean.
        Phys., 6, 1284-1294.

Miyokoda, K., and A. Rosati, 1984: The variation of sea surface
        temperature in 1976 and 1977, 2: The simulation with
        mixed layer models. J. Geophys. Res. 89,6533-6541.

Munk, W., 1981. Internal waves and small scale processes.
        Evolution of Physical Oceanography. B.A. Warren and
        C. Wunsch, Eds., The M.I.T. Press, 264-291.

Murty, A.V.S. 1964: Studies on the surface mixed layer
        and its associated thermocline off the west coast
        of India and reference for working out a prediction
        system of the pelagic fisheries of the region. Indian
        J. Fish. 12, 118-135.

Narayana Pillai, V., P.K. Vijayarajan and A.Nanda Kumar, 1980: Oceanographic investigations along the south-west coast of India (1976-78). Field document by F.A.O. of United Nations, Rome, 51 pp.

National Climatic Centre, 1968: TDF-11 Tape Deck Manual, Asheville, N.C.

National Oceanographic Data Centre, 1974: Users Guide to NODC's Data Services, Key to oceanographic documentation No.1, Department of Commerce, Washington D.C., 72 pp.

Neumann, G., 1955: On wind generated wave motion at subsurface levels. Trans. Am. Geophys. Un. 36, 985-992.

Niiler, P.P., 1975: Deepening of the wind mixed layer. J. Mar. Res. 33, 4U5-422.

Niiler, P.P. and E.B. Kraus, 1977: One dimensional models of the upper ocean, 143-172 in Modelling and Prediction of the Upper Layers of the Ocean E.B. Kraus (Ed)., Pergamon Press, Oxford, 325 pp.

O'Brien, J.J. and H.E. Hurlburt, 1972: A numerical model of coastal upwelling. J. Phys. Oceanogr.,2, 14-26

O'Brien, J.J., R.M. Clancy, J.A. Clarke, M. Crepon, R. Elsberry, T.Gammelsrod M. Mac Vean, L.P. Roed and J.D. Thompson, 1977: Upwelling in the ocean; Two and three dimensional models of upper ocean dynamics and variability. Modelling and Prediction of the Upper Layers of the Ocean, E.B. Kraus, (Ed) Pergamon Press, 178-228.

Panikkar, N.K. and R. Jayaraman, 1966: Biological and oceanographic differences between the Arabian Sea and the Bay of Bengal as observed from the Indian Ocean. Proc. Indian. Acad. Sci.,14-B, 231-240.

Patil, M.R., and C.P. Ramamirtham, 1962: Hydrography
         of the Laccadives off-shore waters - A study
         of the water conditions. J. Mar. Biol. Ass. India
         5, 159-169.

Patil, M.R.,C.P. Ramamirtham, P. Udayavarma, C.P.A. Nair
         and P. Myrland, 1964: Hydrography of the west coast
         of India during the premonsoon period of the   year
         1962. J. Mar. Biol. Ass. India, 20, 2319-2324.

Pollard, R.T., 1972: Properties of near surface inertial
         oscillation. Woods Hole Oceanogr. Inst., Contrib.
         2736, 44 pp.

Pollard R.T., and R.C., Millard, 1970: Comparison between
         observed and simulated wind generated inertial
         oscillation. Deep-Sea Res., 17, 813-821.

Pollard,R.T., P.B.Rhines and R.O.R.Y. Thompson, 1973:
         The deepening of the wind mixed layer. Geophys.
         Fluid. Dyn., 3, 381-404.

Pond, S., 1971: Air-sea interaction. Trans. Amer. Geophys
         Un. (IUGG) 52, 389-394.

Pond,S., and G.L. Pickard, 1983. Introductory Dynamical
         Oceanography. Pergamon Press, Oxford, 329 pp.

Prangsma, G.J.and P. Kruseman, 1984: Aspects of mixed
         layer modelling applied to JASIN data. Dyn.
         Atmos. Oceanog. 8, 321-341.

Privett, D.W., 1959: Monthly charts of evaporation from
         the N. Indian Ocean (including the Red Sea and
         Persian Gulf). Quart. J. Roy. Meteorol. Soc.
         85, 424-428.

Quraishee, G.S., 1984: Circulation in the north Arabian
         Sea at Murray Ridge during S.W. Monsoon. Deep-
         Sea Res., 31, 651-664.

Qasim, S. Z., 1982: Oceanography of the northern Arabian Sea
Deep-Sea Res., 29, 1047-1068.

Raghavan, K., 1969: Satellite evidence of sea-air
interactions during Indian monsoon. Mon. Weather.
Review, 97, 905-908.

Ramage, C.S., F.R. Miller and C. Jefferies, 1972:
Meteorological Atlas of the International
Indian Ocean Expedition, Vol. 1: The surface
climate of 1963 and 1964, National Science
Foundation, Washington, D.C.,

Ramam, K.V.S., P.G.K. Murthy and C.K.B. Kurup, 1979:
Thermal structure variation in the Arabian
Sea (May-July, 1973) Mausam, 30, 105-112.

Ramamirtham, C.P. and R. Jayaraman, 1960: Hydrography
of the shelf waters off Cochin. J. Mar. Biol.
Ass. India. 2, 199-207.

Ramasastry, A.A. and P. Myrland, 1959: Distribution of
temperature and salinity and density in the Arabian
Sea along the south Malabar coast (South India)
during the post-monsoonal season. Indian.J. Fish.,
6, 223-255.

Ramesh Babu,V., L.V.G. Rao, M.J. Varkey and P.Udayavarma,
1976: Temperature distribution of the upper layer
of northern and eastern Arabian Sea during Indo-US
Monsoon Experiment. Indian. J. Met. Geophys.
27, 291-293.

Ramesh Babu, V., M.J. Varkey, V. Kesavadas and A.D.Gouvia,
1980: Water masses and general hydrography along
west coast of India during early March. Indian J.
Mar. Sci. 9, 82-89.

Ramesh Babu, V., and J.S. Sastry, 1984: Summer cooling in the
east central Arabian Sea - A process of dynamic
response to the southwest monsoon,Mausam, 35, 17-26.

Rao, D.S., C.P. Ramamirtham and N.P. Kunhikrishnan, 1963:
        Hydrography of the waters along the Gujarat
        coast during the summer period of the year 1963.
        J. Mar. Biol. Ass. India. 21, 133-142.

Rao, R.R., P.G.K. Murthy, M.G. Joseph and K.V.S. Ramam,
        1981: On the space-time variability of ocean surface
        mixed layer characteristics of the central and
        eastern Arabian Sea during Monsoon-77. International
        Conference on early results of FGEE and large scale
        aspects of its monsoon experiments, Geneva, 20-27.

Ray,T.K., 1984: Energy transfer from the Arabian Sea, the
        Bay of Bengal and North Indian Ocean, Mausam,
        35, 503-506.

Reddy, K.G., M.V. Rao, P.H. Prasad and G.R.L. Rao, 1984:
        The net energy exchange at the surface over the
        Arabian Sea during the southwest monsoon. Mausam,
        35, 499-502.

Reed, R.K., 1977: On estimating insolation over the ocean.
        J. Phys. Oceanogr. 7, 482-485.

Reed, R.K. and D. Halpern, 1974: Radiation measurements
        off the Oregon coast. CUEA Data Rep. 13, Dept.
        Oceanogr., University of Washington, 51 pp.

Roberts, J., 1975: Internal Gravity Waves in the Ocean.
        Marcel-Dekker Inc., New York, 263 pp.

Robinson, M.K., R.A. Bauer and E.H. Schroeder, 1979:
        Atlas of North Atlantic-Indian Ocean Monthly Mean
        Temperatures and Mean Salinities of the Surface
        Layer, Naval Oceanographic Office, Washington, D.C.,
        213 pp.

Rooth, C.G., and W. Duing, 1971: On the detection of
        "internal" waves with pycnocline followers.
        J. Phys. Oceanogr. 1, 12-16.

Rossby, C.G., and R.B. Montgomery, 1935: The layer of
    frictional influence in wind and ocean currents.
    Papers in Physical Oceanography and Meteorology,
    3, 101 pp.

Saha K.R., 1974: Some aspects of the Arabian Sea summer
    monsoon, Tellus, 26, 464-476.

Sastry, J.S. and R.S. D'Souza, 1970 : Oceanography of
    Arabian Sea during southwest monsoon, Part 1:
    Thermal structure. Indian J. Met. Geophys.
    21, 367-382.

Sastry, J.S. and V. Ramesh Babu, 1985: Summer cooling of
    the Arabian Sea - a review . Proc. Indian Acad.Sci.
    94, 117-128.

Schott, F., 1971a: On horizontal coherence and internal
    wave propagation in the North Sea. Deep-Sea Res.,
    18, 291-307.

Schott, F., 1971b: Spatial structure of inertial-period
    motion in a two-layered sea, based on observations.
    J. Mar. Res., 29, 85-102.

Schott, G., 1902. Oceanographic and Maritime Meteorology.
    Wissenschaftlishe Ergebnisse der Deutschen Tiefsee-
    Expedition auf dem Dampfer, Valdivia, 1898-1902.

*Sewel, R.B.S., 1929: Geographic and Oceanographic research
    in Indian waters, Part V: Temperature and salinity of
    surface waters of the Bay of Bengal and Andaman Sea
    with reference to the Laccadive Sea. Mem. Asiat.
    Soc. Beng.9, 207-355.

Sharma, G.S., 1966: Thermocline as an indication of
    upwelling. J. Mar. Biol. Ass. India., 8, 8-19.

Sharma, G.S. 1968: Seasonal variation ot some hydrographic
        properties of the shelf waters off the west coast
        of India. Bull. Natl. Inst. Sci. India. 38, 263-276.

Shetye, R.S, 1984: Seasonal variability of temperature
        field off southwest coast of India. Proc. Indian
        Acad. Sci., 93, 399-411.

Smith,S.D., and E.G. Banke, 1975: Variation of the sea
        surface drag coefficient with wind speed. Quart.
        J. Roy. Meteorol. Soc., 101, 665-673.

Sverdrup, H.U., M.W. Johnson and R.H. Fleming, 1942:
        The Oceans, their Physics, Chemistry and General
        Biology. Prentice-Hall, New York, 1087 pp.

*Tabata, S. and F.M. Boyce, 1962: The relation between
        wind speed and summer isothermal surface layer
        of water at ocean station "P". Fisher. Res. Bd.
        Canada. Pac. Ocean. Group., NANAIMO, B.C.

Toba, Y.M.Iokuda, K. Okuda and S. Kawai, 1975: Forced
        convection accompanying wind waves. J. Oceanogr.
        Soc. Japan., 31, 192-198.

Turner, J.S., 1981: Small scale mixing processes.
        Evolution of Physical Oceanography, B.A. Warren and
        C. Wunsch, Eds., The M.I.T. Press, 236-262.

Tyler, J.E., and R.C. Smith, 1970: Measurements of Spectral
        Irradiance Underwater, Gorden and Breach Science
        Publishers.

Tyler, J.E., 1968: The Secchi disc. Limnol. Oceanogrr,
        23, 1-6.

U.S. Navy Hydrographic Uffice, 1960: Summary of Uceanographic
        Conditions in the Indian Ocean. Spc. Pub. SP-53,
        Washington D.C., 142 pp.

Varadachari, V.V.R., and G.S. Sharma, 1964: On the
        vergence field in the North Indian Ocean, Bull.
        N.G.R.I. 2, 1-14.

Varadachari, V.V.R., and G.S. Sharma, 1967: Circulation
        of the surface waters in the North Indian Ocean.
        J. Indian Geophys. Un., 4, 61-73

Varma, K.K., V. Kesavadas and A. Gouvia, 1980:Thermocline
        structure and water masses in the Northern Arabian
        Sea during February-April. J. Mar. Sci. 9, 148-155.

Woods, J.D., 1980: Diurnal and seasonal variation of
        convection in the wind mixed layer of the ocean.
        Quart. J. Roy. Met. Soc., 106, 379-394.

Woods, J.D., W. Barkmann, 1986: The response of the upper
        ocean to solar heating. I: The mixed layer.
        Quart. J. Roy. Met. Soc., 112, 1-27.

Wooster, W.S., M.B. Schaefer and M.K. Robinson, 1967:
        Atlas of the Arabian Sea for Fishery Oceanography
        University of California Institute of Marine
        Resources, IMR Ref. 67-12, 35 pp, 140 Figs.

Wyrtki, K., 1971: Oceanographic Atlas of the International
        Indian Ocean Expedition, National Science
        Foundation, NSF-10 E-1, Washington,D.C., 542 pp.